A Study on Syntheses of Semiconductor Nanocrystal/Polymer Hybrids and Their Optical and Distribution Properties

Hiroshi YAO

A Study on Syntheses of Semiconductor Nanocrystal/Polymer Hybrids and Their Optical and Distribution Properties

Graduate School of Science, Hokkaido University

Hiroshi YAO

Contents

Chapter 1. Introduction - Why Semiconductor Nanocrystals or Quantum Dots are Attracting Attentions?

1.1 Outline for the Syntheses of Semiconductor Nanocrystals and the Optical Properties

Sciences and technologies which consider the size of materials have recently been developed. Cluster or mesoscopic science, defined as the materiel sciences of an intermediate (= meso) region between microscopic and macroscopic dimension, is devoted to understanding the changes in fundamental properties of materials as a function of size; a transition from isolated atoms or small molecules to bulk crystals. In the case of semiconductors, this evolution of the science and technology is remarkable.[1,2] Thus, semiconductors of oxides and chalcogenides of various metals (TiO_2, ZnO, WO_3, CdSe, CdS, PbS, Cd_3P_2, MoS_2, In_2S_3, and so forth) have been studied during the past decade by Henglein, Brus, and Wang as pioneers.[3-5] Usually, preparations of the materials are done by precipitations of semiconductor colloids from a homogeneous solution through controlled injection of anions (S^{2-}, HSe^-, etc.), cations (Cd^{2+}, Pb^{2+}, etc.) or forced hydrolysis.[6-8] For example, controlled mixing of a metal ion such as Cd^{2+} with sulfide anions yields colloidal solutions of the relevant metal sulfide. Similarly, forced hydrolysis can be employed for preparations of metal oxides such as TiO_2. The size and the distribution of the colloidal particles can be controlled by varying the experimental parameters such as the concentrations of reactants, temperature (low temperature synthesis yields smaller particles)[9], nature of a stabilizer (hexamethaphosphate,[10] thiophenols,[11] or sodium dodecyl sulfide[12]), and a medium (water phase or organic solvent). Actually, various efforts

have been made to prepare well-defined nanocrystalline particles with narrow size distributions. Other methods of colloidal semiconductor synthesis include reactions in the vapor phase, and dissolution of crystalline powders of layered semiconductors.[13,14]

Investigations for preparing nanocrystals in various heterogeneous environments were also performed. Encagement of semiconductor crystals in an organized medium controls both the morphology and also the photocatalytic properties of semiconductors. Typical examples for this are the preparations using micelles,[15] vesicles,[16] zeolites,[27] Langmuir-Blodgett films,[18] clays,[19] and silica glasses.[20] Such preparations provide isolated small semiconductor nanocrystals which are stabilized in an organized medium.

In most of these studied, CdS has been an popular choice for a semiconductor since it can be prepared readily by chemical precipitation and characterized by its optical spectra such as absorption and emission. In the case of CdS, for example, the band gap energy can be varied between 4.5 and 2.5 eV as the size is increased from the molecular regime to a bulk crystal, and the radiative lifetime for the lowest allowed transition changes from tens of ps to several ns.[21] The pressure required to reduce transformation from a four- to a six-coordinate phase decreases from 9 to 2 GPa with the decrease in the crystal size.[22] Besides these, many interesting and characteristic features of semiconductor nanocrystals are known. In the followings, as a general feature of nanoclusters, some fundamental characteristics which offer interesting, important and anomalous physical and chemical properties are overviewed.

1. Quantum Confinement Effect - In any materials with a reduced size, substantial changes of fundamental electronic and optical properties

will be observed when the electronic energy level spacing exceeds the thermal energy. The energy bands of a solid are centered about atomic energy levels, and the band width is known to relate with the strength of the nearest-neighbor interactions. As a cluster size increases, the center of a band develops first and the edge last.[1,2] In metals, where the Fermi level lies in the center of a band, the relevant energy level spacing is small and, at above a few kelvin, the optical properties resemble those of a bulk, even at relatively small sizes.[23] In van der Waals molecular crystals, the nearest-neighbor interactions are weak, the bands in the

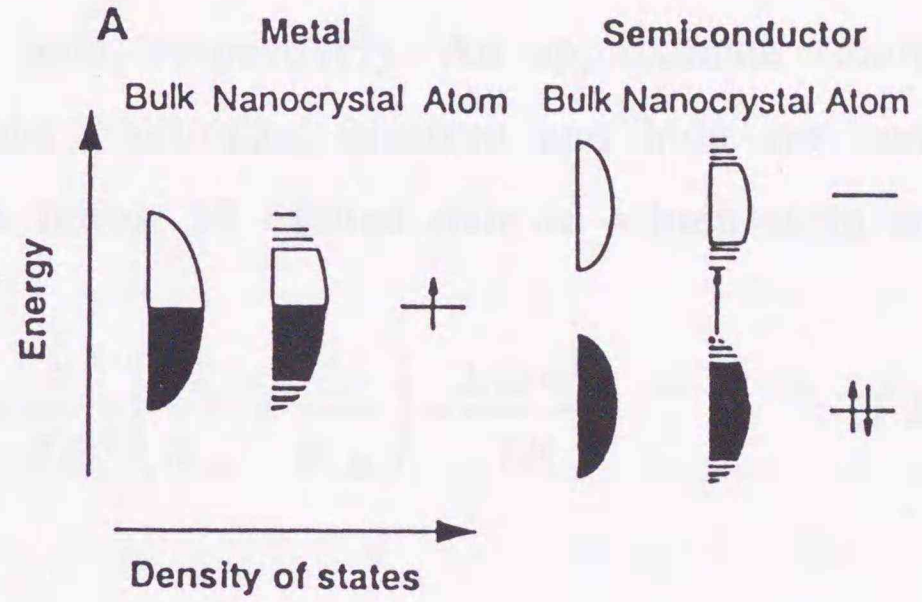

Figure 1.1. Schematic illustration of the density of states in metal and semiconductor nanocrystals.

solid are very narrow and, consequently, very weak size variations in optical and electrical properties are expected or observed in the nanocrystal regime. In semiconductors, however, the Fermi level lies between two bands, and the edge of the bands dominates the low-energy optical behavior. Hence, optical excitation across the gap depends strongly on the size of clusters (Figure 1.1).

When an electron and a hole combined with Coulomb interaction are confined in a restricted sphere with an infinite potential well of a radius,

R, the quantum states can be calculated. In a simple model, an effective mass approximation can be employed, which indicates that an electron and a hole with effective masses of m_e and m_h freely move in a nanocrystal. The Hamiltonian for the lowest excited electron-hole system is written as in eq. 1.1,[24]

$$H = \frac{p_e^2}{2m_e} + \frac{p_h^2}{2m_h} - \frac{e^2}{\varepsilon|r_e - r_h|} \qquad (1.1)$$

where p_e, p_h, r_e, r_h are the momenta, and the position coordinates of the electron and the hole, respectively. An approximate solution in a strong confinement regime (individual electron and hole are confined) obtained by Brus[24] for the lowest 1S excited state is written as in eq. 1.2,

$$E \approx E_g + \frac{h^2}{8R^2}\left(\frac{1}{m_e} + \frac{1}{m_h}\right) - \frac{1.8e^2}{\varepsilon R} \qquad (1.2)$$

where the first, second, and third terms indicate a bulk energy gap, a kinetic confinement energy, and a Coulomb energy, respectively. This equation shows that when the crystal diameter decreases, the energy increases leading to a spectral blue-shift: quantum size effect.

2. The influence of the surface - The most ideal of a semiconductor nanocrystal might be a mass-selected, isolated in the gas phase, and thermally annealed.[25] Despite apparent perfection of a pure cluster in the gas phase, from the point of view of semiconductor physics, it is a highly defective system. At the surface of a pure tetrahedral inorganic semiconductor, substantial reconstructions in the atomic positions occur, leading to energy levels within the energetically

forbidden gap of a bulk solid.[1] These surface states trap electrons or holes and, change the optical properties of the material. Passivation is a chemical process by which these surface atoms are bonded to another materials, eliminating all of the energy levels inside the gap. Ideal termination will naturally remove structural reconstructions, leaving no strain, and simply produces a jump in the chemical potential for electrons or holes at the interface.

3. Oscillator strength[26] - In a bulk semiconductor, the electron and the hole are bound by the screened Coulomb interaction with a binding energy of a few to tens of meV. This exciton is easily ionized by thermal energies, which accounts for the absence of a strong exciton absorption band at room temperature. By confining an electron and a hole in a small sphere, the binding energy and the oscillator strength can increase due to the enhanced spatial overlap between the electron and hole wave functions (for strong confinement) and to the coherent motion of the exciton (for weak confinement). This effect is responsible for the giant oscillator strength observed for bound excitons in bulk semiconductors,[27] where the electron-hole pair is confined in the potential well established by the shallow defect. The total oscillator strength of the electron-hole pair per nanocrystal is given as[26]

$$f = \frac{8\pi^2 m_0}{h^2} \cdot \Delta E \cdot |\mu|^2 \cdot |U(0)|^2 \qquad (1.3)$$

where m_0, E, μ, and $|U(0)|^2$ are a free electron mass, a transition energy, a transition dipole moment, and a probability of finding the electron and hole on the same site (overlap factor), respectively. The oscillator

strength per unit volume, f/V (V is the volume of the crystal) determines the absorption coefficient.

For nanocrystals in a strong confinement regime, the overlap between the electron and hole wave functions, $|U(0)|^2$, is almost unity. Thus, f is independent of the crystal size. However, the oscillator strength per unit volume, f/V, now increases with decreasing the crystal size and scales approximately with $(a_B/R)^3$ where a_B is an exciton Bohr radius of the semiconductor.[28] Since f/V determines the absorption coefficient, the excitonic absorption band should get stronger with decreasing the crystal size and becomes visible even at room temperature. These phenomena were recently confirmed experimentally by H. Weller *et. al.*[21]

In order to interpret a novel physical phenomenon by examining and modifying the theories, it is important to prepare size-regulated semiconductor nanocrystals with a high quality. Although nanocrystal assemblies or shape-regulated crystal preparation have been recently explored, the trials are still far to be satisfactory.[29] Thus, it is worth investigating various preparation methods of size-regulated semiconductor nanocrystals.

1.2 Applications - Semiconductor Nanocrystals in Organic Polymer Hosts

Ultrafast optical modulations instead of the contemporary electrical modulations are important for constructions of optically integrated circuits as a fundamental of developing new opto-electronics. Such all-optical switching devices are expected to be realized on the basis of nonlinear optical materials. These devices are based on the refractive index changes induced by ultrafast light irradiation.[30] Semiconductor

nanocrystals are thus promising materials for such a nonlinear device, since the oscillator strength will be controlled by a regulating crystal size, a size distribution, and a loading density. For these purposes, CdS is known to be one of the well-investigated and promising semiconductors.[30]

Electrical polarization ($\boldsymbol{P}$) is induced in a material when intense light is irradiated, and optical nonlinearity originates from the fact that $\boldsymbol{P}$ is a nonlinear function of a field amplitude ($\boldsymbol{E}$) of incident light; eq. 1.4,

$$P = \chi^{(1)}E + \chi^{(2)}EE + \chi^{(3)}EEE + \cdots \qquad (1.4)$$

where $\chi^{(1)}$, $\chi^{(2)}$, and $\chi^{(3)}$ represent linear, second-order, and third-order electric susceptibilities, respectively. When $\chi^{(2)}$ or $\chi^{(3)}$ contributes to $\boldsymbol{P}$, various nonlinear optical processes occur. Especially, representative third-order nonlinear optical processes are described as absorption saturation and the relevant refractive index changes. Namely, an absorption coefficient (α) and a refractive indices (n) are dependent on the incident light intensity (I),

$$\alpha = \alpha_0 + \alpha_2 I \, , n = n_0 + n_2 I \qquad (1.5)$$

where α_0, n_0, α_2, and n_2 represent an absorption coefficient with a weak light intensity, a refractive index measured with a weak light intensity, a nonlinear absorption coefficient and a nonlinear refractive index, respectively. The values of α_2 and n_2 are dependent directly on the imaginary and the real parts of $\chi^{(3)}$ (i.e., $\mathrm{Im}\chi^{(3)}$ and $\mathrm{Re}\chi^{(3)}$), respectively.[31] This third-order optical nonlinearity originates from a transient change in the absorption spectrum (and refractive index) of a

material. Once a nanoparticle or molecule absorbs a photon from the ground state to the excited state, the transition can no longer be excited until the excited state relaxes back to the ground state. During this period, if one measured the absorption spectrum of the nanoparticle, one would observe reduction in absorption at the lowest transition energy (bleaching). If the excited state has transitions to higher states in the wavelength region probed, then, additional induced absorption can be observed. The changes in the absorption coefficient and the refractive index are proportional to the light intensity as described in eq. 1.5 before the saturation regime is reached. For semiconductor nanocrystals, a large $\chi^{(3)}$ (absolute value of $\chi^{(3)}$) value is expected due to concentration of the oscillator strength to the discrete electron-hole pair transition.

A maximum $\mathrm{Im}\chi^{(3)}$ value, which is derived under the resonant condition, is proportional to several factors as expressed in eq. 1.6,

$$\mathrm{Im}\,\chi^{(3)} \propto \frac{f_x^{\,2}}{h\gamma_L\gamma_T^{\,2}} N \qquad (1.6)$$

where f_x, γ_L, γ_T, N are an oscillator strength of the transition concerned with nonlinearity, a longitudinal relaxation constant, a transverse relaxation constant, and the crystal number density, respectively.[32] For an ideal case, large $\chi^{(3)}$ is obtainable when f_x and N make large, γ_L and γ_T make small. In order to achieve the condition, crystal size control with a very narrow size distribution is important, since this leads to concentration of the notable transition. Also, dense dispersion of the crystals are indispensable. For applications to nonlinear optical (NLO) materials, moreover, photo-reaction or photo-degradation should be prevented and crystal sizes should not be change during a long period.

Thus, semiconductor nanocrystals are to be embedded in solid matrices, especially, in organic polymers as a host.

Studies on semiconductor/organic polymer composites have been so far scarcely reported. The advantages of using organic polymers are as follows: (i) stable dispersion of nanocrystals is possible, (ii) an appropriate choice of functional groups of a polymer is expected to control nanocrystal-host interactions, (iii) various colloidal preparation methods can be applied.[33,34] Interesting properties of nanocrystals in organic polymers, different from those in solution, will be expected. Thus, development of novel preparation methods for size-regulated semiconductor nanocrystals and nanocrystals-doped organic polymer materials are worth to be explored. Interactions between nanocrystals and host polymers, or crystal formation mechanisms are to be fundamentally investigated. In view of applications, third-order optical nonlinearities should be also studied. Keeping these aspects in mind, researches along the line mentioned above were performed.

1.3 Content of This Thesis

The thesis consists of 6 chapters.

Chapter 1 describes a general features of semiconductor nanocrystals. In **chapter 2**, *photocatalytic size-controlled preparations* of CdS nanocrystals under monochromatic laser light irradiation are described. Third-order optical nonlinearities of the prepared CdS nanocrystals incorporated in an organic polymer host were also analyzed in special reference to the effects of the size distribution. In **chapter 3**, preparations of CdS nanocrystals in host polymers are explored by focusing *the effects of the shapes and/or sizes of the polymer matrices.*

Studies of interactions between CdS nanocrystals and polymer matrices are also described. In **chapter 4**, taking an application into consideration, a *method of dense loading* of CdS nanocrystals in polymer matrices was studied in order to enhance the optical nonlinearity by using a polymer stabilizer; polyvinyl pyrrolidone (PVP). Linear and nonlinear optical properties were also investigated. In **chapter 5**, moreover, an enhancement of $\chi^{(3)}$ values with *a binary system* was studied by an application of the preparation method described in Chapter 4. In **chapter 6**, the summary and general conclusions of the research are described.

1.4 References and Notes

(1) Alivisatos, A. P. *Science* **1996**, *271*, 933.

(2) Brus, L. E. *Appl. Phys.* **1991**, *A53*, 465.

(3) Henglein, A. *Top. Curr. Chem.* **1988**, *143*, 113.

(4) Brus, L. E. *IEEE J. Quantum Electr.* **1986**, *QE22*, 1909.

(5) Wang, Y; Herron, N. *J. Phys. Chem.* **1987**, *91*, 5005.

(6) Bahnemann, D.; Henglein, A.; Lilie, J.; Spanhel, L. *J. Phys. Chem.* **1984**, *88*, 709.

(7) Spanhel, L.; Anderson, M. A. *J. Am. Chem. Soc.* **1991**, *113*, 2826.

(8) Nenadovic, M. T.; Rajh, T.; Micic, O. I.; Nozik, A. J. *J. Phys. Chem.* **1984**, *88*, 5827.

(9) Rossetti, R.; Hull, R.; Gibson, J. M.; Brus, L. E. *J. Chem. Phys.* **1985**, *82*, 552.

(10) Fojtik, A.; Weller, H.; Koch, U.; Henglein, A. *Ber. Bunsenges. Phys. Chem.* **1984**, *88*, 969.

(11) Nosaka, Y.; Ohta, N.; Fukuyama, T.; Fujii, N. *J. Colloid. Interface. Sci.* **1993**, *155*, 23.

(12) Kuczynski, J. P.; Milosavijevic, B. H.; Thomas, J. K. *J. Phys. Chem.* **1983**, *87*, 3368.

(13) Visca, M.; Matijevic, E. *J. Colloid Interface Sci.* **1979**, *68*, 308.

(14) Peterson, M. W.; Nenadovic, M. T.; Rajh, T.; Herak, R.; Micic, O. I.; Goral, J. P.; Nozik, A. J. *J. Phys. Chem.* **1988**, *92*, 1400.

(15) Meyer, M.; Wallberg, C.; Kurihara, K.; Fendler, J. H. *J. Chem. Soc., Chem. Commun.* **1984**, 90.

(16) Tricot, Y. M.; Emerson, A.; Fendler, J. H. *J. Phys. Chem.* **1985**, *89*, 4721.

(17) Wang, Y.; Herron, N. *J. Phys. Chem.* **1987**, *91*, 257.

(18) Smotkin, E. S.; Lee, C.; Bard, A. J.; Campion, A.; Fox, M. A.; Mallouk, T. E.; Webber, S. E.; White, J. M. *Chem. Phys. Lett.* **1988**, *152*, 265.

(19) Stramel, R. D.; Nakamura, T.; Thomas, J. K. *Chem. Phys. Lett.* **1986**, *130*, 423.

(20) Ekimov, A. J.; Onushchenko, A. *JETP Lett.* **1984**, *40*, 1136.

(21) Vossmeyer, T.; Katsikas, L.; Giersig, M.; Popovic, I. G.; Diesner, K.; Chemseddine, A.; Eychmueller, A.; Weller, H. *J. Phys. Chem.* **1994**, *98*, 7665.

(22) Goldstein, A. N.; Echer, C. M.; Alivisatos, A. P. *Science* **1992**, *256*, 1425.

(23) Cohen, M. L.; Chou, M. Y.; Knight, W. D.; deHeer, W. A. *J. Phys. Chem.* **1987**, *91*, 3141.

(24) Brus, L. E. *J. Chem. Phys.* **1984**, *80*, 4403.

(25) Liu, A.; Zang, Q.-L.; Tittel, F. K.; Curl, R. F.; Smalley, R. E. *J. Chem. Phys.* **1986**, *85*, 7434.

(26) Wang, Y.; Herron, N. *J. Phys. Chem.* **1991**, *95*, 525.

(27) Stoneham, A. M. *Theory of Defects in Solids*; Clarendon Press: Oxford, UK, 1985.

(28) Kayanuma, Y. *Phys. Rev.* **1988**, *B38*, 9797.

(29) Weller, H. *Abstracts in International Chemical Congress of Pacific Basin Society*; Honolulu, 1995, Anal Chem. 110.

(30) Hanamura, E. *Solid State Commun.* **1987**, *62*, 465.

(31) Gibbs, H. M. *Optical Bistability, Controlling Light with Light*; Academic Press: New York, 1987.

(32) Takagahara, T. *Phys. Rev.* **1989**, *B39*, 10206.

(33) Wang, Y.; Suna, A.; Mahler, W.; Kasowski, R. J. Chem. Phys. 1987, 87, 7315.

(34) Hayashi, T. *Abstracts in International Symposium on Nonlinear Photonic Materials*, Japan, 1994, 243.

Chapter 2. Size Control of CdS Nanoparticles under Monochromatic Laser Irradiation[1-3]

2.1 Introduction

The most striking property of semiconductor nanocrystals (quantum dots) is large changes in optical properties as a function of size. As size is reduced, the electronic excitations shift to higher energies, and the oscillator strength is concentrated into just a few transitions. Thus, semiconductor nanocrystals are widely interested for applications to nonlinear optical materials/devices. An important problem, to be solved, is to optimize preparation methods of nanocrystals, which makes the size and its distribution regulated for not only elucidating basic physical and chemical properties of the materials but also developing nonlinear optical materials/devices and so on.

Nanocrystal preparations (many of them are for CdS or CdSe) have been heretofore developed by applying selected stabilizer addition methods and/or mechanical separation methods using centrifugation. These methods are of course important, and have a high potential to achieve precise size control. However, principles or mechanisms of the size regulation are not well-known. A new principle of a novel nanocrystal size regulation method is highly desired, and worth to be developed.

The energy state of the first electronic excitation (excitonic state) is dependent sensitively on the size of a nanoparticle. For a simple electron-hole confinement in a sphere as described in chapter 1,[4] the lowest energy eigenvalue is given,

$$E_g + \frac{h^2\pi^2}{2\mu R^2} - 1.8\frac{e^2}{\varepsilon R} \qquad (2.1)$$

where E_g, μ, R, ε are a bulk band gap, a reduced electron-hole effective mass ($\mu^{-1} = m_e^{-1} + m_h^{-1}$,: m_e and m_h are electron and hole effective masses), a nanoparticle radius and the dielectric constant of the semiconductor, respectively. The excitonic energy increases with decreasing a particle diameter. The energy level also becomes discrete.

In the case of CdS, the relation between the excitonic energy level and the particle diameter has been calculated more precisely on the basis of a tight-binding method,[5]; an LCAO calculation. Figure 2.1 shows a relation between the first excitonic energy of CdS and the nanoparticle diameter.[5]

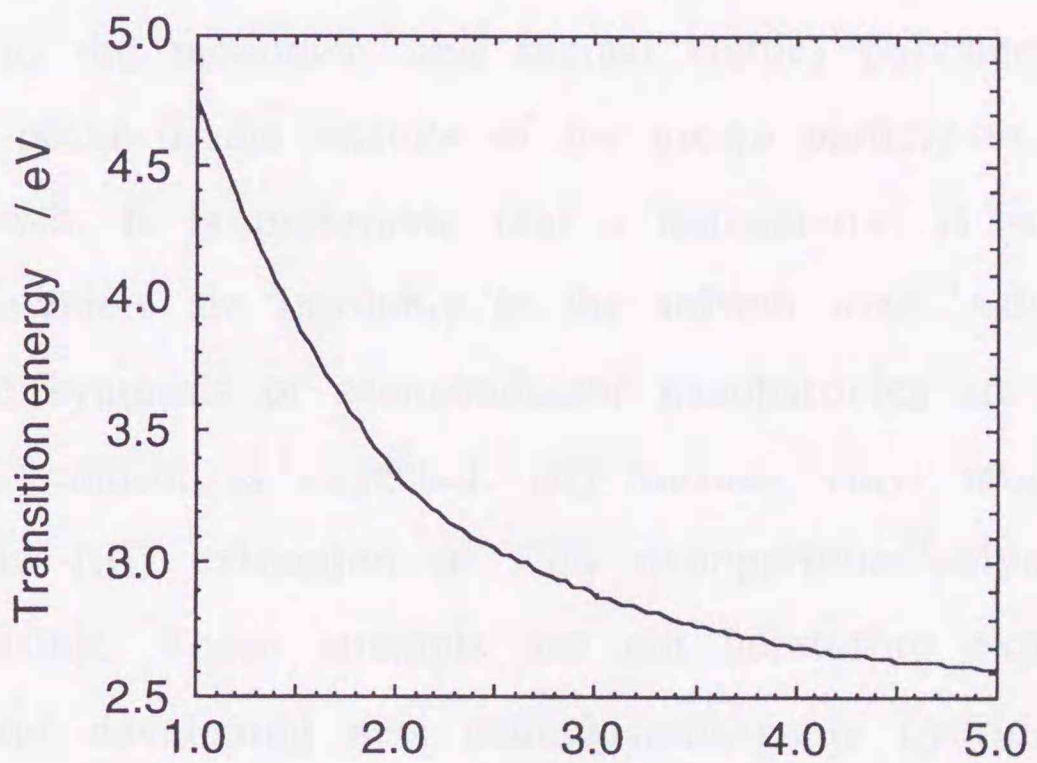

Figure 2.1. A relation between the first excitonic transition energy (1S-1S) and the particle diameter of CdS, which was calculated by a tight-binding method.[5] The figure indicates that one transition energy reflects one particle diameter.

The figure demonstrates, for instance, that light with an energy of 2.9 eV (~425 nm) corresponds to a nanoparticle with a diameter of 3.0 nm. This indicates that single absorption light energy corresponds to a single nanoparticle diameter. If one utilizes such the relation, a novel size-regulated preparation of CdS nanoparticles is expected.

An outline of a size-controlled nanoparticle preparation method by using single wavelength light is described in Figure 2.2. Usually, CdS is slowly synthesized by a reaction of a cadmium salt and a sulfur source in solution. Nanoparticles growth can be controlled by photoirradiating single wavelength light during the reaction. Namely, when the particle grows to the size corresponding to the incident light wavelength (Figure 2.1), the particle first absorbs incident light and then, an electron-hole pair is photogenerated in the particle. If a polymerizable monomer is involved in the solution, the photogenerated electron or hole is transferred to the monomer, and radical (ionic) polymerization will be expected to occur in the vicinity of the grown particle to prevent further particle growth. It is preferable that a monomer(s) is soluble, and the generated polymers are insoluble in the solvent used. Advantages of the photoinduced synthesis of semiconductor nanoparticles are as follows: (i) precise size control is expected, (ii) various vinyl monomers can be selected, and (iii) extraction of CdS nanoparticles/polymer composites will be possible. These attempts are not heretofore explored, and are significant for developing new nanocluster/organic hybrids.

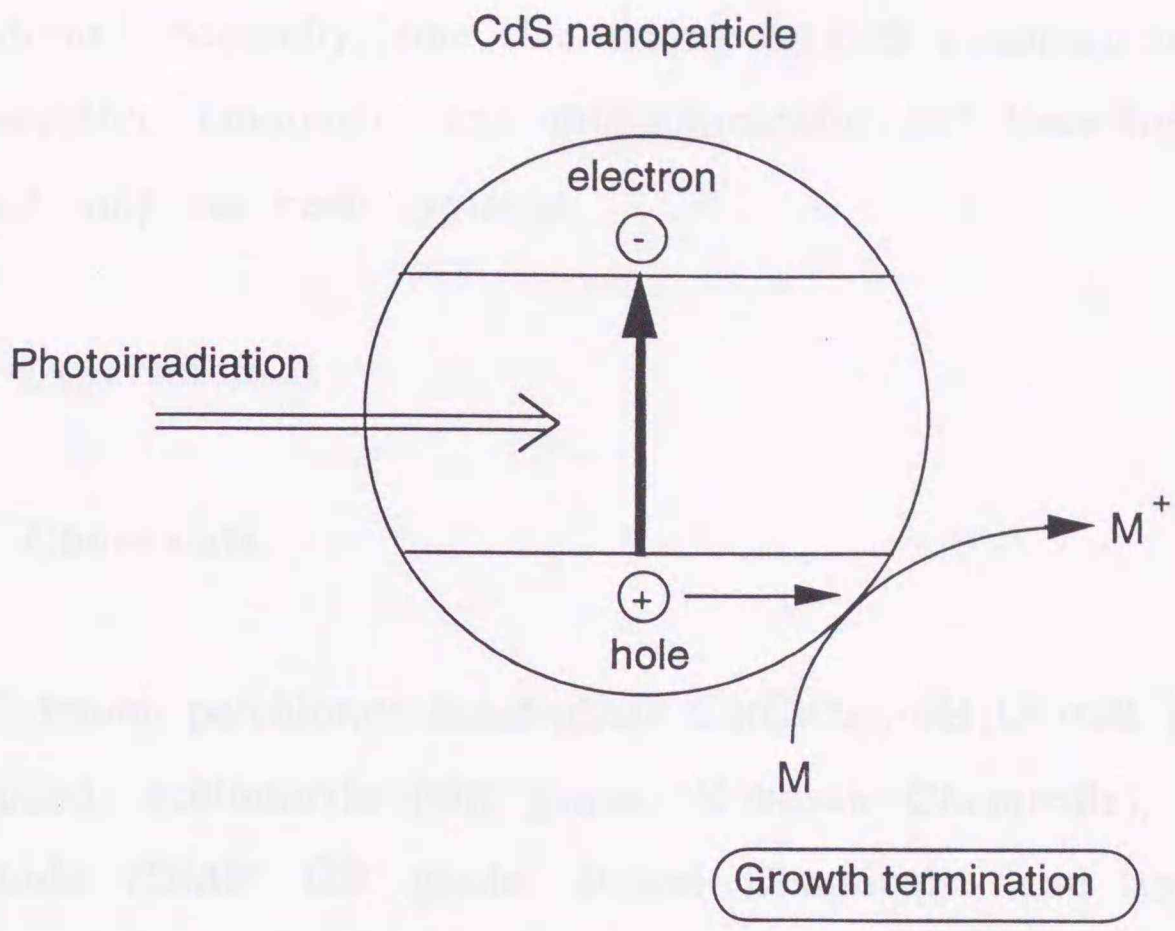

Figure 2.2. Schematic illustration of size regulation of semiconductor nanoparticles under monochromatic light irradiation.

In this chapter, firstly, a novel preparation method for size-controlled CdS nanoparticles is described. Styrene is used for a representative monomer. Under irradiation of 457.9 nm laser light from an Ar^+ laser, the narrowest size distribution of CdS was achieved. The third-order optical nonlinearities of laser-regulated CdS nanoparticles embedded in acrylonitrile-styrene (AS) copolymer films are also discussed. Optically transparent AS copolymer was preferable for loading CdS nanoparticles. It is noteworthy that the lowest excitonic state of CdS has much larger $\chi^{(3)}$ value owing to the larger longitudinal relaxation time than higher energy states. Thus, a decrease in the overlap between the lowest and higher excited states with decreasing the particle size distribution would expect to bring about the enhancement of $\chi^{(3)}$ per unit absorption

coefficient.[6] Secondly, fine size tuning of CdS nanoparticles by selecting polymerizable monomers and monochromatic Ar^+ laser light (from 457.9 to 514.5 nm) has been explored.

2.2 Experimental

2.2.1 Chemicals.

Cadmium perchlorate hexahydrate $Cd(ClO_4)_2 \cdot 6H_2O$ (GR grade, Soekawa Chemicals), acetonitrile (GR grade, Kokusan Chemicals), N,N-dimethyl-formamide (DMF: GR grade, Junsei Chemicals) and an acrylonitrile-styrene copolymer (AS copolymer: [acrylonitrile]/[styrene] = 25/75, Mitsui Toatsu Chemicals, Inc.) were used as received. A styrene monomer (St: Junsei Chemicals) was washed with an aqueous sodium hydroxide solution (5%), followed by distillation under reduced pressure. 1-Vinylimidazole (1-VIm: Tokyo Kasei) was purified by distillation under reduced pressure.

2.2.2 Preparation of CdS Nanoparticles.

Two different methods were employed to prepare CdS nanoparticles. Procedures are as follows (Figure 2.3).

1. CdS nanoparticles prepared with a St monomer.

The main purpose of the experiments is to demonstrate inhibition of particle growth larger than the CdS size corresponding to the irradiation wavelength, and simultaneous incorporation of the particles in polymer films. To study this, the following samples were prepared.

After bubbling an N_2 gas for about 10 min, a gas mixture of H_2S/He (0.02 vol% H_2S, flow rate of 270 mL/min) was bubbled into an acetonitrile solution (45 mL) of $Cd(ClO_4)_2$ (2.0×10^{-3} M) and styrene (4.0×10^{-2}M) under stirring in a quartz cuvette (35 x 35 x 50 mm, optical path length: 50 mm) equipped with a gas inlet and an outlet. During the reaction, the solution was irradiated with an Ar^+ laser beam (Coherent, Innova 70) which was expanded through a concave lens and reflected with a normal mirror on the rear side of the cuvette to facilitate photoexcitation. A single Ar^+ line selected was 488 or 457.9 nm. The laser intensity at each wavelength was set at 0.02 W/cm^2, and monitored with a power meter.

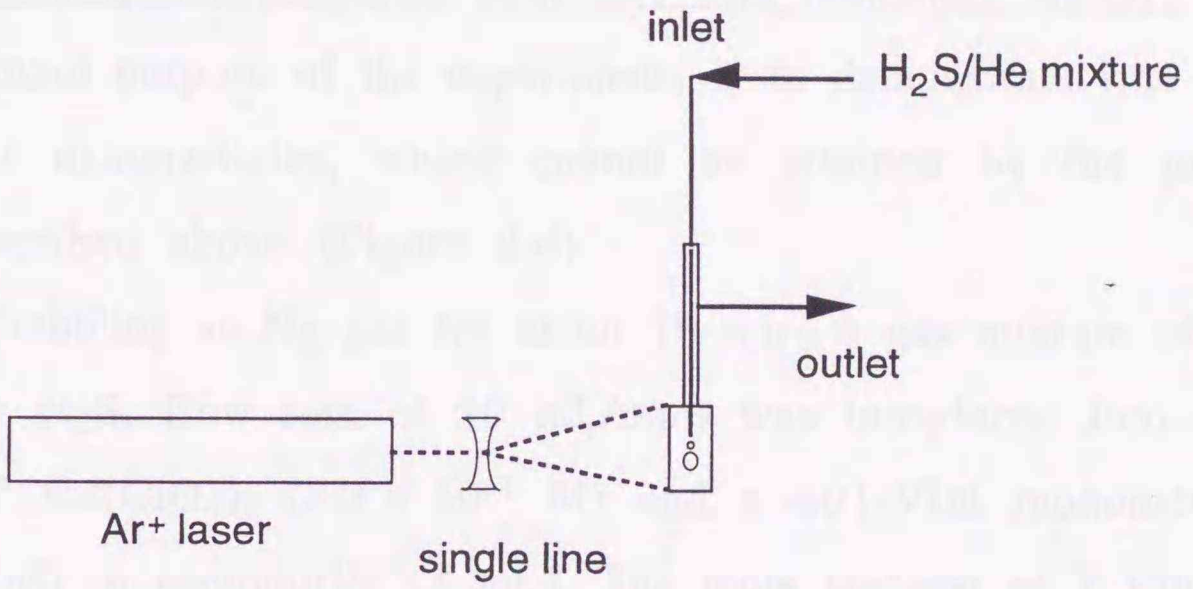

Figure 2.3. Experimental setup for preparation of size-controlled CdS nanoparticles under monochromatic Ar^+ laser irradiation.

After preparing the colloidal solution, the solution was condensed to ca. 4 mL at reduced pressure. The AS copolymer (0.2 g) dissolved in DMF (3 mL) was added to the condensed solution, which was then further dried on a glass plate at reduced pressure. This procedure did not make the CdS particle size larger. The procedures gave AS copolymer-CdS

nanoparticle hybrid films with 160 μm thickness. The sample preparation procedures are summarized in Figure 2.4.

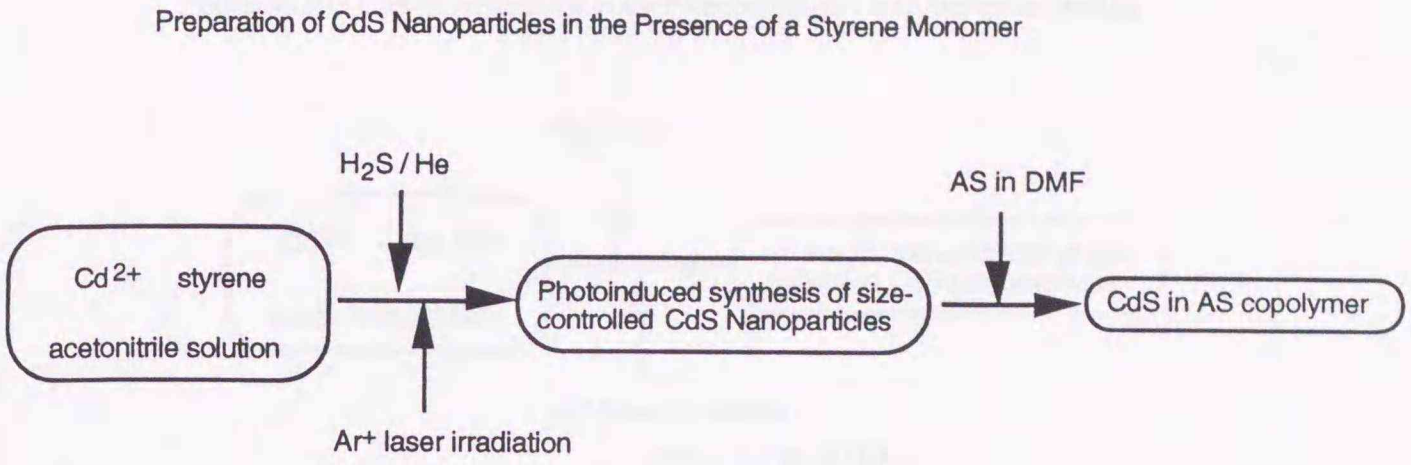

Figure 2.4. Sample preparation procedures for CdS nanoparticles in the presence of St under monochromatic Ar^+ laser irradiation.

2. CdS nanoparticles prepared with St/1-VIm monomer mixture.

The main purpose of the experiments is to demonstrate fine tuning of the size of nanoparticles, which cannot be attained by the preparation method described above (Figure 2.4).

After bubbling an N_2 gas for about 10 min, a gas mixture of H_2S/He (0.02 vol% H_2S, flow rate of 10 mL/min) was introduced into a stirring solution of $Cd(ClO_4)_2$ (2.0×10^{-3} M) and a St/1-VIm monomer mixture (4.0×10^{-2} M) in acetonitrile (3 mL). The mole fraction of 1-VIm was set at 4% in the monomer ratio; [1-VIm]/([1-VIm] + [St]) = 0.04. When only 1-VIm was used, the concentration was adjusted to 1.6×10^{-3} M. A quartz cuvette (optical path length: 10 mm) was used as a reaction vessel. The reaction between He-diluted H_2S and Cd^{2+} under irradiation of an Ar^+ laser was performed for 40 min. Each sample solution was purged by an N_2 gas stream with a rate of 10 mL/min for 10 min after the reaction. A monochromatic line from an Ar^+ laser was chosen by a wavelength selector prism (from 514.5 to 457.9 nm). The beam power

was about 0.02 W/cm^2 at any wavelength selected. The sample preparation procedures are summarized in Figure 2.5.

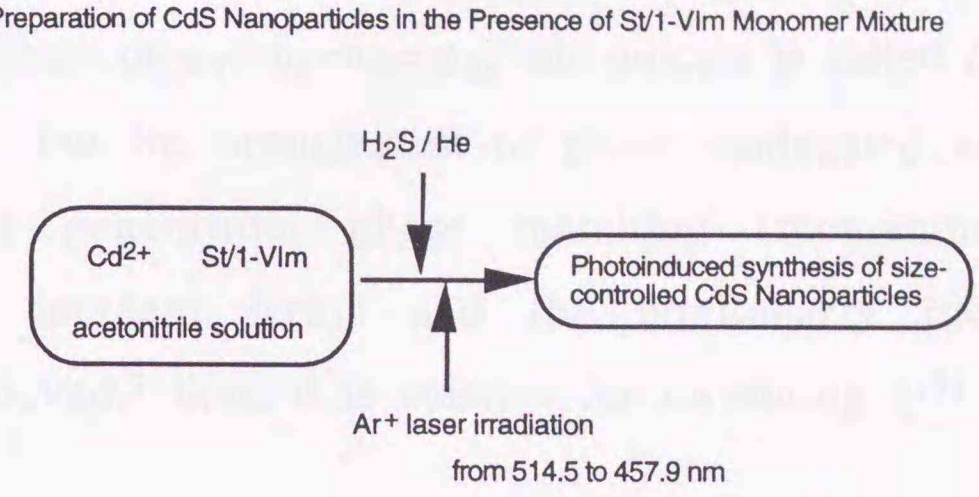

Figure 2.5. Sample preparation procedures for fine tuning of the size of CdS nanoparticles under Ar^+ laser irradiation.

2.2.3 Measurements of Linear Optical Properties.

UV-vis absorption spectra were measured with a Shimadzu UV-2200 spectrophotometer. Emission spectra were recorded on a Shimadzu RF-5000 fluorimeter with a Hamamatsu R-928 photomultiplier. A transmission electron microscope (Hitachi H-7000 or JEOL JEM-100CX) was used to determine the particle diameters of CdS nanoparticles. Particle size distribution histograms were obtained by measuring the diameter of the particles in the photographs.

2.2.4 Measurements of Third-Order Optical Nonlinearity.[7]

One of the optical nonlinearities of the samples was evaluated by a four wave mixing technique. Figure 2.6 shows a Degenerate Four Wave Mixing (DFWM) experimental setup for measuring the third-order optical nonlinear susceptibility $\chi^{(3)}$.

The four wave mixing process is one of the third-order nonlinear processes, which shows a sum or differential frequency generation (ω_4) by irradiation of three incident light with angular frequencies of ω_1, ω_2, and ω_3. In the case of $\omega_1=\omega_2=\omega_3=\omega_4$, this process is called *Degenerate* Four Wave Mixing. For the arrangement of phase conjugated wave (one of the output wave) generation, phase matching (momentum conservation between the incident lights and the nonlinearly induced light) is naturally achieved,[7] thus, it is suitable for measuring $\chi^{(3)}$ values.

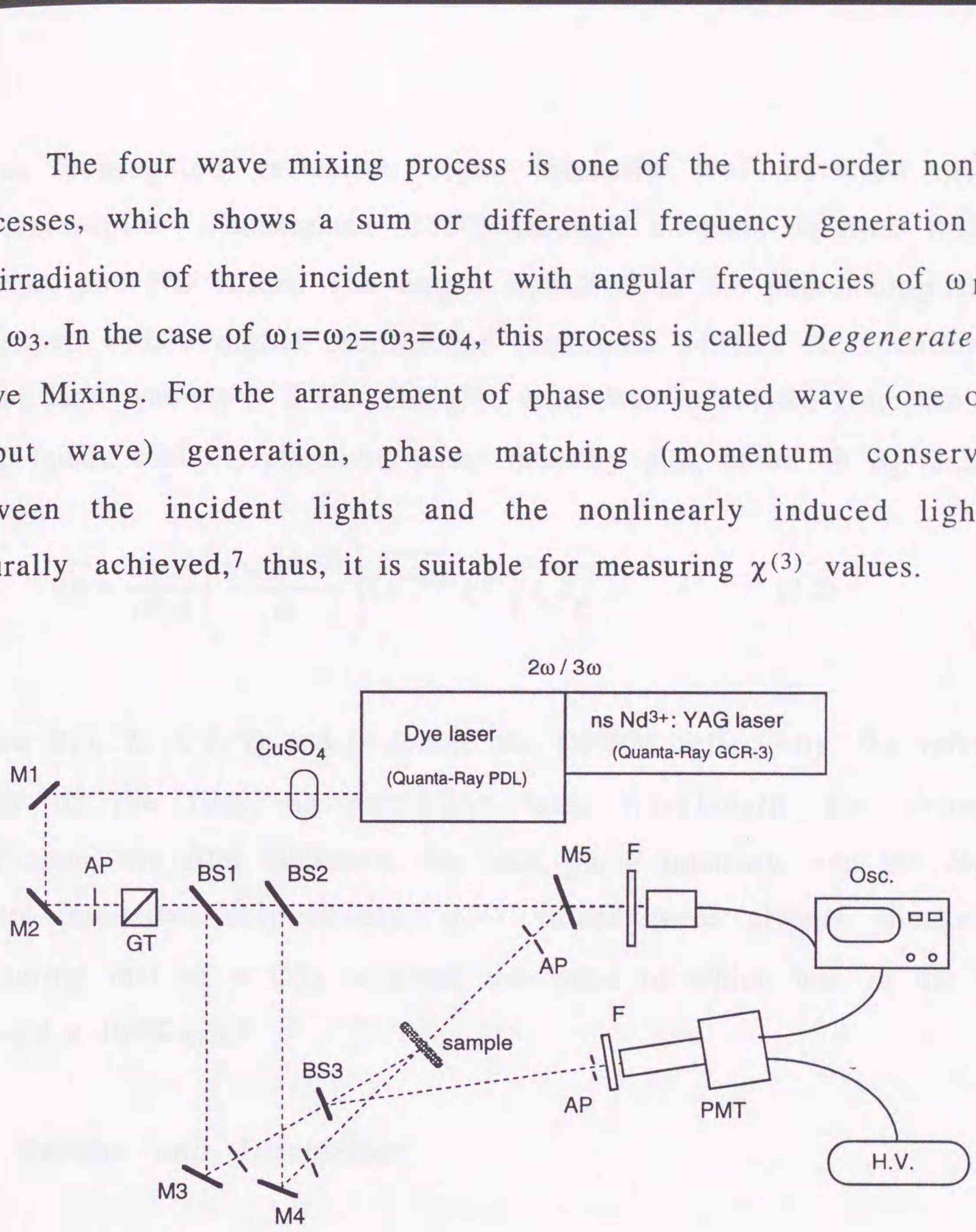

Figure 2.6. Experimental setup for measuring $\chi^{(3)}$ by a Degenerate Four Wave Mixing (DFWM) with a phase conjugation mode.

Excitation laser pulses at 430 ~ 480 nm were generated with a dye laser (Quanta Ray PDL), pumped by a third harmonics (355 nm) of ns output pulses from a Nd^{3+}:YAG laser (Quanta-Ray GCR-3). Three excitation pulses were introduced simultaneously to the sample, and the

phase conjugated reflection light intensity was detected with a photomultiplier (Hamamatsu R329) through a beam splitter BS3, an aperture and ND filters. The output signals from the photomultiplier was processed with a digital oscilloscope (Tektronix 2431L). A repetition rate of the laser was set to 2 Hz. The $\chi^{(3)}$ value was calculated from the slope of a square root of reflectivity-pump intensity plot, based on eq. 2.2,[8]

$$\sqrt{R} = \frac{64\pi^3}{n^2 c\lambda}\left(\frac{1-e^{-\alpha L}}{\alpha}\right)\sqrt{e^{-\alpha L}}\chi^{(3)}\sqrt{I_b I_f}\,, \qquad (2.2)$$

where R, n, λ, α, L, I_b and I_f denote the DFWM reflectivity, the refractive index of the film, an excitation laser wavelength, the absorption coefficient, the film thickness, the back pump intensity, and the forward pump intensity, respectively. $\chi^{(3)}$ values were always checked by measuring that of a CS_2 solution, the value of which was in the range $1.6\sim1.8 \times 10^{-12}$ esu.[9]

2.3 Results and Discussion

2.3.1 CdS Nanoparticles Prepared in the presence of a St monomer

1. Absorption Spectra of CdS and Nanoparticle Size Distribution.

When CdS nanoparticles were prepared under irradiation with a 488.0 or 457.9 nm laser line and loaded in the AS copolymer, the absorption onset wavelength of CdS was blue-shifted from 510 nm (unirradiated sample) to 480-460 nm, as shown in Figure 2.7. An excitonic shoulder appeared at around 430 nm under irradiation of 488.0

or 457.9 nm light, indicating that most probable particle diameters were similar for both samples and independent of the irradiation wavelength. However, the shoulder became more pronounced for the sample irradiated by the shorter wavelength.

High-resolution TEM (transmission electron microscopy) was used to obtain high-magnification photomicrographs and electron beam diffractograms. Figure 2.8 shows a TEM image of a the sample prepared by 488.0 nm laser irradiation. The image shows coagulated particles consisting of ~3 nm CdS in diameter. Lattice images are also clearly observed. The electron diffraction patterns agreed better with a hexagonal crystal structure rather than a cubic structure.

Figure 2.9 shows size distributions of the CdS nanoparticles prepared with and without photoirradiation. The data are relevant to the samples shown in Figure 2.7. With irradiating shorter wavelength light (457.9 nm), the size distribution becomes narrower and the CdS diameter is reduced compared to the sample irradiated at 488 nm. Thus, photoirradiation is concluded to be very useful and advantageous for nanoparticle size regulation.

Factors affecting the size regulation and the absorption spectra of CdS nanoparticles were studied in detail.

The irradiation light intensity is one of the important factors for sharpening and shifting the absorption onset. In the usual experiments, the laser was operated at a maximum output power at 457.9 nm. However, when the light intensity was set weaker, the onset moved slightly to a longer wavelength and the excitonic shoulder became discernible.

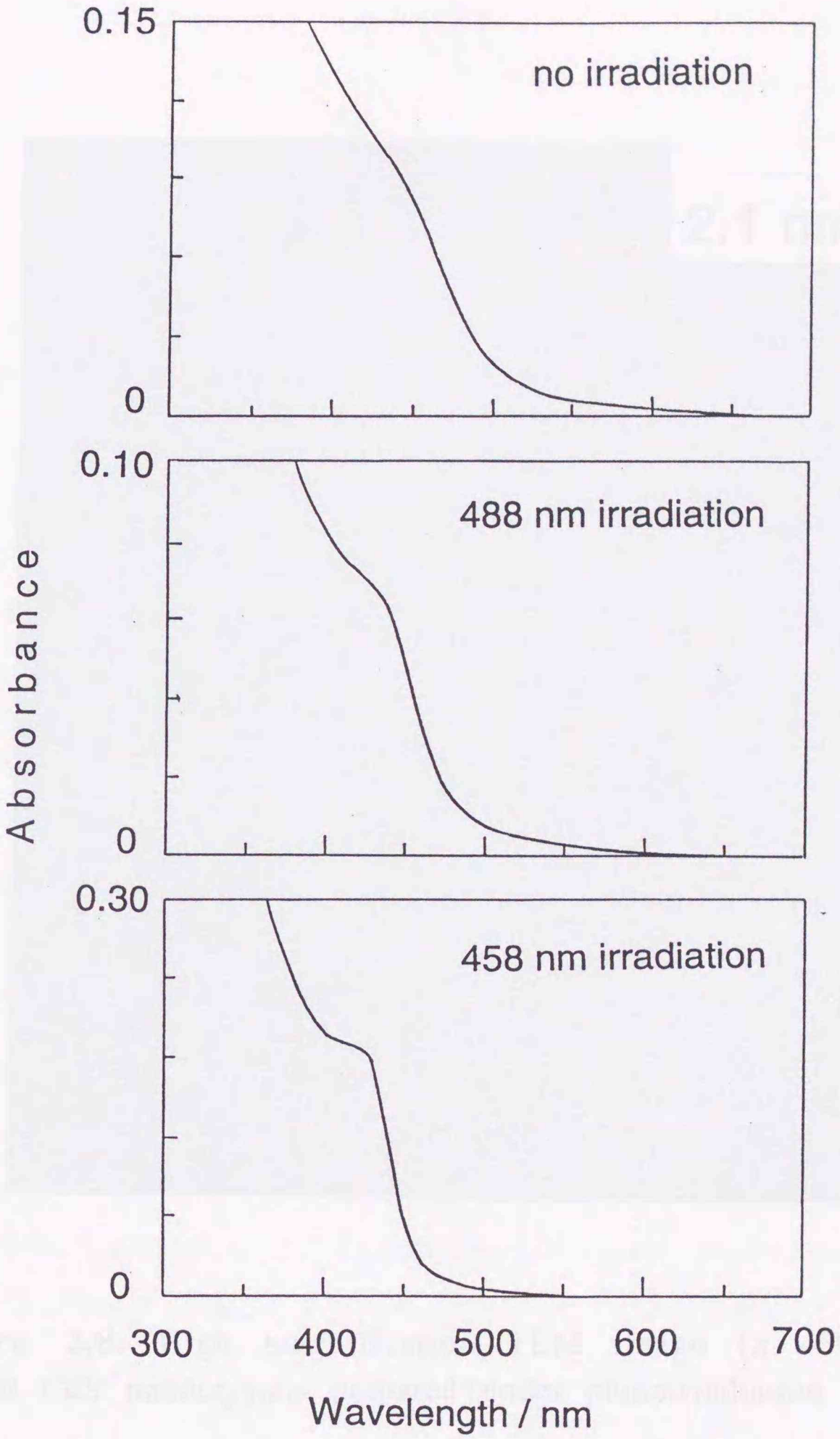

Figure 2.7. Absorption spectra of CdS nanoparticles in AS copolymer films (~0.2 vol%). Upper: without irradiation, middle: irradiation of 488 nm light, lower: irradiation of 457.9 nm light.

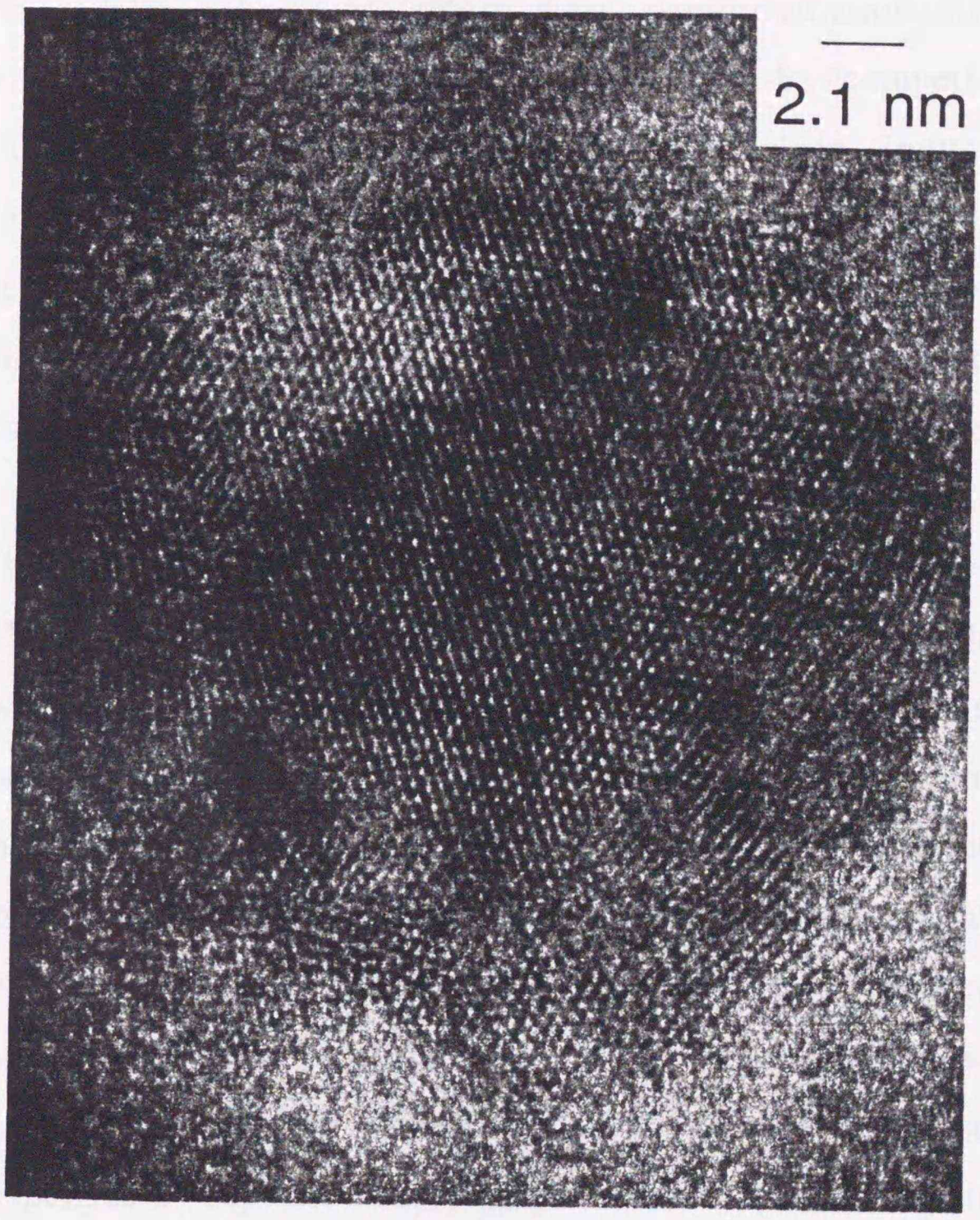

Figure 2.8. High magnification TEM image (x 4800000) of a coagulated CdS nanocrystals prepared under photoirradiation of 488 nm.

Photobleaching (photo-dissolution), giving rise to smaller particles, is not the reason. When a previously-prepared CdS colloidal solution was irradiated in the absence of H_2S and O_2 for a few tens of min, almost no

change in optical absorbance was observed. Thus, photo-dissolution of CdS does not occur without oxygen.

When the concentration of St was decreased to one order of magnitude (~10^{-4} M), an extremely weak photoirradiation effect on the CdS size was observed. This would be explained by competition of the CdS particle growth with the photo-polymerization induced growth termination. Namely, the photoirradiation effect is expected to become more effective, when the CdS formation rate (V_f: linear velocity of the particle diameter) is slow enough so that the growth termination due to the photoreaction takes place, before the growing particle becomes larger than the size corresponding to the irradiation light wavelength. In fact, a decrease in the H_2S concentration in the H_2S/He gas mixture from 0.25 to 0.02 vol% resulted in a shift of the absorption onset wavelength to a shorter wavelength even under the same irradiation conditions.

Termination of the particle growth takes place by a photocatalytic reaction(s) between the excited CdS and St through a photogenerated electron-hole pair, electron transfer from CdS to the substrate (St), or interactions between the particle surface and the activated St. The photoinduced hole transfer from CdS to a St monomer is the most probable candidate for the photocatalytic reaction. The presence of St was indispensable for the observation of the photoirradiation effect. Photocatalytic activation of St and the successive polymerization in the vicinity of the surface of nanoparticles would create a polymer (oligomer) adhering on the particles to prevent the further particle growth.

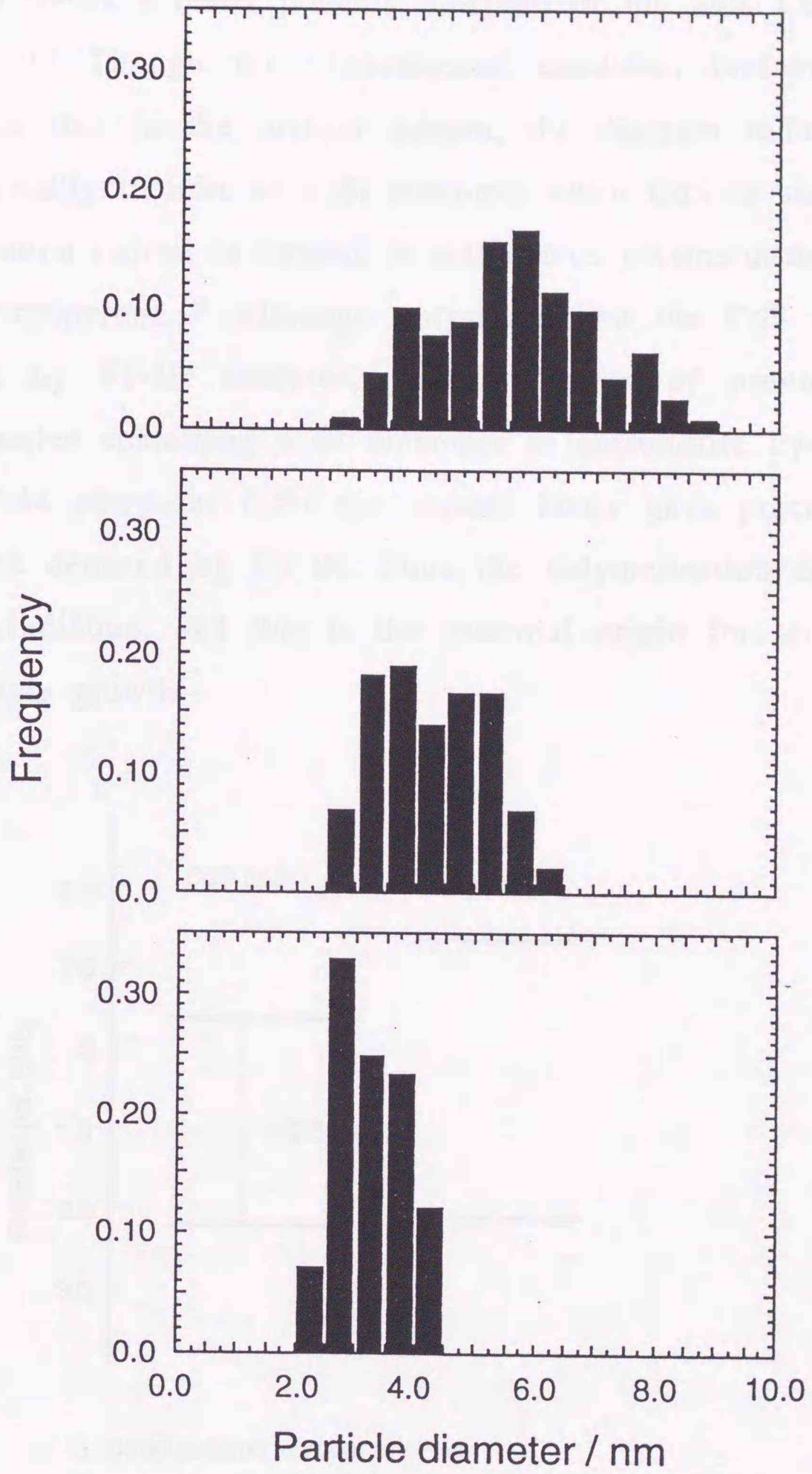

Figure 2.9. Size distributions of CdS nanoparticles prepared with and without irradiation. Upper: without irradiation, middle: irradiation of 488 nm light, lower: irradiation of 457.9 nm light.

Figure 2.10 shows a redox potential diagram of the bulk CdS and a St monomer.[10-12] Though the experimental condition (solvent used) is different from that in the present system, the diagram indicates that a hole would readily transfer to a St monomer when CdS is size-quantized. When a St cation radical is formed, it will induce polymerization as in the case of 1-vinylpyrene.[13] Although polystyrene on the CdS surface was not detected by FT-IR analyses, photoirradiation of previously-grown CdS nanoparticles containing a St monomer in acetonitrile by a Xe lamp through a Y-44 sharp-cut filter for several hours gave precipitations of polystyrene as detected by FT-IR. Thus the polymerization of St occurs under photoirradiation, and this is the essential origin for termination of the CdS particle growth.

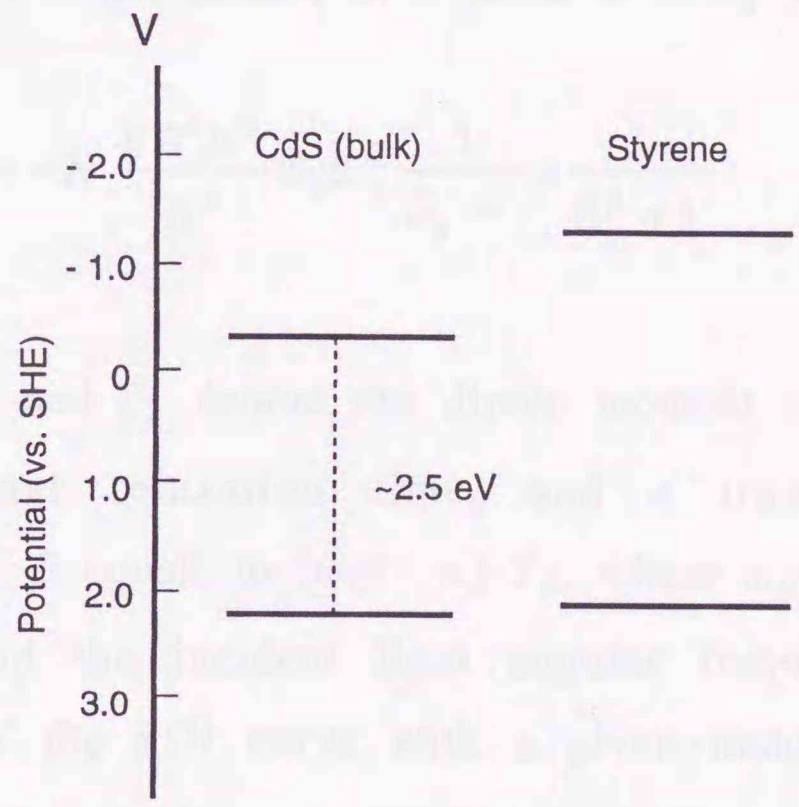

Figure 2.10. Redox potentials of bulk CdS and a styrene monomer.

2. Nonlinear Optical Properties.

Figure 2.11 shows experimental results of $\chi^{(3)}$ for the CdS nanoparticles embedded in the AS copolymer prepared under 457.9 nm irradiation together with the simulated values. The $\chi^{(3)}$ values were determined at the excitation wavelengths between 490 and 430 nm (stepped by 10 nm) in order to study the effect of the excitonic level of CdS on the nonlinearity. With shortening the excitation wavelength from 490 nm to the excitonic peak (430 nm) of the CdS sample, the $\chi^{(3)}$ value increased. By excitation of the excitonic shoulder at 430 nm, $\chi^{(3)}$ of ~5 x 10^{-9} esu was obtained. A calculation of $\chi^{(3)}$, arising from the exciton state (1S-1S transition) of CdS nanoparticles, was performed to compare with the experimental observations. According to Takagahara,[14] $\chi_a^{(3)}$ for particles with single radius, a, is given in as eq. 2.3,

$$\chi_a^{(3)} = -N \frac{8\pi^3\mu^4}{h^3} T_1 T_2^2 \frac{1}{\delta_a - i} \cdot \frac{1}{\delta_a^2 + 1} \qquad (2.3)$$

where μ, T_1, and T_2 denote the dipole moment of the excitonic transition, a longitudinal relaxation time, and a transverse relaxation time, respectively. δ equals to $(\omega_0{}^a - \omega)\cdot T_2$, where $\omega_0{}^a$ and ω are the excitonic transition and the incident light angular frequencies, respectively. For simulation of the $\chi^{(3)}$ curve with a given nanoparticle size distribution, the measured particle size distribution (Figure 2.9, bottom histogram) was assumed to be log-normal:

$$f(a) = \frac{1}{\sqrt{2\pi}\sigma} \exp\left[-\frac{\ln^2\left(a/a_0\right)}{2\sigma^2} \right] \qquad (2.4)$$

where σ and a_0 are a standard deviation and the center radius of the distribution, respectively. Figure 2.12 shows the simulated log-normal distribution with $\sigma = 0.2$ and $a_0 = 1.5$ nm. This function reproduced fairly well the observed histogram. Thus $\chi^{(3)}$ is given as in eq. 2.5,

$$\chi^{(3)} = \int \chi_a^{(3)} \cdot f(a)\, d\ln a \qquad (2.5)$$

Here resonant DFWM measurements can provide the absolute $\chi^{(3)}$ values. The solid curve in Figure 2.11 shows the result of the simulation. As the excitation wavelength becomes shorter, the $\chi^{(3)}$ value increases up to 430 nm. However, the value is predicted to decrease at the wavelength shorter than 430 nm, indicating the nonlinearity is attributed to the lowest energy transition. There are some discrepancies between the observed data and the simulated curve. If the size distribution becomes narrower than that assumed, some discrepancies will still remain. This would be owing to neglecting trapped carriers or/and a contribution of other resonant states.[3] To the best of our knowledge, however, this is the first demonstration for the wavelength dependence of $\chi^{(3)}$ on size-regulated CdS nanoparticles.

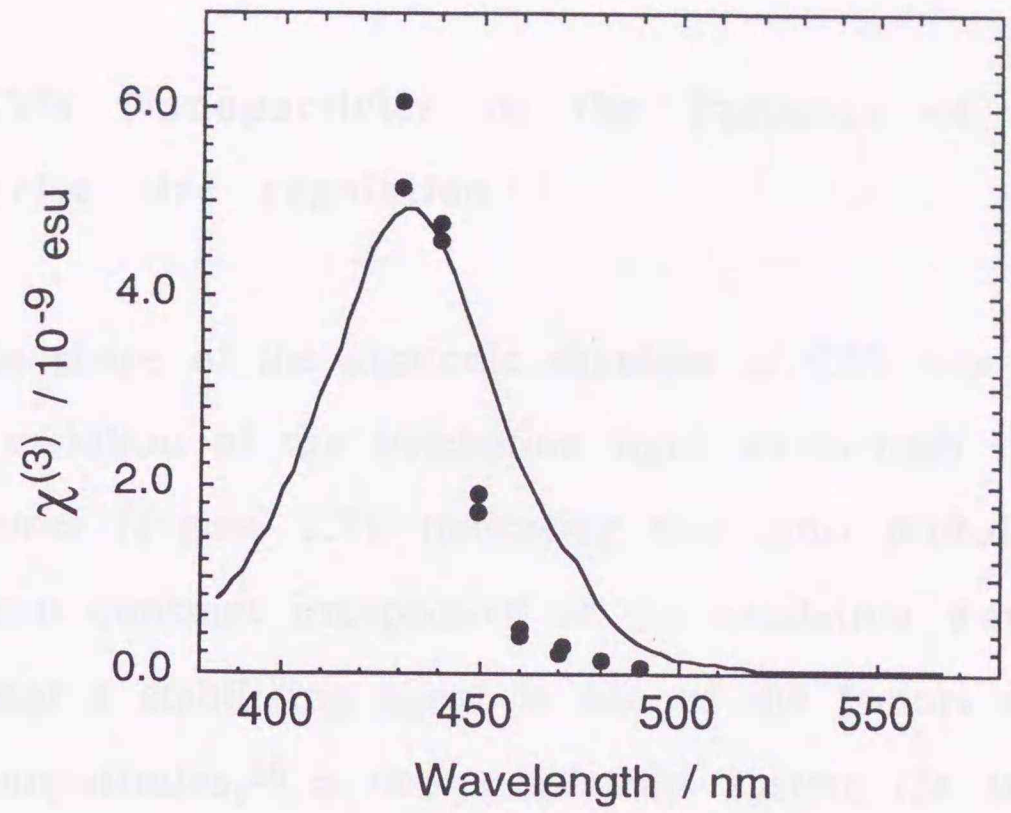

Figure 2.11. Wavelength dependence of the measured and the simulated $\chi^{(3)}$.

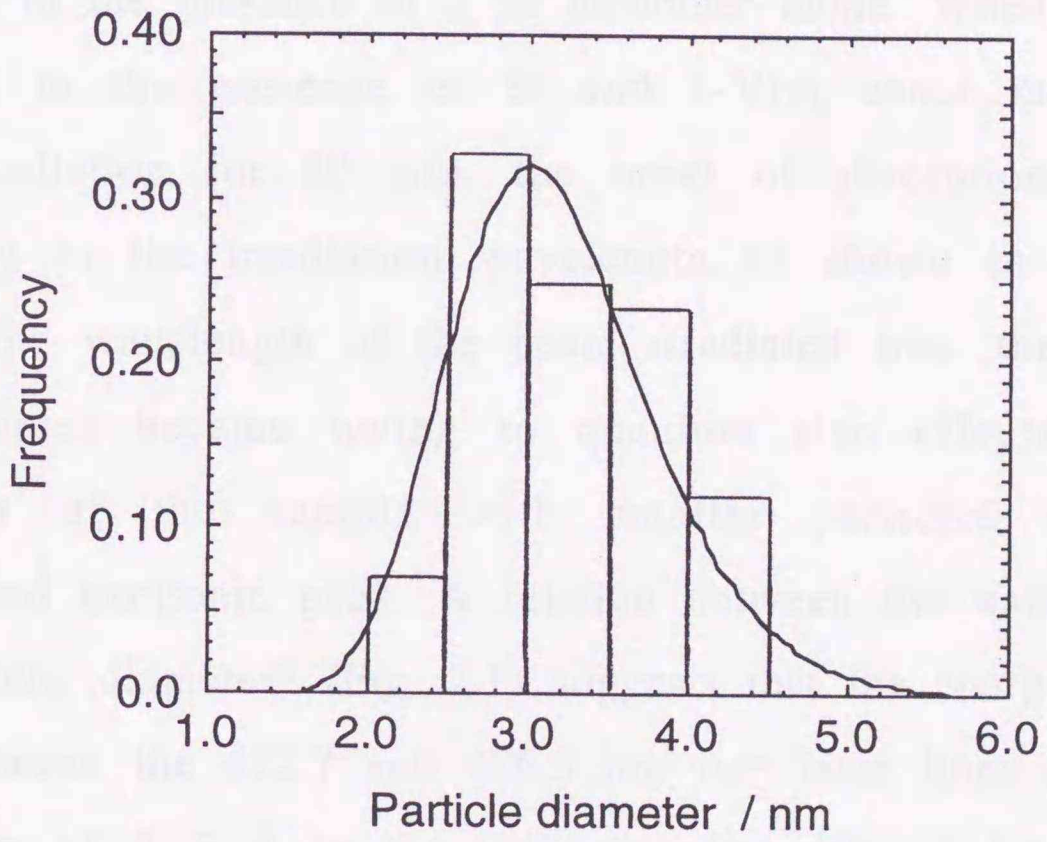

Figure 2.12. Observed particle diameter distribution and the fitted distribution curve by a log-normal function. (σ = 0.2, a_0 = 1.5 nm)

2.3.2 CdS Nanoparticles in the Presence of St/1-VIm mixture for precise size regulation.[15]

The shape of the excitonic shoulder of CdS was hardly changed even for the variation of the irradiation light wavelength in the presence of a St monomer (Figure 2.7), indicating that most probable particle diameter was almost constant irrespective of the excitation wavelength. Since it is known that a stabilizing agent is one of the factors affecting the size of CdS nanoparticles,[16] a two-components system (St and 1-VIm) has been examined for a voluntary size control of CdS nanoparticles.

A broad and red-shifted spectrum was observed for the CdS colloids prepared in the presence of both St and 1-VIm without photoirradiation, whose spectral features were similar to those observed for the sample prepared in the presence of a St monomer alone. When the colloids were prepared in the presence of St and 1-VIm under monochromatic Ar^+ laser irradiation for 40 min, the onset of absorption was blue-shifted according to the irradiation wavelength as shown in Figure 2.13. The shorter the wavelength of the beam irradiated was, the smaller the CdS nanoparticles became owing to quantum size effects. The absorption spectrum of the sample with smaller particles exhibits a more pronounced excitonic peak. A relation between the band gap energy and the particle diameter[6] (Fig. 2.1) suggests that the energy difference of 21 meV between the 472.7 and 476.5 nm Ar^+ laser lines corresponds to the difference of 2~3 Å in the CdS diameter. This value would nominally correspond to one atomic layer. The effect of a small energy difference of irradiation light was reflected on the absorption spectrum of CdS.

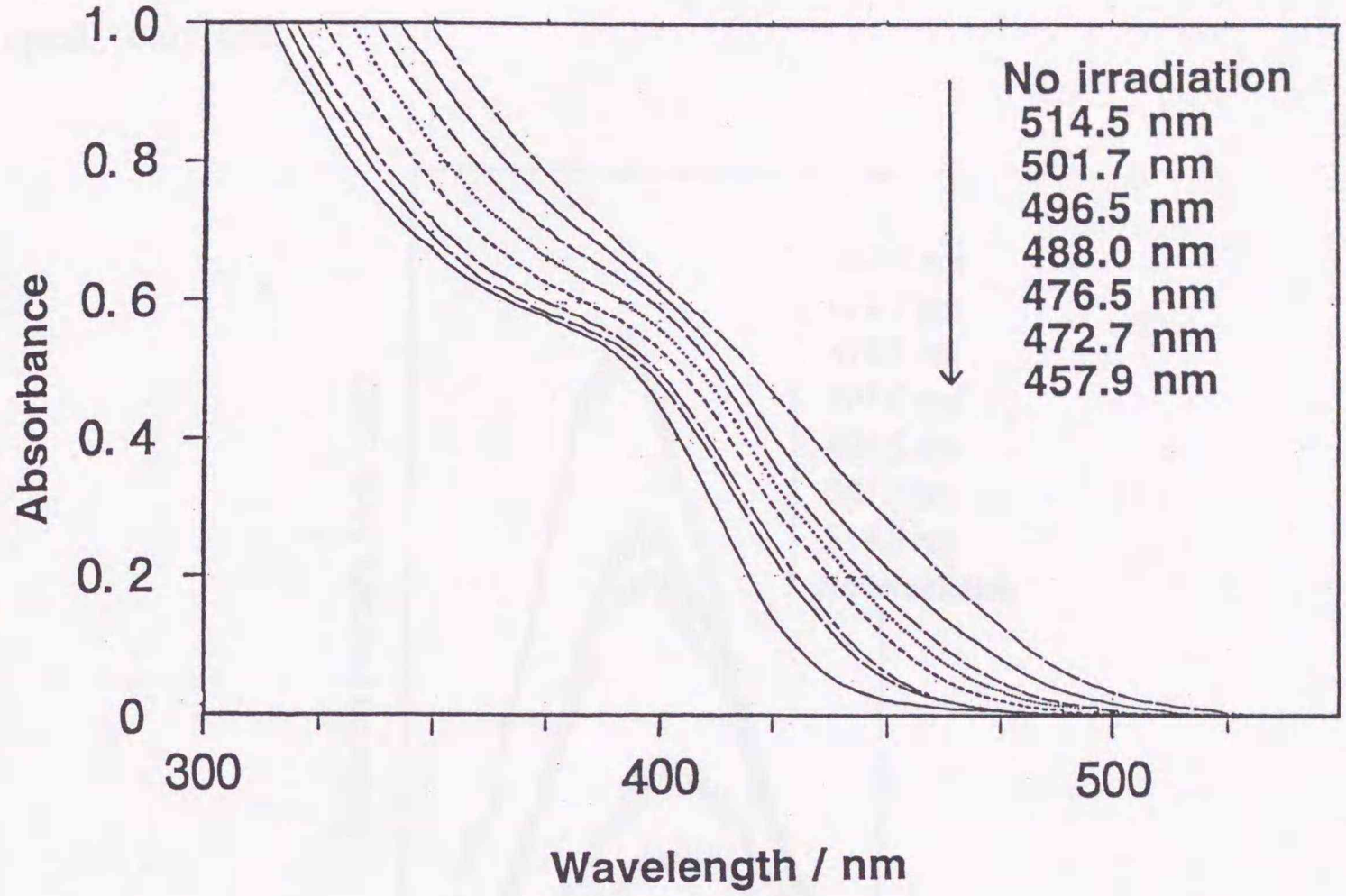

Figure 2.13. Absorption spectra of CdS prepared under irradiating monochromatic Ar+ laser beam at various wavelengths in the presence of styrene and 1-vinylimidazole. The spectrum of CdS without irradiation is also shown.

The emission spectra of the CdS nanoparticles prepared photocatalytically are shown in Figure 2.14. All the spectra showed Stokes-shifts as compared with the absorption spectra, and no edge emission was observed. The spectra indicated that smaller CdS nanoparticles showed shorter wavelength emission with a higher intensity, according to the irradiation wavelength of a monochromatic Ar^+ laser beam. The red emission would originate from recombination of surface trapped carriers.[17] This is a quantum size effect of the emission of the trapped state. Namely, the emitting energy and the recombination

probability of trapped carriers became higher with a decrease in the particle size, probably due to a decrease of the distance between the trapped carriers.

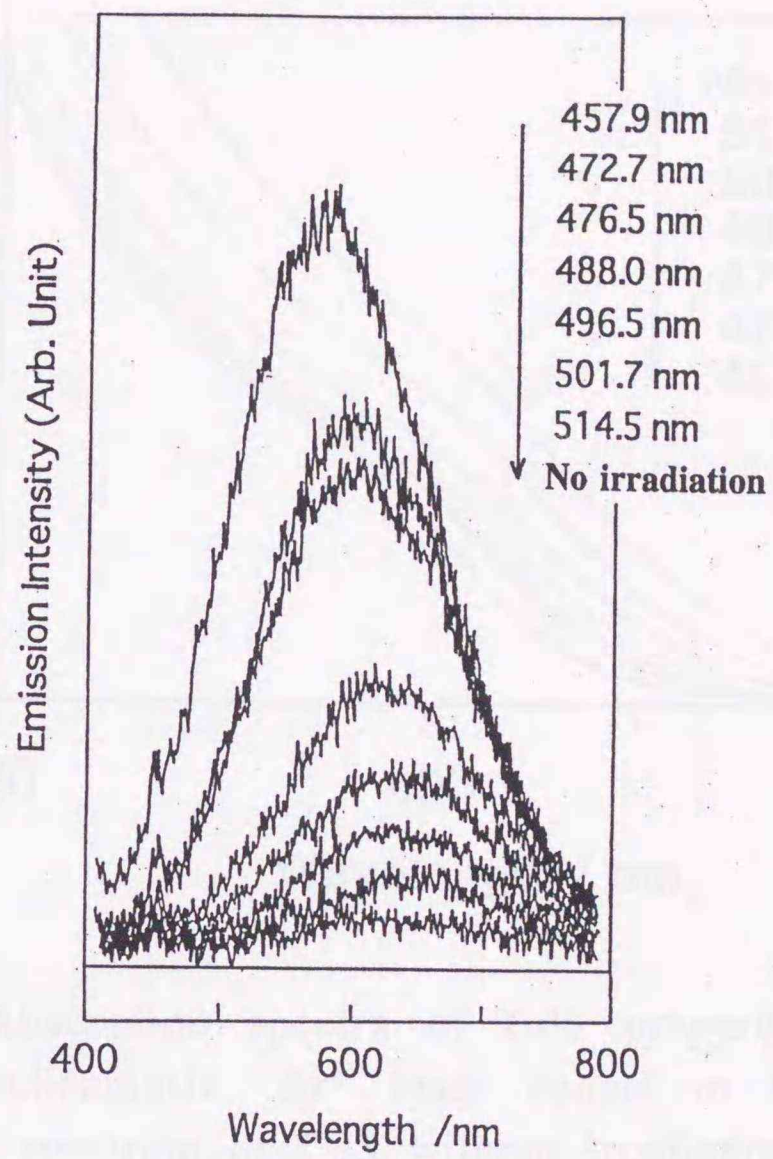

Figure 2.14. Emission spectra of CdS with and without irradiating various wavelengths of an Ar^+ laser.

When styrene was used as a monomer stabilizer under photoirradiation of an Ar^+ laser beam at 457.9 nm as size regulation light, the absorption spectrum of CdS was considerably red-shifted compared to that of the sample prepared with both St and 1-VIm. Although the absorption tail of CdS was lessened by using St alone, a successive spectral shift corresponding to the change in the irradiation wavelength was scarcely observed. 1-VIm would play a role in

diminishing the particle size and also in inducing the efficient photocatalytic reaction associated with the size regulation.

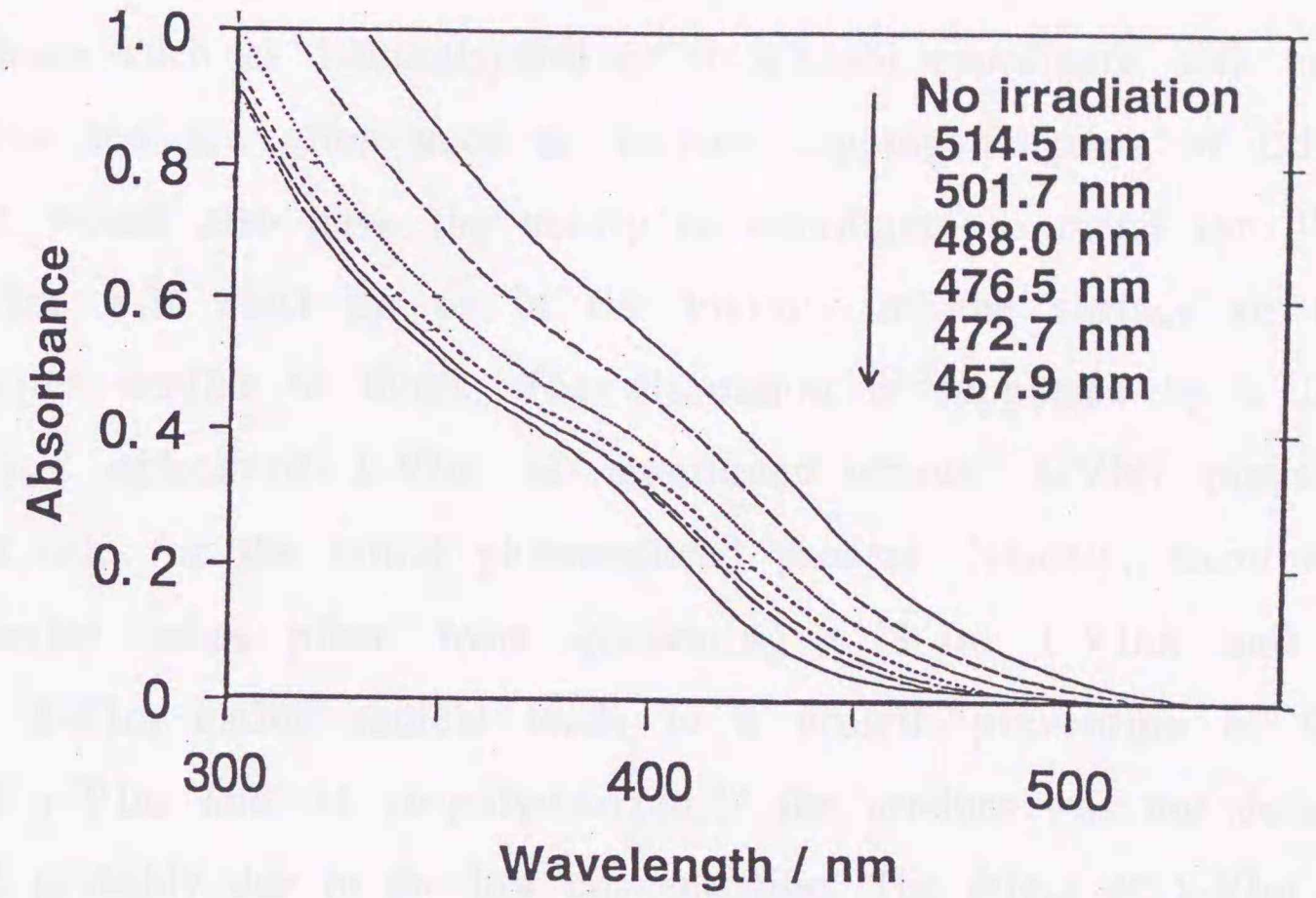

Figure 2.15. Absorption spectra of CdS prepared under irradiation of various monochromatic Ar^+ laser beams in the presence of 1-vinylimidazole. The spectrum of CdS without irradiation is also shown.

Figure 2.15 shows a set of the absorption spectra of the CdS samples synthesized under photoirradiation in the presence of 1-VIm alone. A remarkable photoirradiation effect was observed; the spectrum depended upon the wavelength of irradiation light. As compared with the results in Figure 2.13, each spectrum in Figure 2.15 is broader. Thus, St is necessary to exhibit a pronounced excitonic shoulder or peak. When 1-VIm (1×10^{-2} M; high concentration which was used in the experiments of section 2.3.1) was used for preparation of CdS nanoparticles without photoirradiation, large blue-shifted spectrum was

observed and the absorption onset moved shorter than 457.9 nm. Thus the preparation of CdS under photoirradiation with the same concentration of 1-VIm was not applied, since large stabilization by 1-VIm for decreasing particle sizes of CdS occurred.

Thiols such as 1-thioglycerol or thiophenol coordinate with heavy metal ions and are often used as surface capping reagents of CdS.[18] Imidazole would also have the ability to coordinate to metal ions,[19] so that 1-VIm will exist on or in the vicinity of the surface of CdS nanoparticles similar to thiols. The discussion is supported by a large stabilization effect of 1-VIm as mentioned above. 1-VIm plays an important role for the initial photoinduced process. Namely, electron or hole transfer takes place from generating CdS to 1-VIm, and the resulting 1-VIm cation radical leads to a growth prevention of CdS. Although 1-VIm and St co-polymerized,[20] the product was not detected by FT-IR probably due to the low concentration. The effect of 1-VIm was not enough to make the particle size fairly uniform as demonstrated by the absorption spectra in Figure 2.15. When St co-existed with 1-VIm, the spectral shoulders of CdS prepared under photoirradiation were better-resolved and larger size regions of the particle distribution lessened. Since absorbance of CdS prepared with 1-VIm under short-wavelength irradiation became smaller than that under long-wavelength irradiation, growth prevention of CdS would be concerned with not only the rate of St activation leading to surface attaching of the polymer, but also photo-dissolution of CdS nanoparticles without oxygen.

2.4 Summary

(1) Size-regulated CdS nanoparticles were prepared by introducing a H_2S/He gas mixture into an acetonitrile solution of Cd^{2+} and styrene, while the solution was irradiated with a monochromatic Ar^+ laser beam (488.0 and 457.9 nm). The UV-vis absorption onset wavelength of CdS prepared under photoirradiation was blue-shifted and showed a pronounced excitonic peak in comparison with those for the sample without photoirradiation. Characterizations of the particle size distribution were performed by TEM, and the narrower size distribution was obtained under irradiation at 457.9 nm. Particle growth prevention was related to photoinduced hole transfer from generating CdS to a styrene monomer and subsequent polymerization in the vicinity of the CdS particle. Thus, the size regulation based on a new principle using photocatalytic reactions was achieved. These CdS nanoparticles were dispersed in acrylonitrile-styrene (AS) copolymer films and the CdS/polymer hybrids were shown to be applicable to nonlinear optical materials, as demonstrated by $\chi^{(3)}$ values.

(2) CdS nanoparticles were grown in the presence of a styrene and 1-vinylimidazole mixture under monochromatic Ar^+ laser beam irradiation. With changing the irradiation wavelength from 514.5 to 457.9 nm, the absorption onset and excitonic shoulder of CdS were blue-shifted accordingly due to the quantum size effect. Especially, the energy difference of 21 meV between 472.7 and 476.5 nm of Ar^+ laser lines reflected on the difference of the particle diameter, which corresponded to that of 2~3 Å. This phenomenon is important for the precise size control of nanoparticles.

2.5 References and Notes

(1) Hayashi, T.; Yao, H.; Takahara, S.; Mizuma, H. *J. Phys. Chem.* **1992**, *96*, 2866.

(2) Hayashi, T.; Mizuma, H.; Yao, H.; Takahara, S. in *Organic Materials for Non-Linear Optics* (Ashwell, G. J.; Bloor, D., Eds), **1993**, 197.

(3) Hayashi, T.; Mizuma, H.; Yao, H.; Takahara, S. *Nonlinear Opt.* **1995**, *13*,135.

(4) Brus, L. E. *J. Chem. Phys.* **1984**, *80*, 4403.

(5) Lippens, P. E.; Lannoo, M. *Phys. Rev.* **1989**, *B39*, 10935.

(6) Roussignol, Ph.; Ricard, D.; Flytzanis, C. *Appl. Phys.* **1987**, *A44*, 285.

(7) Jain, R. K.; Klein, M. B. in *Optical Phase Conjugation* (Fisher R. A. Eds.); Academic Press, San Diego, 1983, 307.

(8) Jain, R. K.; Steel, D. G. *Appl. Phys. Lett.* **1980**, *37*, 1.

(9) Sakai, T.; Kawabe, Y.; Ikeda, H.; Kawasaki, K. *Appl. Phys. Lett.* **1990**, *56*, 411.

(10) Fox, M. A. *Topics in Current Chemistry*, vol 142; Springer-Verlag, Berlin, 1987, 71.

(11) Hoffman, A. J.; Yee, H.; Mills, G.; Hoffmann, M. R. *J. Phys. Chem.* **1992**, *96*, 5540.

(12) Sommer, F. Breitenbach, J. W. *IUPAC International Symposium on Macromolecular Chemistry*, Budapest, 1969, 257.

(13) Kamat, P. V.; Todesco, R. V. *J. Polym. Sci. Part A Polym. Chem.* **1987**, *25*, 1035.

(14) Takagahara, T. *Phys. Rev.* **1987**, *36*, 9293.

(15) Hayashi, T. *Kobunshi* **1995**, *44*, 26.

(16) Fojtik, A.; Weller, H.; Koch, U.; Henglein, A. *Ber. Bunsenges. Phys. Chem.* **1984**, *88*, 969.

(17) Chestony, N.; Harris, T. D.; Hull, R.; Brus, L. E. *J. Phys. Chem.* **1986**, *90*, 3393.

(18) Vossmeyer, T.; Katsikas, L.; Giersig, M.; Popovic, I. G.; Diesner, K.; Chemseddine, A.; Eychmuller, A.; Weller, H. *J. Phys. Chem.* **1994**, *98*, 7665.

(19) Gygaz, H. R. *J. Discuss. Faraday Soc.* **1968**, 227.

(20) Yasuda, H.; Tamai, H. *Hyomen*, **1992**, *30*, 895.

Appendix

Generation of a phase conjugated wave related to $\chi^{(3)}$ is schematically illustrated in Figure 2.14.

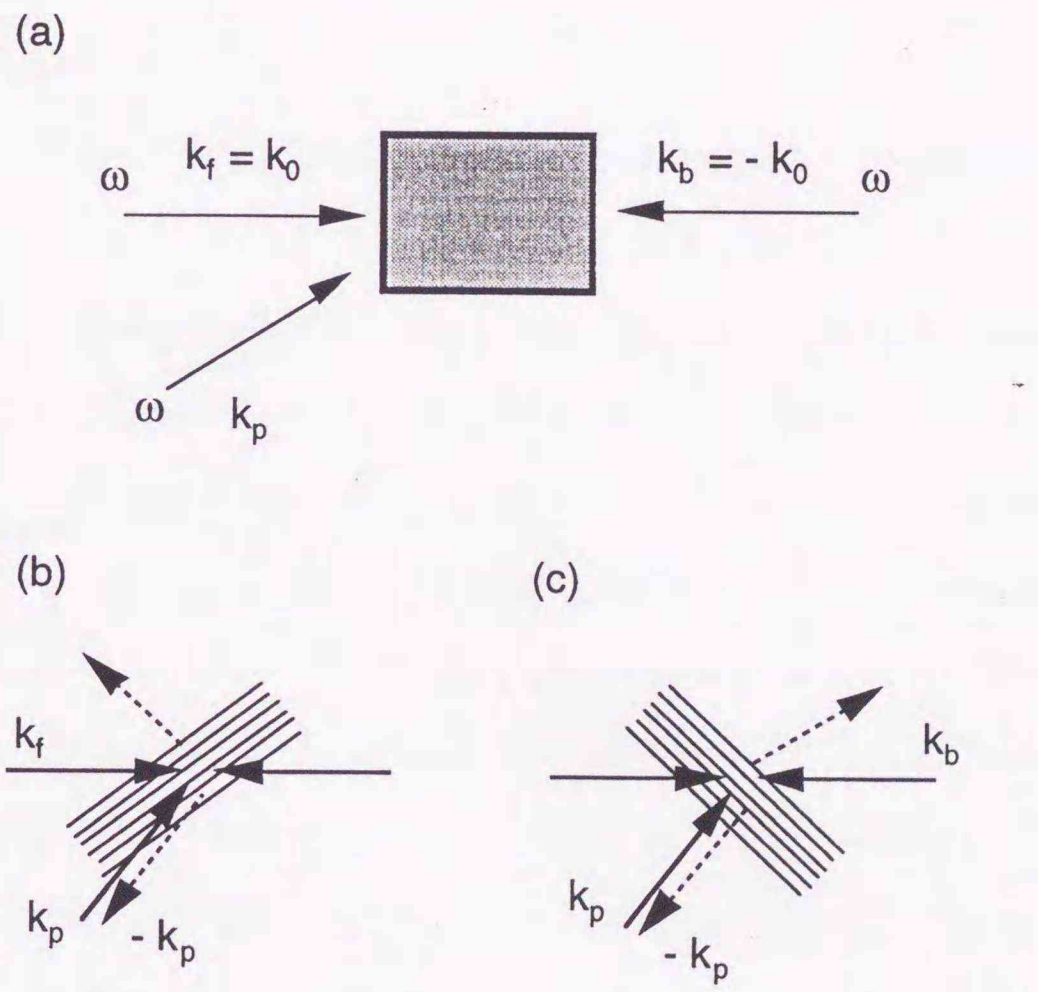

Figure 2.14. Mechanism of formation of a phase conjugated wave by a DFWM technique.

As shown in Fig. 2.14 (a), two counter propagating pump beams (ω; k_f and ω; k_b) and a probe beam (ω; k_p) were simultaneously irradiated into a nonlinear medium. A population grating with a wave vector k_f-k_p, which is an interference resulted from density differences between the excited and the ground states, was generated by a pump beam k_f and a probe beam k_p, as shown in Fig. 2.14 (b). The other pump beam, k_b, is diffracted by the population grating to be propagated with a wave vector -k_p. This beam is a phase conjugated wave. For 2.14 (c), the population grating made of k_b and k_p diffracts k_f to a generate phase conjugated wave toward k_p. These processes are results of the third-order nonlinear optical phenomena.

Chapter 3. CdS Nanocrystals in Chelate Polymer Microparticles: Optical and Distribution Properties[1]

3.1 Introduction

Dense dispersion of semiconductor nanocrystals[2] and understanding of the relevant dispersion characteristics in dielectric host media are desired for fundamental physics and device applications.[3,4] However, since a single nanocrystal consists of only a small number of atoms (100~10000), an elucidation of the interactions between the crystal surface and the host matrices is absolutely necessary to understand the electronic properties of nanocrystals.[5]

In Chapter 2, the size control of CdS nanocrystals by monochromatic irradiation is discussed. The approach is quite potential for size-controlled preparations of CdS through a variation of the incident light wavelength. Besides such the approach, simultaneous control of the crystal size and nanocrystal distributions in host matrices is quite important for development of nanocrystal hybrid assemblies. Solid materials such as glasses and polymers act as dielectric host matrices and are considered to be useful for preventing particle flocculation. In particular, *in situ* crystal synthesis in polymer matrices is very interesting since the interactions between nanocrystal surfaces and functional molecular groups in polymers are expected to be controlled by the properties of the host polymers. Furthermore, correlations between the crystal size/dispersion properties of nanocrystals and the chemical structural/three dimensional structural features of the host polymers are worth to be studied for future applications of the nanocrystal hybrid systems. Thus, a preparation of CdS nanocrystals in micrometer-sized

chelate polymer particles was explored and its optical characteristics were studied in detail.

As a host polymer matrix, polymer particles having chelating ligands are very favorable for homogeneous and dense loading of Cd^{2+} ions in the host matrix via interactions between the ion and the ligand.[6] When CdS crystals grow in the polymer particle by nucleation of Cd^{2+} with an appropriate S^{2-} source, the crystal size and its distribution, morphological structures, and their electronic properties will be affected by the electrostatic interactions between the crystal surface and the ligands. According to a theoretical model of ion-exchange mechanisms in polymer resin beads, furthermore, the reaction of Cd^{2+} ions with a sulfur source is expected to be controlled through several factors such as the concentration of the sulfur source and the surface area of the polymer particle.[7] Although characterization of a single microparticle is in general difficult, a microspectroscopy technique, applicable to a single microparticle in solution, has been developed. Therefore, the optical properties of CdS nanocrystals can be studied for individual polymer particles.

In this chapter, preparations and characterizations of CdS nanocrystals embedded in chelate polymer particles are described. A particular emphasis of the study is, (i) an observation of a polymer size dependence of the optical properties of CdS based on the quantum size effect, and (ii) a modulation of the CdS crystal size and its distribution characteristics with an added electrolyte; NaCl. Peculiar dispersion structures of CdS in polymer particles observed under certain preparation conditions and the factors governing the size and the distribution of CdS are also described.

3.2 Experimental

3.2.1 Chemicals.

Chelate polymer microparticles (Chelex 100: 200-400 mesh, Analytical Grade, Bio-Rad Laboratories), made of styrene-divinylbenzene copolymers, having iminodiacetate groups ($-N(CH_2COO^-)_2$) were used as a host matrix to prepare CdS nanocrystals. The beads were soaked in distilled water and washed successively with methanol, aqueous HCl (2 M), aqueous NaOH solutions (2M), and then thoroughly with water. After treating with ethanol, the beads were dried under vacuum. Cadmium acetate $Cd(CH_3COO)_2 \cdot 2H_2O$ (GR grade, Wako Pure Chemicals), sodium sulfide $Na_2S \cdot 9H_2O$ (GR grade, Wako Pure Chemicals), and sodium chloride NaCl (GR grade, Kanto Chemicals) were used as received.

3.2.2 Preparations of CdS Nanocrystals in Chelate Polymer Microparticles.

Several procedures were employed to prepare CdS nanocrystals. *Sample I* was prepared in the absence of any electrolyte except for Na_2S while *sample II* was prepared to study NaCl effects on CdS size and its distribution in the polymer particle. Preparation methods are described separately.

1. Samples I.

The chelate polymer (0.087 g, dried weight) mentioned above was soaked in an aqueous $Cd(CH_3COO)_2$ solution (0.1M, 0.5 mL) for 10 min under supersonication, and stored for 2 d at room temperature. All the Cd^{2+} ions were confirmed to be incorporated into the polymer, as judged

by the fact that the supernatant solution no longer reacted with a Na_2S solution to form CdS. The Cd^{2+}-incorporated chelate polymer was then washed with distilled water several times. Preparations of CdS nanocrystals in the polymer were performed by adding an aqueous Na_2S solution to the Cd^{2+}-polymer samples. Diffusion of sulfide anions into the polymer particles is expected to depend on the initial concentration of Na_2S (discussed later in detail). Therefore, CdS-polymer samples were prepared by the following two methods, employing a different initial concentration of the Na_2S solution.

Sample Ia: The Cd^{2+}-polymer beads described above were redispersed in 1 mL of water, and 2.6 mL of an aqueous Na_2S solution (1.8×10^{-2} M) were added into the solution under vigorous stirring. The polymer particles immediately turned pale yellow due to CdS formation. After stirring for further 30 min, the mixture was left standing for 1 d. The supernatant solution was removed and the particles collected by filtration were washed repeatedly with water and ethanol. The sample was dried in vacuo.

Sample Ib: A dilute Na_2S solution was used to prepare CdS nanocrystals. In order to adjust the total amount of the S^{2-} ion to that in *sample Ia*, 50 mL of an aqueous Na_2S solution (9.2×10^{-4} M) were added to the Cd^{2+}-polymer particles dispersed in 10 mL of water. The solution was stirred for 2 h and then left standing for 1 d. After working up procedures analogous to those for *sample Ia*, the particles were dried under vacuum. Preparation procedures of *samples Ia* and *Ib* are summarized in Figure 3.1.

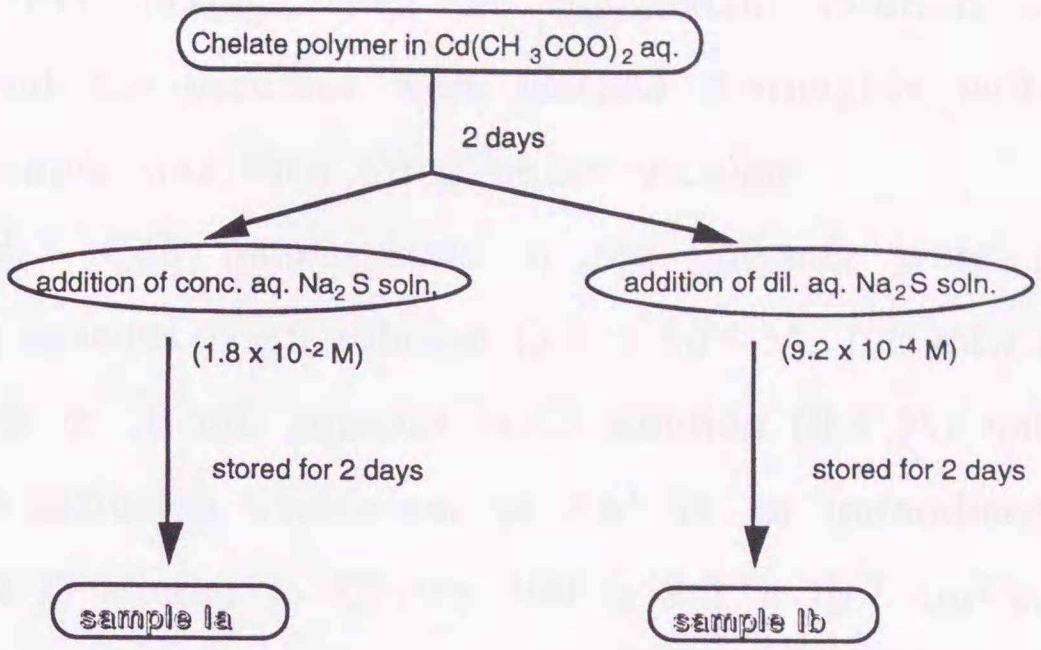

Figure 3.1. Sample preparation procedures of CdS in chelate polymer microparticles.

2. *Samples II*.

The chelate polymer particles of 0.107 g (dried weight) were soaked in an aqueous $Cd(CH_3COO)_2$ solution (8.4×10^{-3} M, 5.0 mL) for 10 min under supersonication, and stored for 2 d at room temperature. Here, the concentration of an aqueous Cd^{2+} solution was adjusted to be lower than that for *sample I*. Hence, CdS nanocrystal formation in each polymer particle is expected to be proceed homogeneously compared to that for *samples I*. The Cd^{2+}-incorporated chelate polymer particles were then washed with distilled water several times.

Sample IIc: CdS nanocrystals in the polymer were prepared by adding a dilute aqueous Na_2S solution (3.8×10^{-4} M, 100 mL) to the Cd^{2+}-polymer particles in 10 mL distilled water under vigorous stirring. The polymer particles turned slowly pale yellow owing to formation of CdS. After stirring for 2 h, the solution was kept standing for 2 d at room temperature. In order to obtain a time profile of absorbance of CdS in the

polymer particle, an aliquot of the solution (several mL) was sampled at various times after mixing. Then the supernatant solution was removed by filtration, and the particles were washed thoroughly with water and ethanol. The sample was then dried under vacuum.

Sample IId: CdS nanocrystals in the polymer were prepared by adding a dilute aqueous Na_2S solution (3.8×10^{-4} M, 100 mL) to the Cd^{2+}-polymer particles in 10 mL aqueous NaCl solution (0.5 M) under vigorous stirring. As the diffusion coefficient of Na^+ in an iminodiacetate chelate resin (Dowex A-1) similar to Chelex 100 is 1.2×10^{-7} cm^2/s,[8] 10 min is considered to be enough for homogeneous diffusion of the ion in the polymer particle with the diameter of about 100 μm. The polymer particles turned pale yellow slowly, but faster than *sample IIc*. After 2 h stirring, the solution was kept standing for 2 d at room temperature. After working up procedures analogous to those for *sample IIc*, the particles were dried in vacuo. Preparation procedures of *samples IIc* and *IId* are summarized in Figure 3.2.

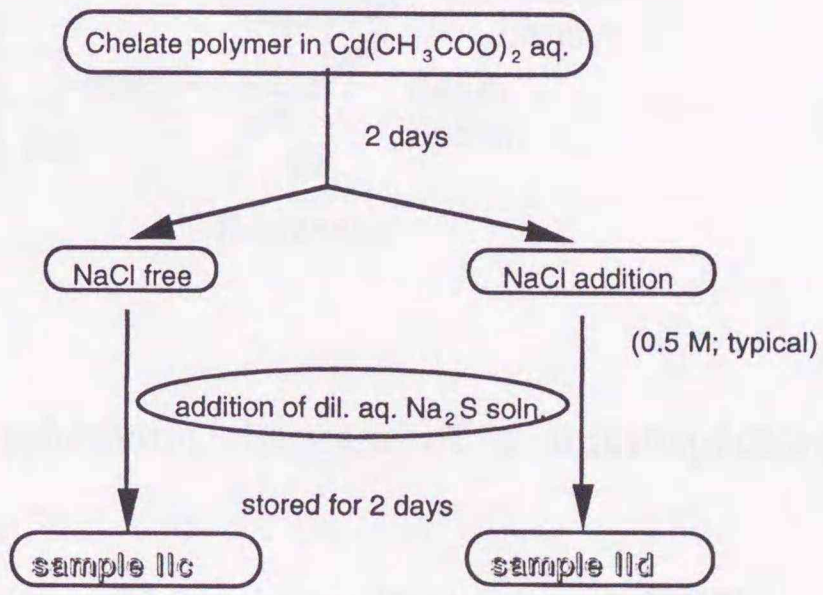

Figure 3.2. Sample preparation procedures of CdS in chelate polymer microparticles.

3.2.3 Apparatus.

Absorption spectra of CdS in single polymer particles were measured by a microspectroscopy system (shown in Figure 3.3) consisting of an optical microscope (Nikon, Optiphoto-2) and a polychromator (Oriel; Multispec 257)-multichannel photodetector (Princeton Instruments; ICCD-576E/G) set.[9]

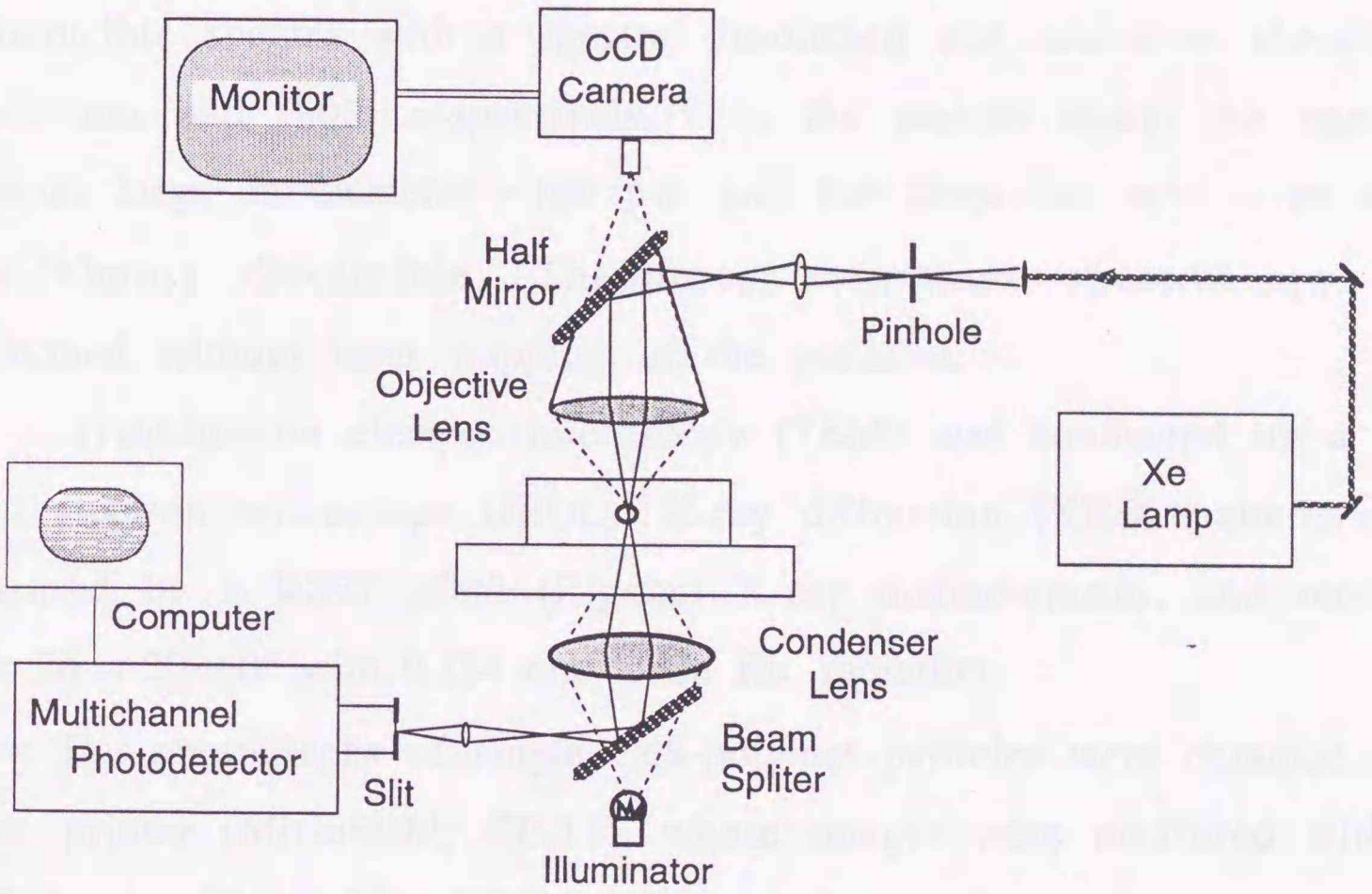

Figure 3.3. A schematic diagram of a microspectroscopy system.

A 150 W Xe lamp (Hamamatsu Photonics; L2273) was used as a light source for absorption spectroscopy. In the case of the dried CdS-polymer samples, the incident Xe beam was scattered by the particle under the microscope, so that the sample was dispersed in water just before optical measurements to reduce light scattering. The chelate polymer swelled in

water approximately ~1.5 times and the diameter of the particle was determined for the solution sample. Chelex 100 did not show any absorption in the wavelength region above ~400 nm. For the calculation of absorbance, therefore, the incident light intensity (I_0) was determined by the light beam being passed near a sample particle, while the transmitted light intensity through a CdS-polymer particle (I) was measured by passing the beam at the center of the particle. For organic dye-doped Chelex 100 particles, these procedures always afforded reproducible spectra with a spectral resolution and minimum absorbance of ~2 nm and 0.05, respectively.[10] In the present study, the particles were as large as diameter ~100 μm and the Brownian motion in water was almost discernible. Therefore, absorption spectroscopy was performed without laser trapping of the particles.

Transmission electron microscopy (TEM) was conducted by a JEM 2010 electron microscope (JEOL). X-ray diffraction (XRD) patterns were measured by a RINT 2000 (Rigaku) X-ray diffractometer, and recorded over $2\theta = 20\sim60°$ with 0.154 nm of Cu Kα radiation.

The photographs of single CdS-polymer particles were obtained by a video printer (Mitsubishi; CP-11), whose images were measured with an CCD camera (Sony; Model DXC-930) equipped to the microscope.

3.2.4 Simulation of the Absorption Spectra.

Simulation of the absorption spectra of *sample Ia* was performed based on a theoretical model reported by Roussignol *et al.*[11] Under an effective mass approximation, an electron-hole pair is assumed to be confined in a sphere of radius R (= d_{CdS} / 2, where d_{CdS} is the crystal

diameter of CdS) with an infinite potential barrier. In this model, the transition energies of a CdS nanocrystal (E_{nl}^R) are described as in eq. 3.1,

$$E_{nl}^R = E_g + h^2\phi_{nl}^2 / (8\pi^2 m^* R^2) - 1.8e^2 / (\varepsilon R) \qquad (3.1)$$

where E_g is the band gap energy of bulk CdS (2.5 eV).[12] The second term represents the confined kinetic energy of a particle, where m^* is the effective reduced mass, taken here to be approximately $0.2m_0$ as a mobile electron mass,[12] and ϕ_{nl} is the n-th root of the spherical Bessel function of l-th order. In the present study, the lowest three quantized transition energies of 1S-1S, 1P-1P, and 1D-1D which correspond to ϕ_{10} (= 3.14), ϕ_{11} (= 4.49), and ϕ_{12} (= 5.75), respectively are considered. The Coulomb interaction energy between an electron and a hole in a semiconductor with a dielectric constant of ε was taken as the third term of the right-handed side of eq. 3.1.[13,14] Although the spin-orbit splitting interaction would be considered for any three transitions, this might lead to an overestimation of homogeneous broadening tails in the simulation. Therefore, only the transition from the 1S spin-orbit split-off band ($\triangle_{SO}$ = 64 meV[15]) to the lowest 1S electron level was taken into account.[16] The absorption coefficient, $\alpha^R(\omega)$, at a given frequency (ω) is the sum of the contributions from the 1S-1S, $1S_{SO}$-1S, 1P-1P, and 1D-1D transitions and each transition possesses a homogeneous line width of $1/T_2$ and an intensity caused by level degeneracies.[11] A crystal size distribution can be expressed as a log normal distribution function $f(R)$ with a standard deviation of σ. The center radius of the size distribution, R_0, described in eq. 2.4 (Chapter 2), was evaluated by analyzing the TEM images of the samples (discussed later). The absorption spectral shape ($\alpha(\omega)$) can be simulated by eq. 3.2, by taking a proportional factor of k into account.

$$\alpha(\omega) = k \int \alpha^R(\omega)\ f(R) \cdot d\ln(R) \qquad (3.2).$$

In actual simulation, the line shape parameter (T_2) was fixed to 10 fs[17] and the absorption spectrum was fitted by two parameters: σ and R_0.

3.3 Polymer Size Dependence of the Optical Properties of CdS Nanocrystals in Polymer Microparticles.

3.3.1 Optical Properties of CdS Nanocrystals in *Samples I*.

Figures 3.4a and 3.4b show the absorption spectra of CdS in individual polymer particles prepared from the concentrated (*sample Ia*) and dilute (*sample Ib*) aqueous Na_2S solutions, respectively. It is noteworthy that the S/N values of the spectra around 400~420 nm are worse compared with those in the longer wavelength region. This is because transmittance of the microscope objective decreases with shifting incident light (I_0) to the shorter wavelength, particularly, below 420 nm. However, the present microspectroscopy technique enabled reproducible measurements of the spectra for individual polymer microparticles (see the experimental section), so that quantitative discussion could be made on the basis of the data in Figure 3.4.

As clearly seen in Fig. 3.4, the absorption spectra of CdS were strongly dependent on the preparation method. The important results are as follows. Firstly, the onset wavelength, below which the absorbance increased sharply, was around 500 nm for *sample Ia* while that for *sample Ib* was shifted to a longer wavelength (520 nm). For CdS crystals,

it is well-known that the onset wavelength shifts to a shorter one with decreasing the crystal size.

(a)

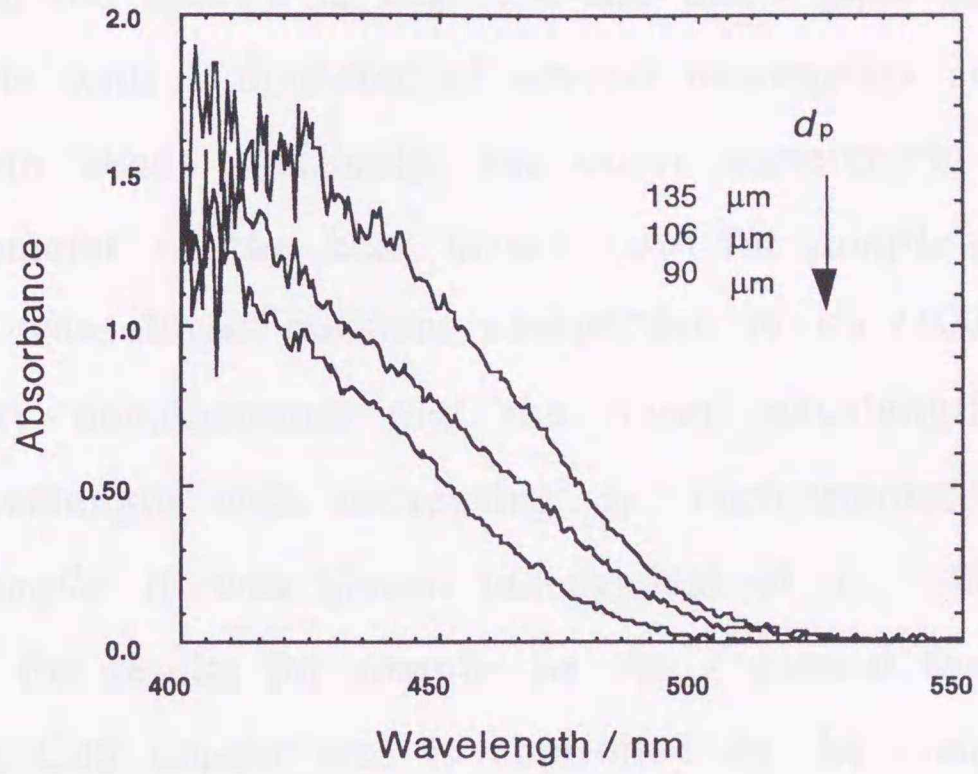

(b)

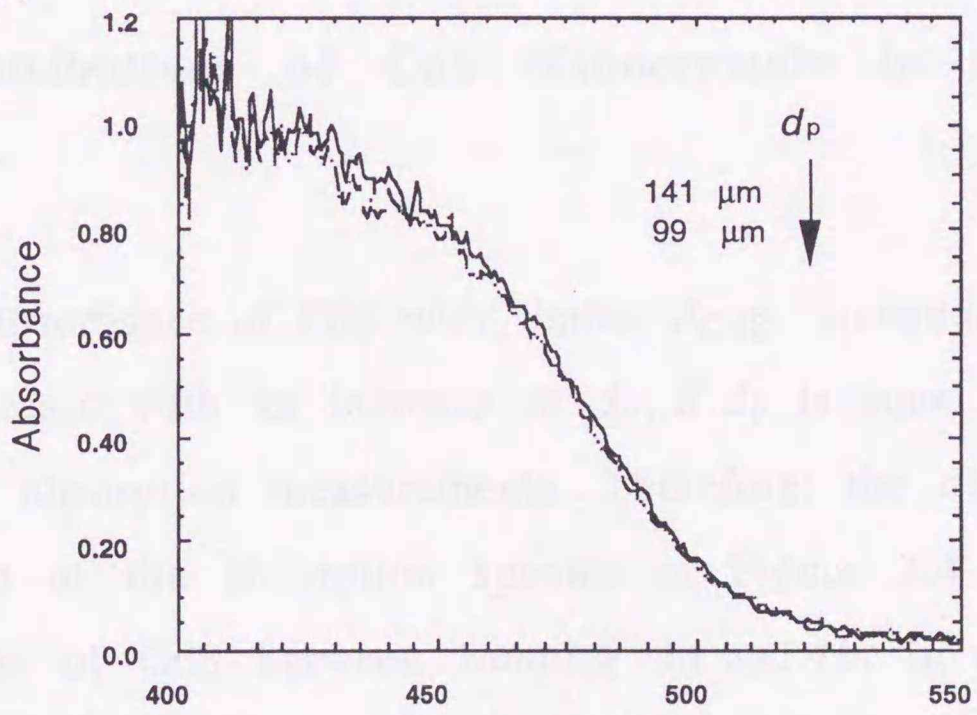

Figure 3.4. Absorption spectra of CdS nanocrystals embedded in the chelate polymers. (a) *sample Ia* prepared from a concentrated Na_2S solution, (b) *sample Ib* prepared from a dilute Na_2S solution.

Actually, Weller and his co-workers have reported that the band gap energy, related to the onset wavelength of CdS, increases from 2.4 to 3.9 eV with decreasing average CdS diameter from 9.6 to 1.4 nm.[18] As judged from the spectra in Fig. 3.4 and those reported by Weller *et al.*, CdS crystals with a diameter of several nanometers are produced in the chelate resin beads. Secondly, the onset wavelength strongly depended on the diameter of the host matrix (d_P) for *sample Ia* while that for *sample Ib* was almost constant irrespective of d_P (100~140 μm). Figure 3.4a clearly demonstrates that the onset wavelength shifts toward a shorter wavelength with decreasing d_P. Furthermore, the absorbance of CdS for *sample Ib* was almost independent of d_P, which was in marked contrast to the results for *sample Ia*. As a general feature of the present results, the CdS cluster size is controlled by the concentration of added Na_2S and the diameter of the host polymer bead.

3.3.2 Distributions of CdS Nanocrystals in Chelate Polymer Particles.

The absorbance of CdS with similar d_{CdS}, embedded in the polymer, should increase with an increase in d_P, if d_P is equal to the optical path length for absorption measurements. Therefore, the difference in the d_P dependence of the absorption spectra in Figure 3.4 indicates those in distributions of CdS between *samples Ia* and *Ib*. In order to investigate distributions of CdS nanocrystals in the polymer particles, transmission electron microscopy (TEM) measurements were performed. Since chelate polymer particles swelled in water, elaborated efforts were necessary to make thin sliced samples. Figure 3.5 shows the TEM images of both the surface and center areas of the CdS-polymer *samples Ia* and *Ib*. For

sample Ia, the TEM pictures in Figures 3.5a and 3.5b demonstrate that small CdS nanocrystals (recognized as black spots) are dispersed densely and homogeneously in both the surface layer and the center area of the polymer particle. According to the results from the TEM observation, the size distribution of CdS is fairly narrow with a crystal diameter (d_{CdS}) of ~3 nm. The results agree with the d_P dependence of the absorption spectra. In Figure 3.4a, actually, the increase in d_P from 90 to 135 μm (1.5 fold) results in that of the absorbance of ~1.5 at 420 nm, indicating that the diameter of the polymer particle corresponds to the optical path length. On the basis of both absorption and TEM experiments, therefore, CdS nanocrystals are concluded to be distributed homogeneously in the entire host matrix for *sample Ia*. The size distribution of CdS in *sample Ia* (d_P = 135 μm) determined by the TEM image (Figure 3.5a) is shown in Figure. 3.6. It is noteworthy that the size distribution can be well fitted by the log normal distribution function in eq. 2.4 with the parameters of $2R_0$ = 2.7 nm and σ = 0.37. This is the important result for simulation of the absorption spectral shape of CdS, as described in the following section.

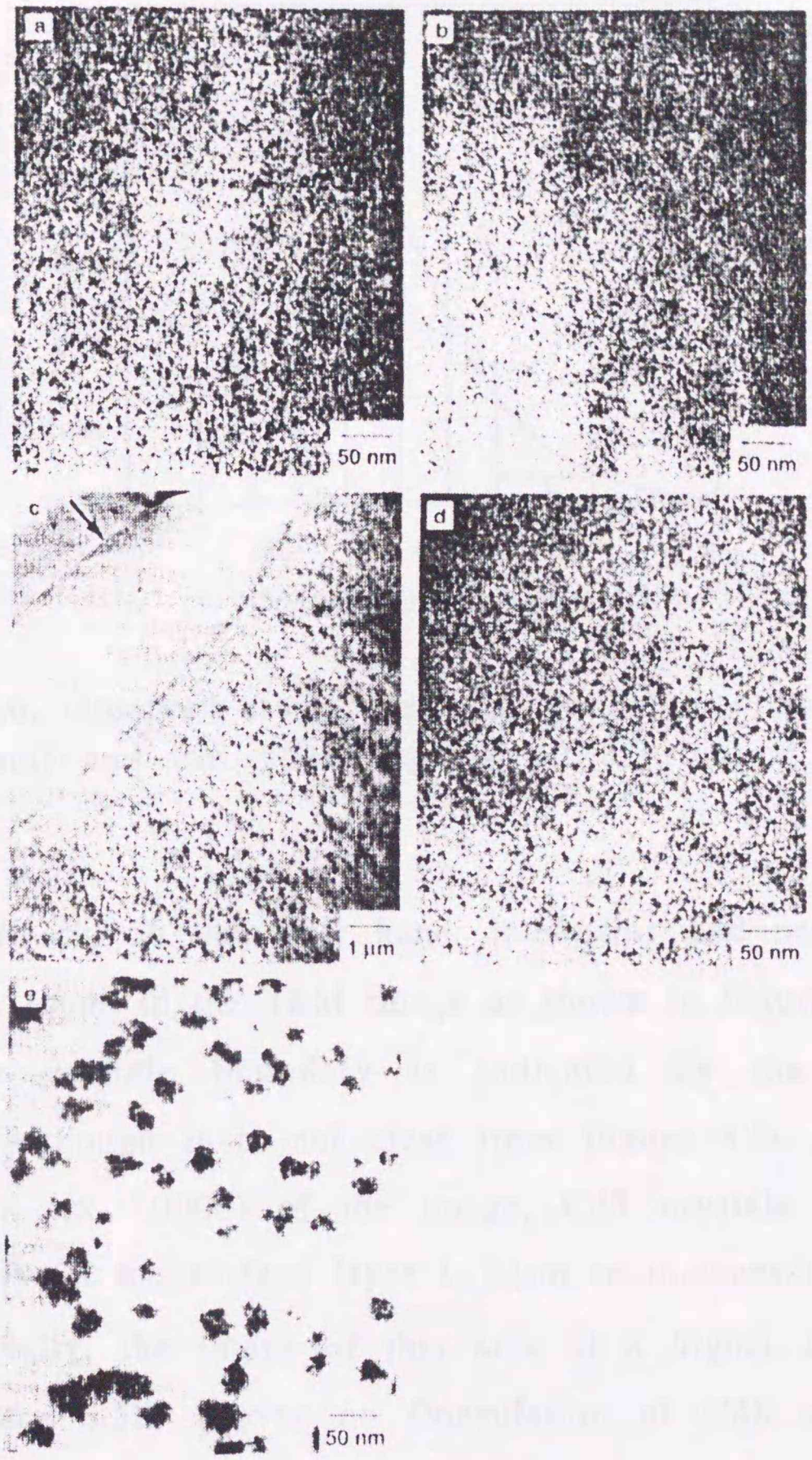

Figure 3.5. TEM images of the CdS-polymer particles. (a) and (b) show the surface and center images of the particle (*sample Ia*, x 300000), respectively. (c) and (d) represent TEM images of the surface areas of the particle (*sample Ib*) with the magnification of 10000 and 300000, respectively. (e) is the image of the particle (*sample Ib*) ~5 μm inner from the surface (x 300000). The arrow indicated in the figure (c) represents the polymer particle boundary.

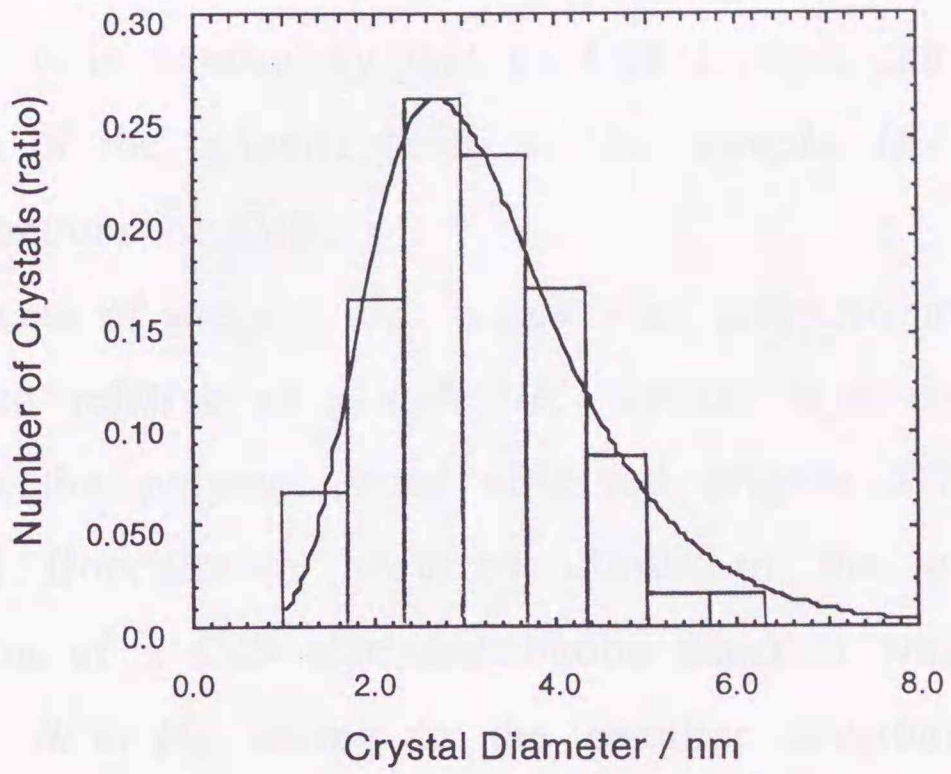

Figure 3.6. Observed crystal size distribution of *sample Ia* (d_p = 135 μm; histogram) and the fitted log normal distribution function (solid curve).

For *sample Ib*, on the other hand, interesting and peculiar dispersion textures were found in the TEM image as shown in Figure 3.5c, in which the polymer particle boundary is indicated by the arrow in the photograph. Although it is not clear from Figure 3.5c due to the low magnification (x 10000) of the image, CdS crystals are precipitated homogeneously in the surface layer (~5 μm in thickness) of the polymer particle. Actually, the image of this area at a higher magnification (x 300000, Figure 3.5d) proves no flocculation of CdS and the average diameter of the crystals has been shown to be ~3 nm. On going from the particle surface to the inner area, the size of the CdS crystals increases as can be recognized by the fact that the morphology changes from the upper left (surface) to the lower right (inner part) in Figure 3.5c. The magnified TEM image of the area inner from the surface by ~5 μm shown in Figure 3.5e indicates that CdS nanocrystals with a diameter of 5~7 nm

flocculate each other to produce larger particles with a diameter of 20~30 nm. It is noteworthy that no CdS crystals can be observed at the central part of the polymer bead, so that *sample Ib* possesses layer-by-layer distributions of CdS.

In the case of *sample IIc*, which was prepared under a lower Na_2S concentration relative to *sample Ib*, similar layer-by-layer distributions of CdS in the polymer were observed (Figure 3.7; left side), while nanocrystal flocculation occurred closer to the polymer surface. A determination of a CdS size distribution function was thus very difficult for *sample Ib* or *IIc* owing to the peculiar distribution structures. The optical microscope image of the microparticle for *sample IIc* is shown in Figure 3.7 (right-handed side) as a typical example. The ring structure was observed at around 8 μm inside from the polymer surface. The TEM image with a lower magnification (x 16000) indicates that this ring structure corresponds to the edge of generated CdS nanocrystals (schematically shown in Figure 3.7; center). Thus, the length from the polymer surface to the ring structure (L) represents the width of the CdS layer in the polymer particle. This boundary is probably appeared due to the inhomogeneous distributions of CdS in the polymer, which leads to the changes in the light scattering intensity. The optical properties of CdS nanocrystals are governed by the sample preparation method (i.e., concentration of the added Na_2S solution) through the changes in the distributions of the crystals in the host polymer particles (discussed later again).

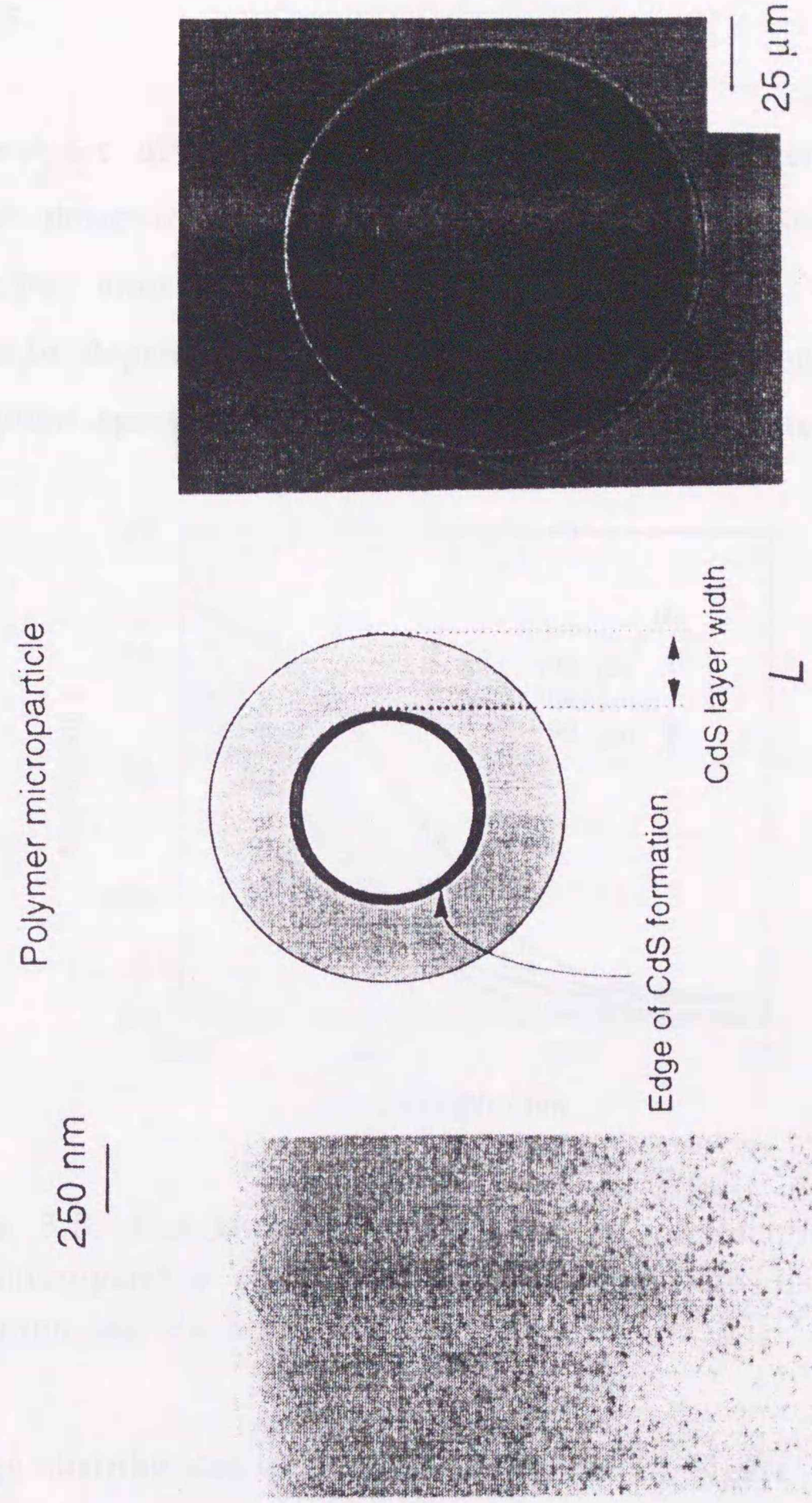

Figure 3.7. (Left) An TEM image of the CdS-polymer cross section of *sample IIc*. (Center) Schematic picture of the CdS nanocrystal distribution. (Right) An optical microscope image of *sample IIc*. Similar image was observed for *sample Ib*.

3.3.3 Simulation of the CdS Distribution in Individual Polymer Particles.

Analyses of single polymer particles are in general very difficult except for those by absorption and emission spectroscopy. Since one of the principal aims of this research is to elucidate the origin of the polymer size dependence of d_{CdS} and the size distribution, simulation of the absorption spectral band shape of CdS was conducted for *sample Ia*.

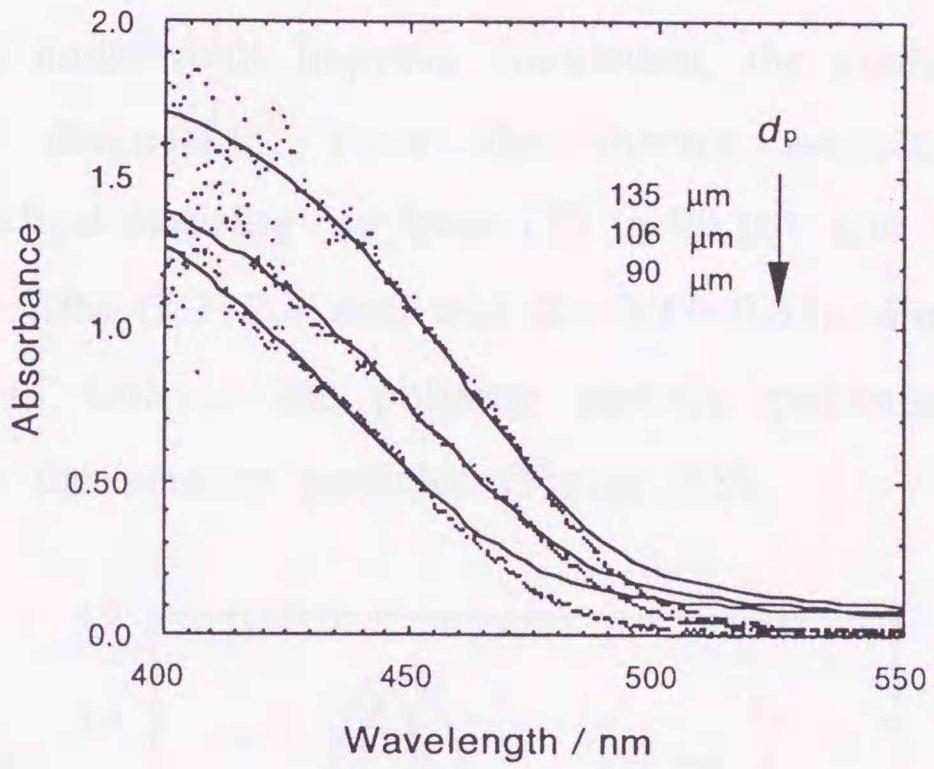

Figure 3.8. Simulated absorption spectra of *sample Ia* with several polymer microparticle diameters; d_p. The CdS size distributions used for the simulation are shown in Figure 3.9.

The d_{CdS} distributions of *sample Ia* shown in Figure 3.6 could be fitted by a log normal function as described in the preceding section. Actually the observed absorption spectrum of the CdS-polymer particle with d_p = 135 μm was reproduced fairly well by using the parameters with $2R_0$ = 2.7 nm and σ = 0.37 (see also experimental section and eq. 3.1), except for the absorption tail towards 550 nm (solid curve in Figure 3.8). The

results indicate that the crystal size distributions can be estimated from the absorption spectra. Therefore, simulation of the absorption spectra of the CdS-polymer particle with d_P = 106 and 90 μm was also conducted, and the results are included in Figure 3.8. The parameters obtained for the polymers with d_P of 106 and 90 μm were $2R_0$ = 2.4 nm, σ = 0.37 and $2R_0$ = 2.4 nm, σ = 0.31, respectively, and the d_{CdS} distributions are summarized in Figure 3.9. The deviation of the simulated spectra from the observed one around 480~550 nm may be due to the assumption of the common line-shape function for all the transitions. Although a more sophisticated model will improve simulation, the analyses are enough for the present discussion, since the shorter wavelength shift of the spectrum with decreasing d_P from 135 to 90 μm can be explained by the decreases in $2R_0$ (2.7~2.4 nm) and σ (0.37~0.31). Furthermore, the size distribution of CdS in the polymer particle estimated by simulation is narrower for the smaller particles (Figure 3.9).

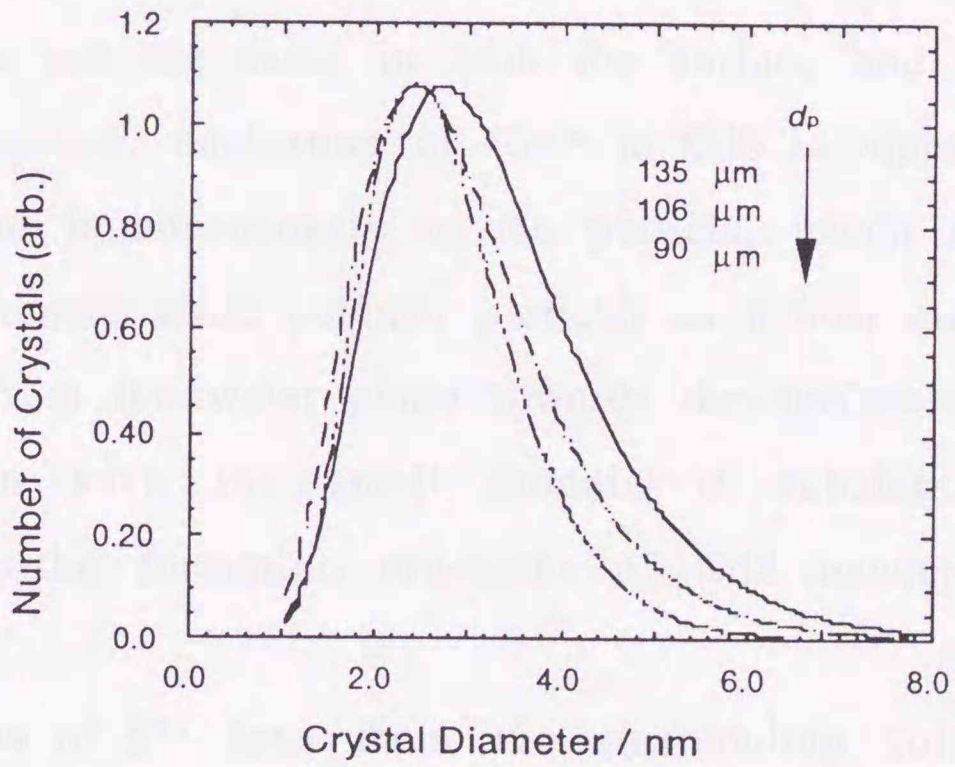

Figure 3.9. Simulated nanocrystal size distributions of *sample Ia* with various d_P.

Since the effective mass approximation is invalid for CdS particles smaller than 3~4 nm, the shift of the absorption tail to the longer wavelength can be ascribed to distributions of larger-sized CdS crystals. Therefore, it is concluded that the size distribution of CdS nanocrystals (d_{CdS} > 3~4 nm) is reasonably estimated by the present simulation method.

3.3.4 Effects of the Polymer Size and the Injection Method of an Na_2S Solution on Nanocrystalline CdS Size Distributions.

The crystal size of CdS was shown to be highly dependent on both the size of the host chelate polymer particle and the injection method of an aqueous Na_2S solution (i.e., concentrated- or dilute-solution injection). The relationships between d_{CdS} and these factors are worth discussing, since this leads to the possibility of precise controls of the size and distribution of CdS nanocrystals. For *sample Ia*, since d_{CdS} and its distribution are the same in both the surface and center areas of the polymer particle, nucleation of Cd^{2+} to CdS is supposed to proceed very quickly and homogeneously in the particle, which can be achieved by using micrometer-sized polymer particles as a host matrix. So the flux of S^{2-} ions from the water phase towards the surface of the host polymer particle in such the small domain is substantially important to understand the formation processes of CdS nanocrystals as discussed below.[19]

The flux of S^{2-} ions from the surrounding solution phase to the polymer surface in unit time is expressed as in eq. 3.3,

$$2\pi d_p D\left[1 + \frac{d_p}{2(\pi Dt)^{1/2}}\right] C_0 \qquad (3.3)$$

where D and C_0 are the diffusion coefficient and the concentration of the S^{2-} ion in the water phase, respectively.[20] Nucleation in the polymer is very fast, so that the reaction between S^{2-} and Cd^{2+} proceeds via pseudo first-order kinetics. The flux of the S^{2-} ion, necessary for nucleation of Cd^{2+} ions in the polymer, can be obtained by dividing eq. 3.3 by the volume of the polymer particle, $\pi d_p^3/6$. By stirring the outer solution, the transient term (the second term in the bracket in eq. 3.3) can be neglected so that the flux of S^{2-} to the polymer surface is proportional to $12DC_0/d_p^2$. This indicates that, at a given C_0, the S^{2-} flux per unit time becomes larger along with a decrease in d_p. Phenomenologically, this is what observed for *sample Ia*. Namely, supersaturation in the smaller polymer particles proceeds more efficiently through S^{2-} diffusion compared to that in larger particles, and this leads to generation of a huge number of CdS nuclei.[21] Therefore, smaller CdS crystals are produced in the smaller polymer particles. Actually, these samples exhibited the polymer size dependence of the optical properties of the CdS nanocrystals.

For *sample Ib*, on the other hand, although the total mole number of S^{2-} in the water phase is equal to that for *sample Ia*, the concentration of S^{2-} is very low (9.2×10^{-4} M; total volume of the water phase = 60 mL) so that nucleation in the polymer phase is restricted by the low S^{2-} flux. The Cd^{2+} ions located in the surface layer of the polymer will be rapidly nucleated to CdS while the S^{2-} flux is insufficient to react with Cd^{2+} ions in the inner volume, rendering the layer-by-layer size distributions of CdS.

The effects of the host polymer particle size and the sample preparation method on d_{CdS} and its distribution are reasonably explained on the basis of the S^{2-} flux to the polymer surface and the degree of

supersaturation in the polymer phase, though more detailed studies are required to elucidate the molecular mechanisms. Preparations of CdS nanocrystals in ion-exchange chelate polymer particles are very unique, and both d_{CdS} and its distribution will be controlled more precisely through optimization of the present preparation methods.

3.4 Electrolyte Effects on CdS Nanocrystal Formation and Its Size in Polymer Microparticles.

3.4.1 Electrolyte Effects on the Size of CdS Nanocrystals.

In Section 3.4, the size- and distribution-control of CdS nanocrystals through d_p and the preparation methods (i.e., *sample I* or *II*) were described in detail. It is noteworthy that these samples are obtained by the preparation method without an external salt other than Cd^{2+} and S^{2-}. As a synthetic method in an aqueous solution, generally, the presence of a foreign electrolyte such as KCl and NaCl is known to interfere generation of small nanoclusters. This is because the addition of a salt brings about a thinner electrical double layer around the surface of nanocrystal, and this leads to crystal flocculation. In homogeneous solutions, therefore, small nanocrystals cannot be prepared in the presence of a foreign KCl or NaCl. In the present study, however, quite characteristic effects of NaCl on the CdS crystal size and its distributions in polymer particles were observed.

Sample II (injection of a low concentrated S^{2-} solution) was prepared with and without NaCl at various reaction times. Figure 3.10a shows absorption spectra of *samples IIc* ([NaCl] = 0) and *IId* ([NaCl] = 0.5 M) prepared with the reaction time of 30 min (d_p ~ 100 μm). Absorbance of

CdS for *sample IIc* at $\lambda < 500$ nm was smaller than that for *sample IId*, indicating generation of a smaller amount of CdS nanocrystals for *sample IIc* during 30 min. When absorbance of *sample IIc* at around 400 nm was normalized to that of *sample IId*, however, two spectra almost coincided with each other, suggesting that both samples had similar crystal size distributions. Figure 3.10b shows absorption spectra of *samples IIc* and *IId* at the reaction time of 48 hr. A blue-shifted spectrum was observed for the sample prepared in the presence of NaCl (*sample IId*). Differential spectra (1st derivatives) relevant to the spectra in Figure 3.10b are shown in Figure 3.11. Although it is not clear from Figure 3.10b, the differential spectra demonstrate a clear shift of the absorption onset and an excitonic shoulder for *sample IId*.

The spectral shift of *sample IId* is caused by the quantum size effect. This is understood by following discussions. The absorption spectra of *samples IIc* and *IId* agree very well with each other as a typical example is shown in Figure 3.10a (reaction time; 30 min). However, Figure 3.10a demonstrates the difference in absorbance ($\lambda < 500$ nm) between two samples. According to the results in Figure 3.10a, the CdS formation rate for *sample IIc* is slower than that for *sample IId*. In order to make a quantitative discussion, a time profile of absorbance at 450 nm (nearly excitonic shoulders) was measured for each sample, as the results were summarized in Figure 3.12.

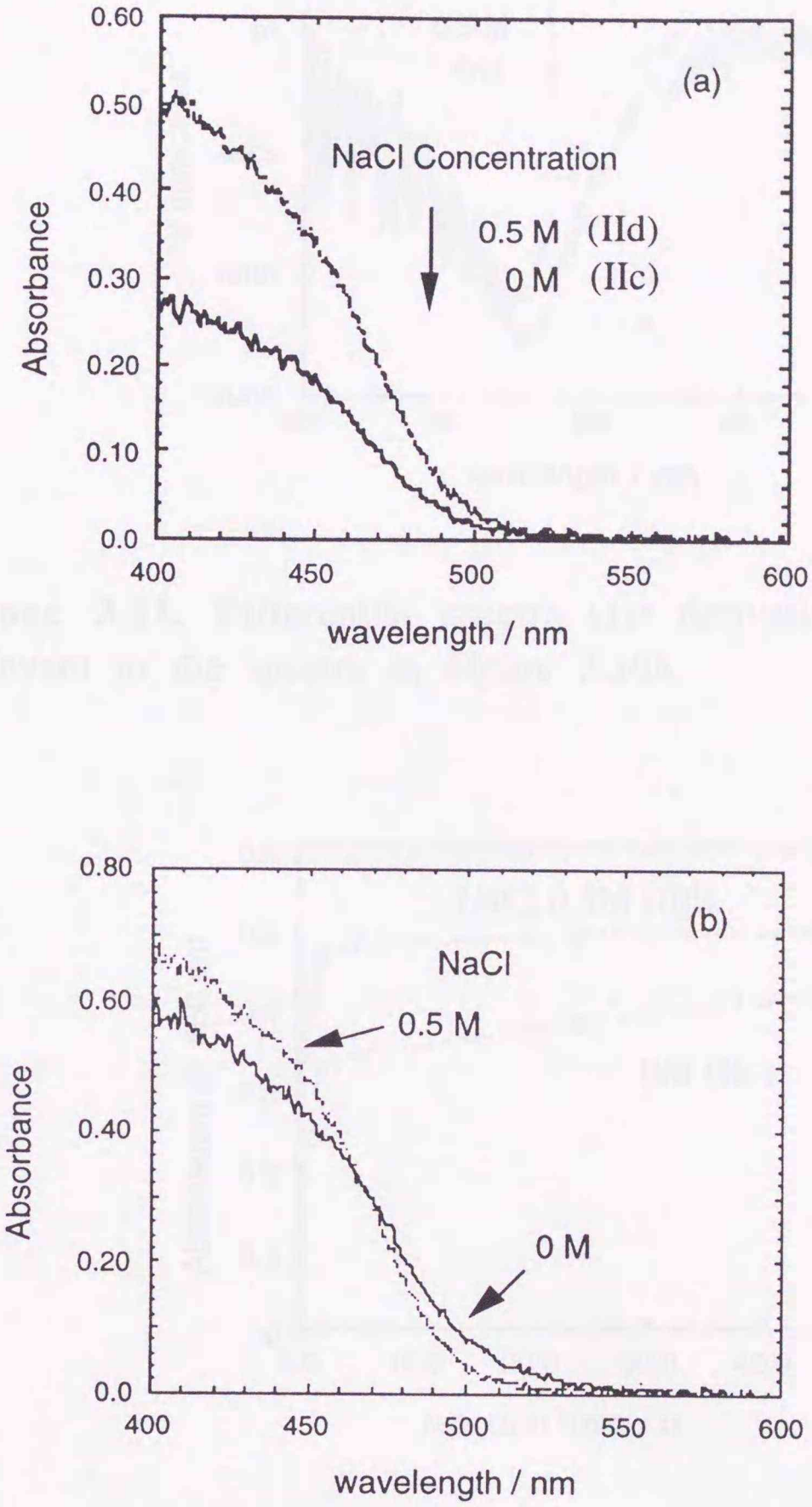

Figure 3.10. Absorption spectra of CdS nanocrystals prepared with or without NaCl at the reaction time of (a) 30 min or (b) 48 h. The diameter of the host chelate polymer used in this study was ~100 μm.

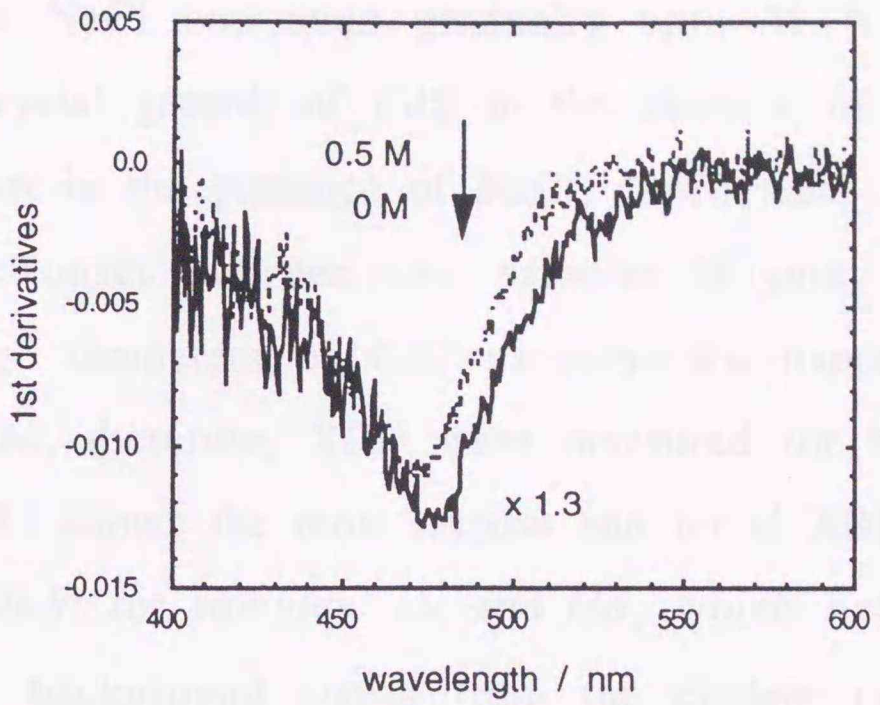

Figure 3.11. Differential spectra (1st derivatives) of *sample IIc* and *IId* relevant to the spectra in Figure 3.10b.

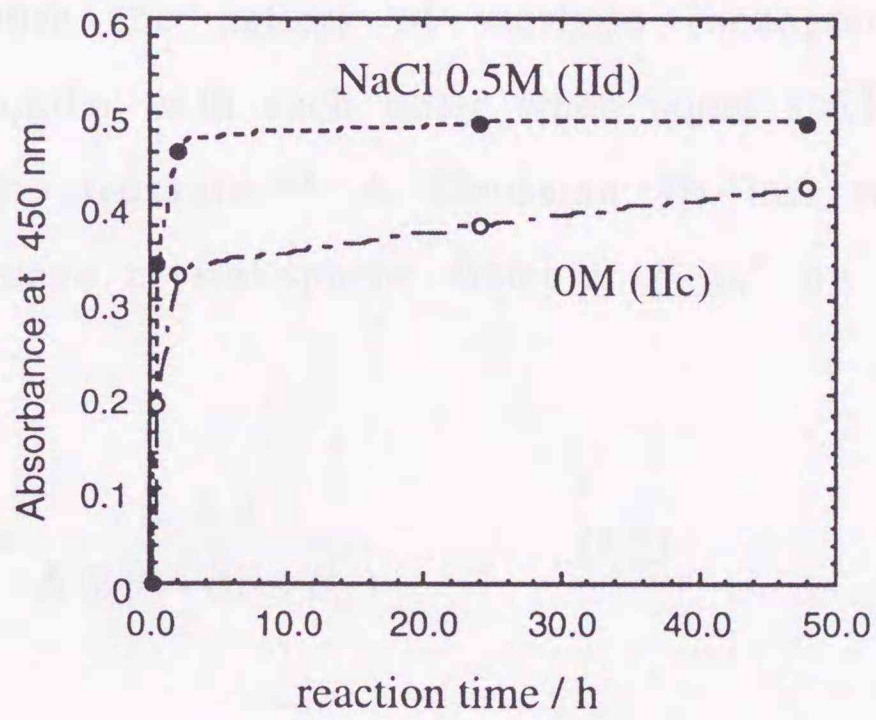

Figure 3.12. Time profiles of CdS formation in the chelate polymer.

Both samples exhibited the fast increase in the absorbance during the first 2 h (discussed later again). However, CdS formation in the polymer particle finished within 2 h in the presence of NaCl (0.5 M), while that in

the absence of NaCl continued gradually upto 48 h. The latter results indicate that crystal growth of CdS in the absence of NaCl is very slow compared to that in the presence of NaCl, which leads to the difference in the absorbance onset between two samples (Figure 3.12). In order to examine average diameters of CdS nanocrystals dispersed in the chelate polymer particles, therefore, XRD were measured for both samples.

Figure 3.13 shows the most intense and broad XRD reflection peak at around $2\theta = 26.5°$ for *samples IIc* and *IId*, which has been obtained by subtracting the background signal from the chelate polymer. Very weak reflection peaks at $2\theta = \sim 44°$ and $\sim 52°$ were also observed. These peaks are supposed to originate from CdS crystalline diffraction patterns, probably from a zincblend (cubic) structure. However, the signals were so weak that complete determination of the crystal structure could not be made, because the patters of wurtzite (hexagonal) and zincblend structures are similar with each other when some stacking faults exist in the hexagonal structure.[22] A Gaussian fit has been performed to determine the mean crystal-sphere diameter $d_{CdS}°$ by the Debye-Scheller formula[23],

$$d_{cdS}{}^{\circ} = \frac{1.2\,\lambda}{\Delta(2\theta)\cdot\cos(\theta_0)} \qquad (3.5)$$

where λ is the wavelength of the X-ray radiation, θ_0 is the angle of reflection of the peak, and $\Delta(2\theta)$ is the full width at half-maximum of the peak (FWHM). Estimated $d_{CdS}°$ for *samples IIc* and *IId* were 3.8 and 3.1 nm, respectively. As expected from the results in Figures 3.10, 11, and 12, it is concluded that smaller CdS nanocrystals are stably prepared in the presence of NaCl in the chelate polymer. This is in marked contrast to

what observed for the preparation of nanocrystals in an aqueous electrolyte solution, by which fast flocculation is induced due to screening of the electrical double layer around the periphery of nanocrystal surfaces, by an added electrolyte.

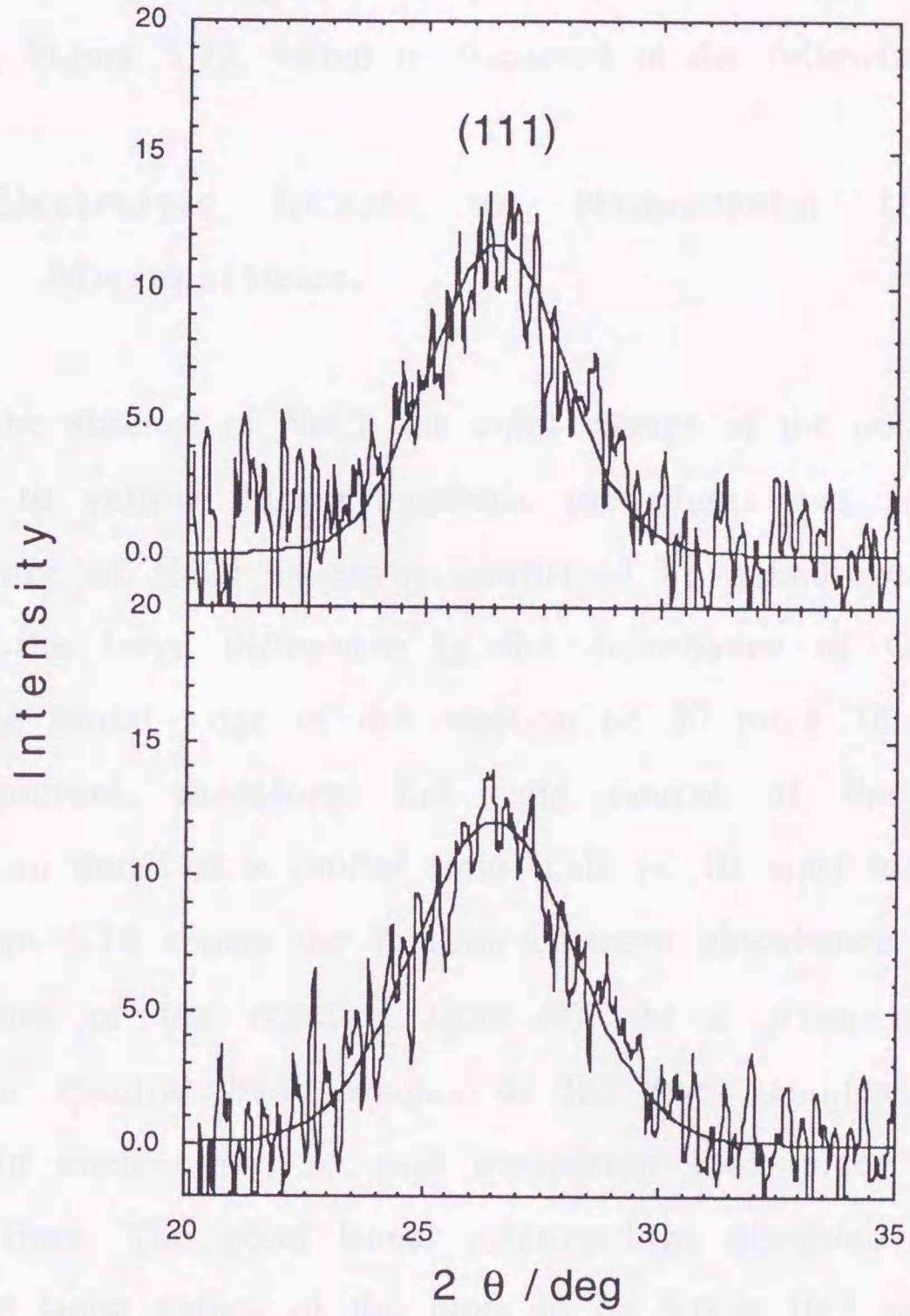

Figure 3.13. XRD diffractograms at around 2θ = 27°. Upper and lower patterns correspond to those of CdS prepared under NaCl free and [NaCl] = 0.5 M conditions, respectively. The solid curves represent Gaussian fits of the patterns.

The characteristic NaCl effects on d_{CdS} would be due to dense distributions of the chelating ligands in the polymer as stabilizing groups, and also to differences in the rate of Na_2S diffusion into the polymer particle. In particular, the diffusion rate of S^{2-} into the Cd^{2+}-polymer particles has been suggested to play an essential role as seen from the results in Figure 3.12, which is discussed in the following sections.

3.4.2 Electrolyte Effects on Nanocrystal Distributions in Polymer Microparticles.

In the absence of NaCl, the color change of the polymer particle from colorless to yellow during synthetic procedures was faster than that in the presence of NaCl as easily confirmed by naked-eyes. In Figure 3.12, actually, the large difference in the absorbance of CdS was observed during the initial stage of the reaction (< 30 min). In order to obtain a clearer picture, therefore, the time course of the absorbance was measured in detail at a shorter time scale (< 10 min) for *samples IIc* and *IId*. Figure 3.14 shows the relation between absorbance at 450 nm and a square root of the reaction time (t). At a given reaction time, the absorption spectral band shapes of the two samples were almost the same with each other, so that nucleation took place according to the reaction time. The good linear relationships observed for both samples afford the slope values of the plots to be 4.6×10^{-3} and 8.9×10^{-3} $s^{-1/2}$ for *samples IIc* and *IId*, respectively. The $(t)^{1/2}$ dependence of the absorbance indicates that S^{2-} ions

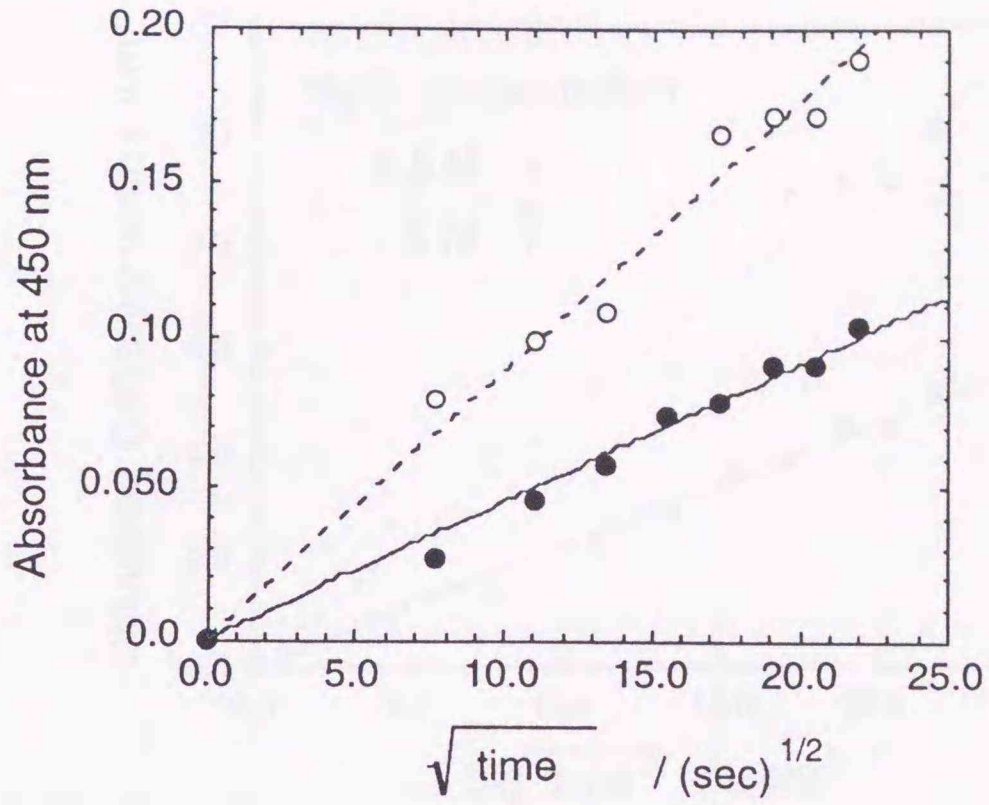

Figure 3.13. Time dependence of CdS absorbance at 450 nm in the initial time region of the reaction ($Cd^{2+} + S^{2-} = CdS$). (•): *sample IIc* ([NaCl] = 0), (o): *sample IId* ([NaCl] = 0.5 M).

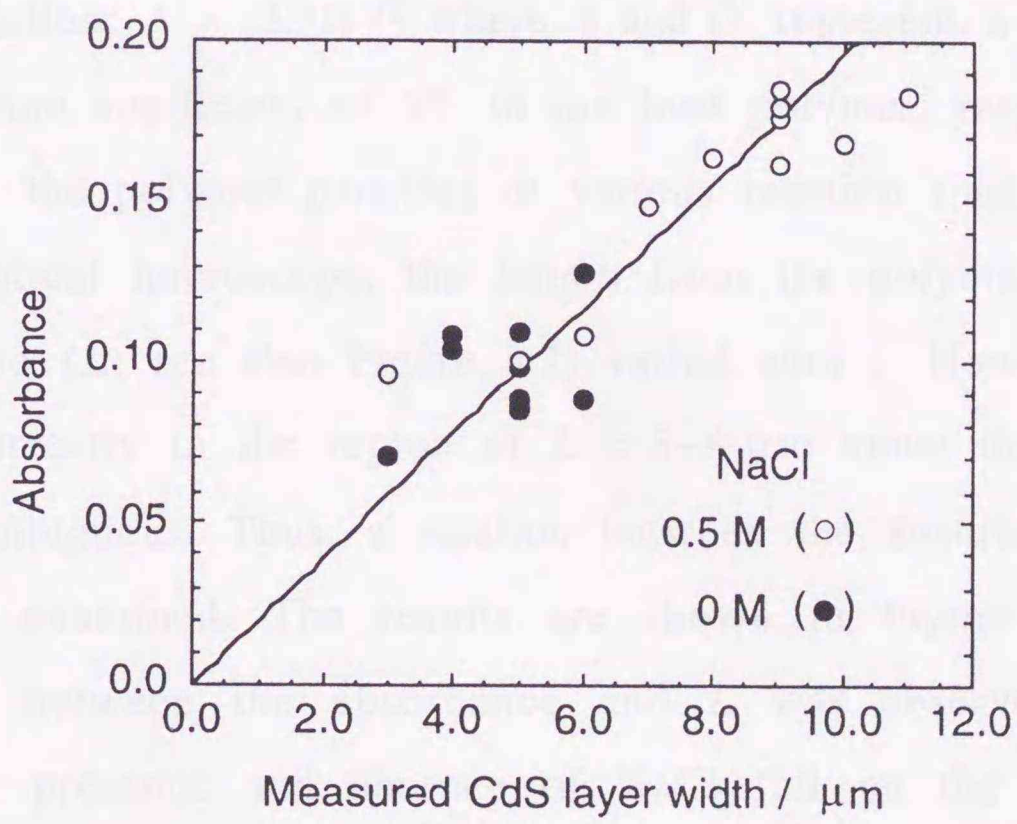

Figure 3.14. Relation between the observed absorbance at 450 nm and *L*.

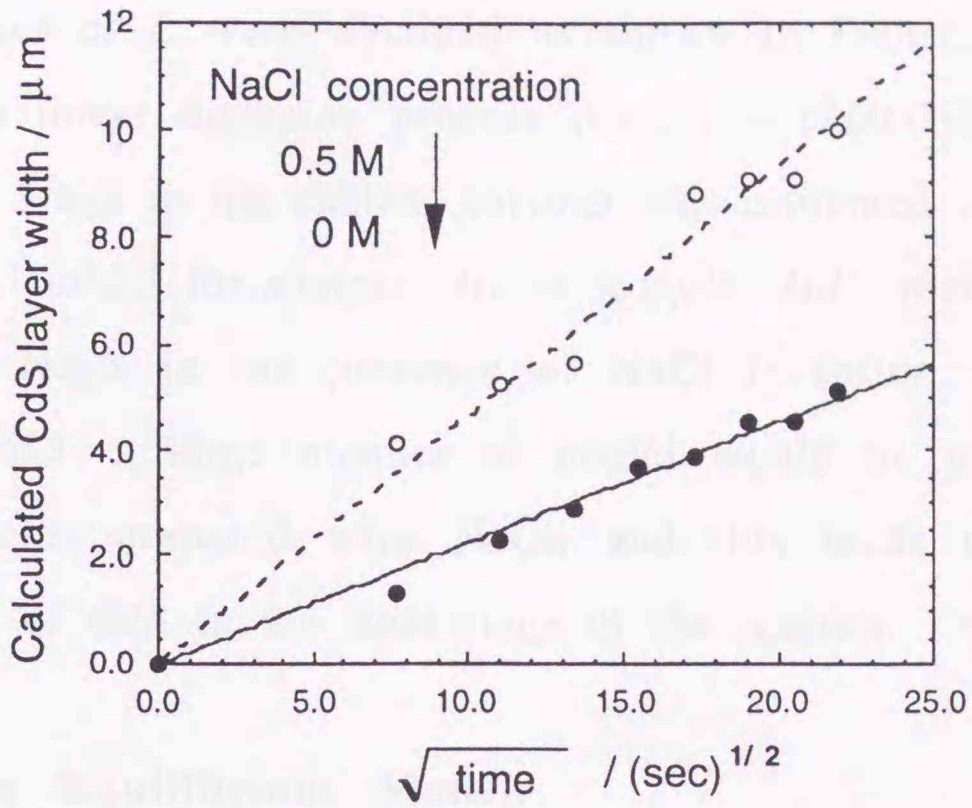

Figure 3.15. Time dependence of L in the initial stage of the reaction. (•): *sample IIc* ([NaCl] = 0), (o): *sample IId* ([NaCl] = 0.5 M).

diffuse into the polymer particle in a quasi-linear fashion as expected from the relation; $\Delta = (2Dt)^{1/2}$ where Δ and D represent a diffusion length and a diffusion coefficient of S^{2-} in the host polymer, respectively.

When the polymer particles at various reaction times were observed under an optical microscope, the length from the polymer surface to the ring structure (L; see also Figure 3.7) varied with t. However, L was not measured correctly in the region of $L < 3\sim4$ μm since the ring boundary was very ambiguous. Thus, a relation between the absorbance at 450 nm and L was examined. The results are shown in Figure 3.14. A linear relationship between the absorbance and L was observed and the data both in the presence and absence of NaCl fall on the same line. The results indicate that L corresponds to the width of CdS nanocrystals distributed in the host polymer and that the density of CdS is the same for both samples. Also, the results demonstrate that L can be calculated from the absorbance at 450 nm. According to Figure 3.13 and 3.14, thus,

the time courses of L were obtained as shown in Figure 3.15. Analyzing the data as a linear diffusion process (i.e., $L = (2Dt)^{1/2}$), the diffusion coefficient of Na_2S in the chelate polymer was estimated to be 2.5×10^{-10} or 1.1×10^{-9} cm^2s^{-1} for *sample IIc* or *sample IId*, respectively. Since diffusion of Na_2S in the presence of NaCl is faster than that in the absence of NaCl, a large number of nuclei would be generated for the polymer particles prepared with NaCl, and this leads to restriction of further growth of CdS in the final stage of the reaction.

3.4.3 Donnan Equilibrium Model.

The electrolyte effects on ionic diffusion in the polymer particles and, thus, those on d_{CdS} and the CdS distributions in the polymer, can be interpreted qualitatively by a Donnan equilibrium model reported by Teorell *et. al.* for charged-membrane systems.[24] According to the model, Donnan potential differences between the water and polymer phases control the rate of Na_2S diffusion in the polymer. Under the present condition, ionic species in the aqueous Na_2S solution are $2Na^+$, SH^- and OH^-.[25] For simplicity, here, the ionic species are assumed to be $2Na^+$ and S^{2-} by considering a charge balance. In the initial stage, Na_2S (Na^+ and S^{2-}) diffuses into the polymer sphere, and an S^{2-} anion reacts with Cd^{2+} to form CdS, while Na^+ becomes free. CdS formation proceeds from the surface to the inner volume of the particle so that Na^+ locates in the surface layer of the particle in the initial stage of the reaction. Without NaCl, thus, Na^+ would distribute to the water phase to generate a Donnan potential difference between the two phases, which makes the potential of the polymer surface to be negative. Moreover, since Na^+ cannot exchange with Cd^{2+} in the chelate polymer, this also contributes to a

generation of a Donnan potential upon distribution of Na^+ into the water phase. Thus, S^{2-} no longer diffuses into the polymer interior due to this potential, and diffusion of the ion in the polymer becomes slow, which is what observed for *samples IIc* (Figure 3.16a). When NaCl is sufficiently added in the water phase, Na^+ and Cl^- ions are distributed into the polymer and this makes the Donnan potential lower than that in the absence of NaCl. Thus, S^{2-} is likely to diffuse into the polymer interior, leading to faster diffusion of S^{2-} for *sample IId* (Figure 3.16b).

(a) *NaCl free*

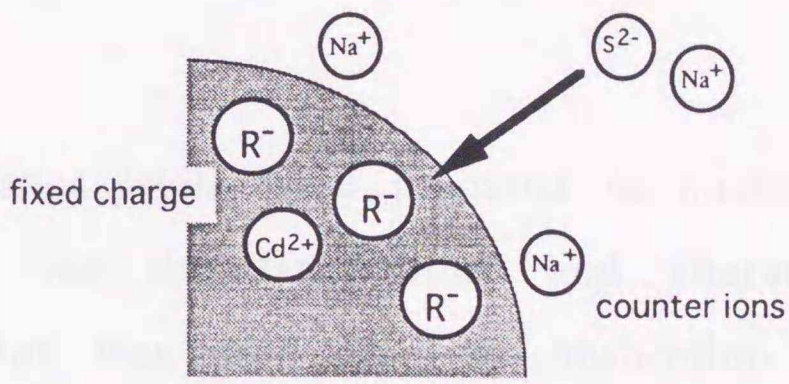

Donnan potential generation

(b) *NaCl*

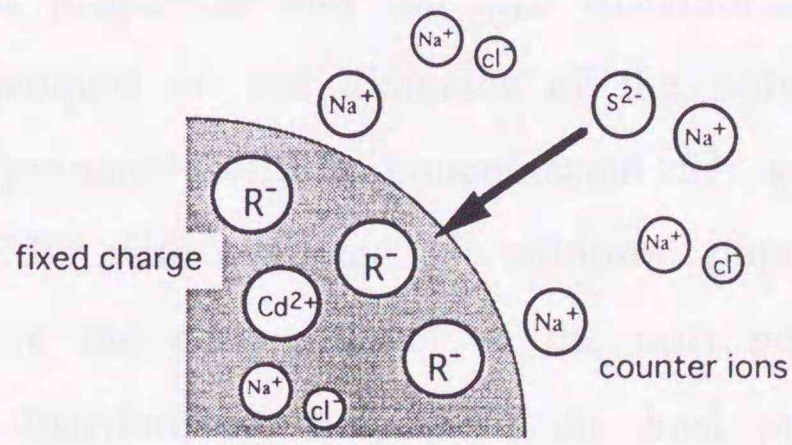

Figure 3.16. Schematic diagrams of the Donnan potential model.

Faster diffusion of S^{2-} into the polymer in the presence of NaCl implies generation of many CdS nuclei. Therefore, small CdS particles are produced quickly (< 2 h as shown in Figure 3.12). Formation of small CdS crystals is proved by the blue-shift of the onset wavelength for *sample IId*. In the absence of NaCl, contrarily, slow diffusion of S^{2-} resulted in slow CdS formation and, thus, relatively large CdS was produced compared to that for *sample IIc*. All the results of the NaCl effects can be thus explained along the single context of the change in the Donnan potential with an added electrolyte and subsequent S^{2-} diffusion.

3.5 Summary

(1) CdS nanocrystals were prepared in micrometer-sized chelate polymer particles for the first time, and characterization of the CdS/polymer hybrids was performed by absorption microspectroscopy, optical microscopy, and TEM measurements. Simulation of the absorption spectral shapes of CdS nanocrystals under an effective mass approximation was also conducted on the basis of the size distributions of the crystals in the polymer, which was estimated by the relevant TEM images. The optical properties and the size distributions of CdS in host polymers were dependent on the diameter of the polymer particle, when the samples were prepared with a concentrated S^{2-} solution. In the case of the reaction of Cd^{2+} with a diluted S^{2-} solution, contrarily, formation of CdS was confined in the surface layer of the host polymer particle with layer-by-layer size distributions. Effects of the host polymer particle size and the concentration of the Na_2S solution on the size distributions and the optical properties of CdS are discussed in terms of the apparent rate of nucleation of Cd^{2+} to CdS.

(2) When the reaction between Cd^{2+}-incorporated chelate polymer and a diluted Na_2S solution was conducted in the presence of NaCl (0.5M), the mean crystal diameter of CdS was shown to be diminished (t > 24 h). In the absence of NaCl, on the other hand, the increase in the mean crystal size was observed after 2 h. Time profiles of CdS formation were thus different; the initial rate of CdS nanocrystal formation was accelerated by an addition of NaCl. The formation rate was proportional to the square root of the reaction time, indicating the difference of diffusion of S^{2-} anions into the polymer particles; the essential origin of the NaCl effects. The results were reasonably explained by the Donnan potential model.

3.6 References and Notes

(1) Yao, H.; Kitamura, N. *Bull. Chem. Soc. Jpn.* **1996**, *69*, 1227.

(2) Shinijima, H.; Yumoto, J. Uesugi, N.; Omi, S.; Asahara, Y. *Appl. Phys. Lett.* **1989**, *55*, 1519.

(3) Alivisatos, A. P. *Science* **1996**, *271*, 933.

(4) Masumoto. Y.; Zimin, L. G.; Naoe, K.; Okamoto, S.; Arai, T. *Mater. Sci. Eng.* **1994**, *B27*, L5.

(5) Colvin, V. L.; Alivisatos, A. P. *J. Chem. Phys.* **1992**, *97*, 730.

(6) Teranishi, T.; Harada, M.; Asakura, K.; Asanuma, H.; Saito, Y. Toshima, N. *J. Phys. Chem.* **1994**, *98*, 7967.

(7) Helfferich, F. *Ion Exchange*; McGraw-Hill, New York, 1962.

(8) Marinsky, J. A. *Ion Exchange*; Marcel Dekker, New York, 1966; Vol 1.

(9) Kitamura, N.; Nakatani, K.; Kim, H.-B. *Pure Appl. Chem.* **1995**, *67*, 79.

(10) Kitamura, N.; Hayashi, M.; Kim, H.-B.; Nakatani, K. *Anal. Sci.* **1996**, *12*, 49.

(11) Roussignol, Ph.; Ricard, D.; Flytzanis, C. *Appl. Phys.* **1990**, *B51*, 437.

(12) Pankove, J. I. *Optical Processes in Semiconductors*; Dover, New York, 1971.

(13) Steigerwald, M. L.; Brus, L. E. *Acc. Chem. Res.* **1990**, *23*, 183.

(14) Nosaka, Y. *J. Phys. Chem.* **1991**, *95*, 5054.

(15) Langer, D. W.; Euwema, R. N.; Era, K.; Koda, T. *Phys. Rev. B: Solid Stete*, **1970**, *B2*, 4005.

(16) Morgan, R. A.; Park, S.-H.; Koch, S. W.; Peyghambarian, N. *Semicond. Sci. Technol.* **1990**, *5*, 544.

(17) In Ref. 11, T_2 was set 15 fs for simulation of the spectrum at low temperature. In the present study, since we measured the absorption spectra at room temperature, discrepancies between the simulated and observed spectra around the band edge were fairly large if we used the value of T_2 at 15 fs. Therefore, we used T_2=10 fs to fit more precisely the spectral band edge.

(18) Vossmeyer, T.; Katsikas, L.; Giersig, M.; Popovic, I. G.; Diesner, K.; Chemseddine, A.; Eychmuller, A.; Weller, H. *J. Phys. Chem.* **1994**, *98*, 7665.

(19) Bard, A. J.; Faulkner, L. R. *Electrochemical Methods. Fundamentals and Applications*; John Wiley & Sons, New York, 1980.

(20) Gerischer, H.; Heller. A. *J. Phys. Chem.* **1991**, *95*, 5261.

(21) Ramsden, J. J. *Surf. Sci.* **1985**, *156*, 1027.

(22) Langford, J. I.; Louer, D. *Powder Diffraction*, **1986**, *1*, 211.

(23) Bawendi, M. G.; Kortan, A. R.; Steigerwald, M. L.; Brus, L. E. *J. Chem Phys.* **1989**, *91*, 7282.

(24) Teorell, T. *Progress Biophysics Biophys. Chem.* **1953**, *3*, 305.

(25) Cotton, F. A.; Wilkinson, G. *Basic Inorganic Chemistry*; *2nd ed.*, John Wiley & Sons, New York, 1987.

Chapter 4. Linear and Nonlinear Optical Properties of CdS and CdSe Nanocrystals Stabilized with Poly(N-vinyl-2-pyrrolidone)[1]

4.1 Introduction

Semiconductor nanocrystals have recently attracted considerable attention because of their mesoscopic enhancement of third-order optical nonlinearities as mentioned in Chapter 1 and 2.[2-5] In relation to the optical nonlinearity, Jain and Lind first reported a large $\chi^{(3)}$ value of 1.3 x 10^{-8} esu for nanometer-sized CdS_xSe_{1-x}-doped glasses by measuring degenerate four-wave mixing (DFWM) signals using a Corning color filter.[6] Saturation properties of DFWM signals and transmission of a 5.0 nm CdS-doped organic polymer film were observed by Wang and Mahler, but they did not determine the $\chi^{(3)}$ value.[7] In Chapter 2 and 3, novel preparation methods of CdS nanocrystals dispersed in polymer matrices have been described. Also, nonlinear optical properties of CdS embedded in the acrylonitrile-styrene copolymer films prepared by the photo-irradiation method have been discussed. In order to elucidate and improve nonlinear optical properties of nanocrystals, however, more systematic studies, including characterization of crystals-polymer film samples, are required. Therefore, linear and nonlinear optical properties of polymer-stabilized CdS are studied in detail. In order to show material differences for an optical nonlinearity, CdSe nanoparticles were also prepared under similar conditions. In particular, the study was focused on CdS and CdSe nanocrystals prepared by an "organo-sol" method.[8] Although a few organic films incorporating CdS or CdSe nanocrystals have been reported,[7,8] their optical nonlinearities have not been clarified compared with those of inorganic ones. Thus it is important to prepare

and characterize optical films incorporating homogeneously CdS or CdSe nanocrystals, which are size-controlled and concentrated in the films.

An organo-sol is a colloid dispersed in an organic solvent. For II-VI binary compounds, preparations in organic solvents such as methanol, 2-propanol and acetonitrile have been reported.[9-11] It is worth to be pointed out that, one of the advantages of preparing nanocrystals in organic solvents is that the distribution of particle sizes is narrower than that in water.[12] Organic solvents are also preferable when nanocrystals are dispersed in organic polymer matrices.

In this chapter, the linear and nonlinear optical properties of CdS and CdSe nanocrystals coated with poly(N-vinyl-2-pyrrolidone) (PVP), prepared by an organo-sol method, are described. Since the role of stabilizers for nanocrystals are not well-known, interactions between the functional groups (conformational interactions) of PVP and CdS nanocrystals were also studied by FT-IR for the first time. The PVP-coated CdS nanocrystals obtained could be densely embedded in organic polymer films similar to the crystals in the acrylonitrile-styrene copolymer or poly(2-hydroxyethyl methacrylate) films. Then large $\chi^{(3)}$ values are expected for these CdS-doped films and will be observed using a resonant DFWM method. The $\chi^{(3)}$ values of nanometer-sized CdSe-doped films were also determined, and the material dependence of the optical nonlinearity was discussed.

4.2. Experimental

4.2.1 Chemicals.

$Cd(NO_3)_2 \cdot 4H_2O$ (99.99%, High Purity Chemicals), $Cd(ClO_4)_2 \cdot 6H_2O$ (GR grade, Soekawa Chemicals), poly(N-vinyl-2-pyrrolidone) (PVP: molecular

weight = 40000, Wako Pure Chemicals), acrylonitrile-styrene (AS) copolymer (Mitsui Toatsu Chemicals, Inc.) and poly(2-hydroxyethyl methacrylate) (PHEMA: Scientific Polymer Inc.) were used as received. Methanol, ethanol, and acetonitrile (GR grade) were used after distillation with calcium hydride under nitrogen atmosphere.

Sodium hydrogen selenide (NaHSe) was prepared by a reaction of selenium (black, High Purity Chemicals) with sodium borohydride ($NaBH_4$, > 95%, Yoneyama Chemical Industries) in ethanol under nitrogen or argon atmosphere, and used to prepare CdSe colloids.[12]

4.2.2 Organo-sol preparation of CdS and CdSe nanocrystals.

CdS nanocrystals in methanol or acetonitrile were prepared as follows. One mL of an H_2S gas was injected into 5 mL of an organic solution containing $Cd(NO_3)_2 \cdot 4H_2O$ (2.0×10^{-4} M) and PVP (0~2 g/L) under vigorous stirring. In the case of a growth-profile observation, the solution was not stirred. The colorless solution turned yellow upon injection of H_2S when methanol was used as a solvent. In acetonitrile, however, the color of the solution did not change.

CdSe nanocrystals were prepared in the following way. After bubbling of an N_2 gas into a stirred 50 mL solution of a Cd salt (2.0×10^{-4} M) and PVP (0~8 g/L) for 20 min, 30 μL of an ethanolic NaHSe solution was injected into the solution. The solution turned red or orange as a result of formation of CdSe nanocrystals.

4.2.3 Preparation of PVP-coated CdS powders.

For the samples prepared by the organo-sol method in the presence of PVP, flocculation of CdS and CdSe nanocrystals can be prevented even if the solvent is evaporated. Two kinds of PVP-coated CdS powders were prepared by evaporating methanol or acetonitrile, in order to study the effect of the polymer functional groups on the properties of CdS through FT-IR measurements. (i) PVP (1.00 g) was dissolved into 150 mL of a $Cd(NO_3)_2$ (3.55×10^{-3} M) methanol solution. With vigorous stirring, 50 mL of an H_2S gas was quickly injected into the solution. After 10 min methanol was removed using a rotary evaporator at 30~35 °C at low pressure. Then *yellow* PVP-coated CdS powder was obtained. The mean particle diameter of CdS was about 6.5 nm, and the standard deviation of the size distribution was about 0.9 nm as judged from the relevant TEM images. (ii) PVP (0.10 g) was dissolved into 50 mL of an acetonitrile solution containing $Cd(NO_3)_2$ (2.0×10^{-4} M). With vigorous stirring, 10 mL of an H_2S gas was quickly injected into the solution. The acetonitrile was removed at low pressure without heating. *White* PVP-coated CdS powder was obtained.

PVP-coated CdSe nanocrystals were also obtained in a similar way by evaporating a colloidal ethanolic solution (2.0×10^{-4} M) which was prepared with PVP (0.08 g/L) without heating.

4.2.4 Preparation of CdS- or CdSe-doped organic polymer films.

In order to obtain optical films containing CdS or CdSe nanocrystals with a high volume fraction, an acrylonitrile-styrene (AS) copolymer or poly(2-hydroxyethyl methacrylate) (PHEMA) was used which could readily dissolve PVP-coated CdS or CdSe nanocrystals. For $|\chi^{(3)}|$ measurements, an AS film was prepared by dissolving (a) 0.008 g, (b)

0.04 g, (c) 0.10 g, or (d) 0.42 g of the *yellow* PVP-coated CdS powder, each containing 0.5 g of the AS copolymer, into 3.0 mL of an N,N-dimethylformamide (DMF) solution. After casting each solution on a glass plate, DMF was evaporated under vacuum and four transparent CdS-doped AS films with different PVP-coated CdS contents were obtained. The thickness of the film (d) was 18 μm for $|\chi^{(3)}|$ measurements, and that of other films was about 100 μm as determined by a micrometer. Preparations of AS films containing the *white* PVP-coated CdS powder were also conducted by similar procedures. However, the AS films turned yellow due to the change in the particle sizes of CdS. Thus, these films were not tested for an optical nonlinearity.

CdS- or CdSe-doped PHEMA films were also used. The *yellow* PVP-coated CdS powder (0.04 g) or PVP-coated CdSe powder was dissolved in a methanol (0.8 mL) solution containing PHEMA (~0.05 g), and dried on quartz plates to prepare thin films.

4.2.5 Apparatus.

Measurements of the resonant third-order nonlinear susceptibility ($|\chi^{(3)}|$) were carried out with a DFWM optical setup of the phase conjugation style, described in section 2.2 and Figure 2.6. Forward pump, back pump, and probe pulses arrive at the sample simultaneously, and the reflectivity R (ratio of the DFWM signal power to the probe power) was measured. The wavelength of both pump and probe laser beams was 465 nm for CdS, and 460 nm for CdSe. The $\chi^{(3)}$ value was calculated from the slope of a square root of a reflectivity-pump intensity plot, based on eq. 2.2.

UV-visible absorption spectra for solution samples were measured in a quartz cell with a 10 mm optical path length using a Shimadzu UV-2200 spectrophotometer. The particle diameter was determined using a Hitachi H-300 transmission electron microscope. FT-IR spectra were recorded using a JASCO FT/IR-8300 spectrometer. As a sample, one drop of the solution containing the PVP-coated CdS powder (*yellow* and *white*) was first placed on a CaF_2 plate and the solvent was immediately evacuated by flowing a dry N_2 gas stream.

4.3. Results and Discussion

4.3.1 Stabilizing effect of PVP for CdS nanocrystals.

Figure 4.1 shows absorption spectra of methanol and acetonitrile solutions of CdS (2.0×10^{-4} M) - PVP (2.0 g/L) colloids measured in a 10 mm optical pathlength cuvette. A well-defined peak at around 330 nm was observed for the acetonitrile solution, indicating a narrow size distribution of CdS nanocrystals. The CdS diameter estimated from the absorption peak using the tight-binding approximation[14] was about 2.0 nm. In the case of the methanol solution, a broad and structureless spectrum was observed in marked contrast to the spectrum in acetonitrile. These colloids did not coagulate so that more detailed experiments were possible. Thus the concentration effect of PVP on the absorption onset of the CdS nanocrystals was studied in detail. Absorption spectra of the CdS nanocrystals at various PVP concentrations in acetonitrile are shown in Figure 4.2. The onset of absorption was blue-shifted with increasing the PVP concentration, which could be explained in terms of the quantum size effect as discussed in detail below.

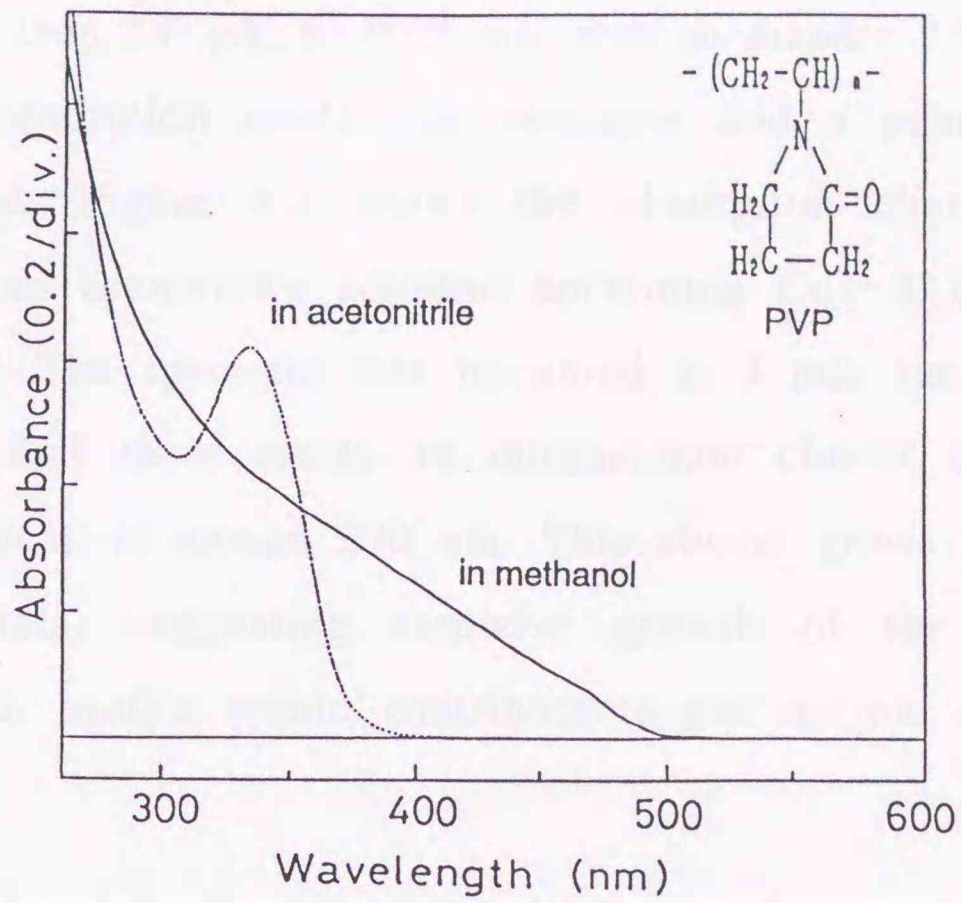

Figure 4.1. Absorption spectra of CdS nanocrystals prepared with PVP (2.0 g/L) in methanol (solid line) and acetonitrile (doted line). The inset shows the structure of PVP.

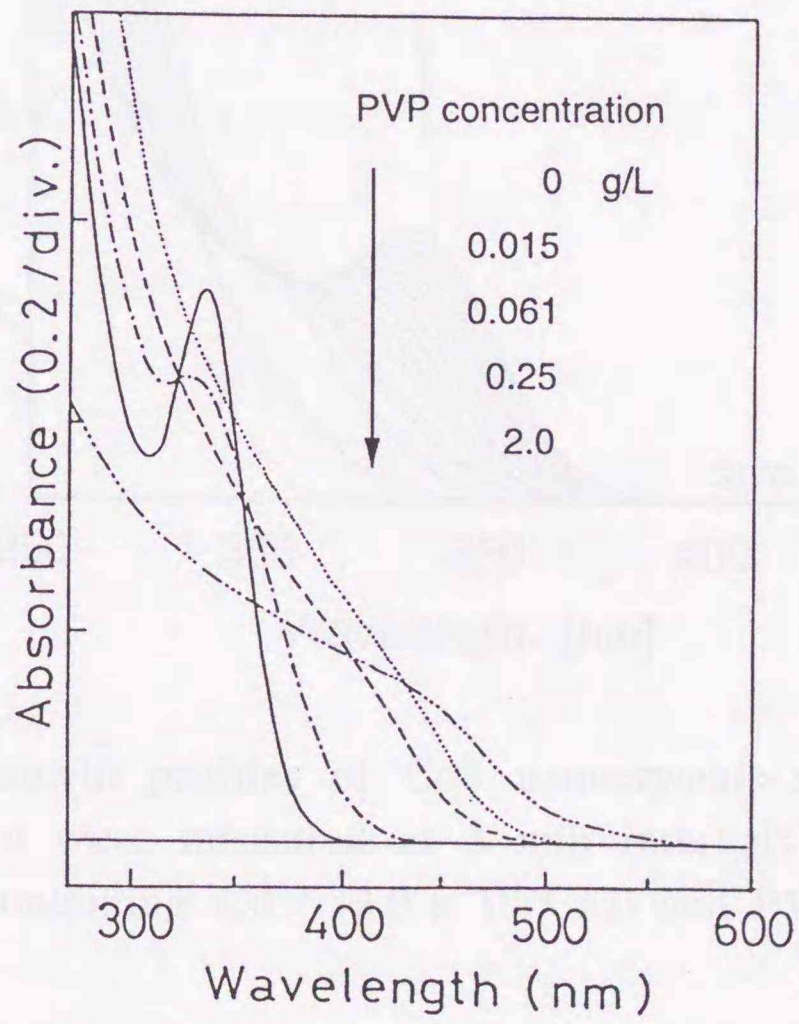

Figure 4.2. Absorption spectra of CdS nanocrystals in acetonitrile with various PVP concentrations.

When more than 2.0 g/L of PVP was used to prepare 2.0×10^{-4} M CdS colloids, the absorption onset was saturated and a peak shift was no longer detected. Figure 4.3 shows the absorption changes after H_2S injection into an acetonitrile solution containing Cd^{2+} (2.0×10^{-4} M) and PVP (8.0 g/L). The spectrum was measured at 3 min intervals. The time course shows that there exists an intermediate cluster characterized by an absorption peak at around 270 nm. This cluster grows to form 2.0 nm CdS nanocrystals, suggesting stepwise growth of the particles. The stepwise growth profile would contribute to the narrow size distribution of CdS.

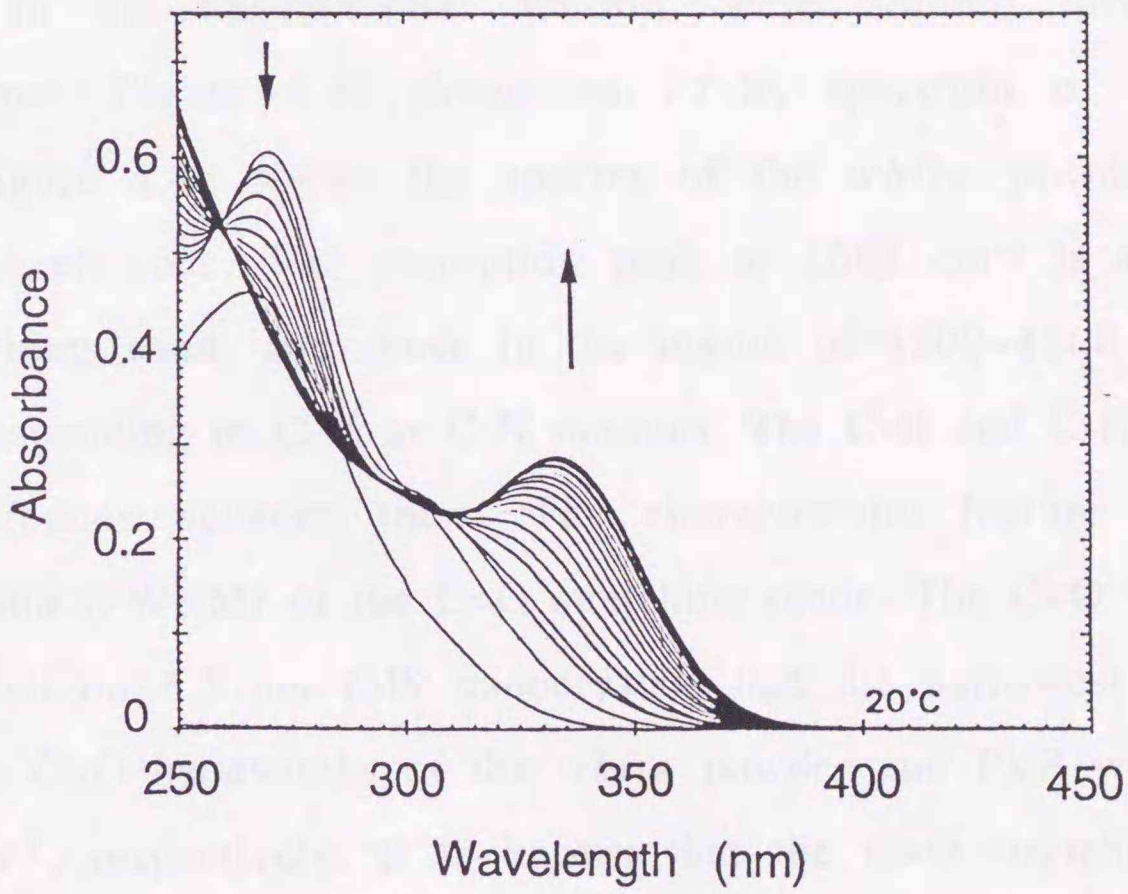

Figure 4.3. Growth profiles of CdS nanocrystals stabilized with PVP. Changes of spectra were measured at 3 min intervals after injecting H_2S into acetonitrile containing Cd^{2+} (2.0×10^{-4} M) and PVP (8.0 g/L).

In the case of a methanol solution, the change in the absorption spectrum was negligible in the PVP concentration range of 0~8 g/L. PVP was found

to play a role in controlling the particle size of CdS nanocrystals under the influence of the solvent. Taking also the concentration effect of PVP into consideration, the dissolved state of PVP, namely, conformational interactions of the PVP chains in organic solvents, would play an decisive role in the size control.

It is important to understand the properties of PVP in the vicinity of the surface of CdS nanocrystals in order to control the particle size and the inorganic/organic interfaces. CdS nanocrystals prepared by the organo-sol method were very stable, and they did not flocculate even under a concentrated (> 0.1 M) condition. Therefore the two PVP-coated CdS powders (*yellow*: coat on 6.5 nm CdS, and *white*: coat on 2.0 nm CdS), described in the experimental section, were studied through FT-IR measurements. Figure 4.4a shows an FT-IR spectrum of the *yellow* powder. Figure 4.4b shows the spectra of the *white* powder and PVP alone as a reference. The absorption peak at 1682 cm^{-1} is assigned to a C=O stretching band, and those in the region of 1500~1200 cm^{-1} to the bands corresponding to C-H or C-N motions. The C-H and C-N bands show little differences between them. The characteristic feature appeared at the bandwidth (FWHM) of the C=O stretching mode. The C=O band of PVP which coated on 6.5 nm CdS nanocrystals had the narrowest width (~30 cm^{-1}). The C=O bandwidths of the *white* powder and PVP were about 37 and 43 cm^{-1}, respectively. It is known that the C=O stretching mode of PVP depends upon its configuration through changes in the surroundings.[15] The bandwidth of the C=O stretch reflects the degree of self-association of the lactam groups owing to the interactions between chain conformations, and it increases with increasing the self-association interaction.[15]

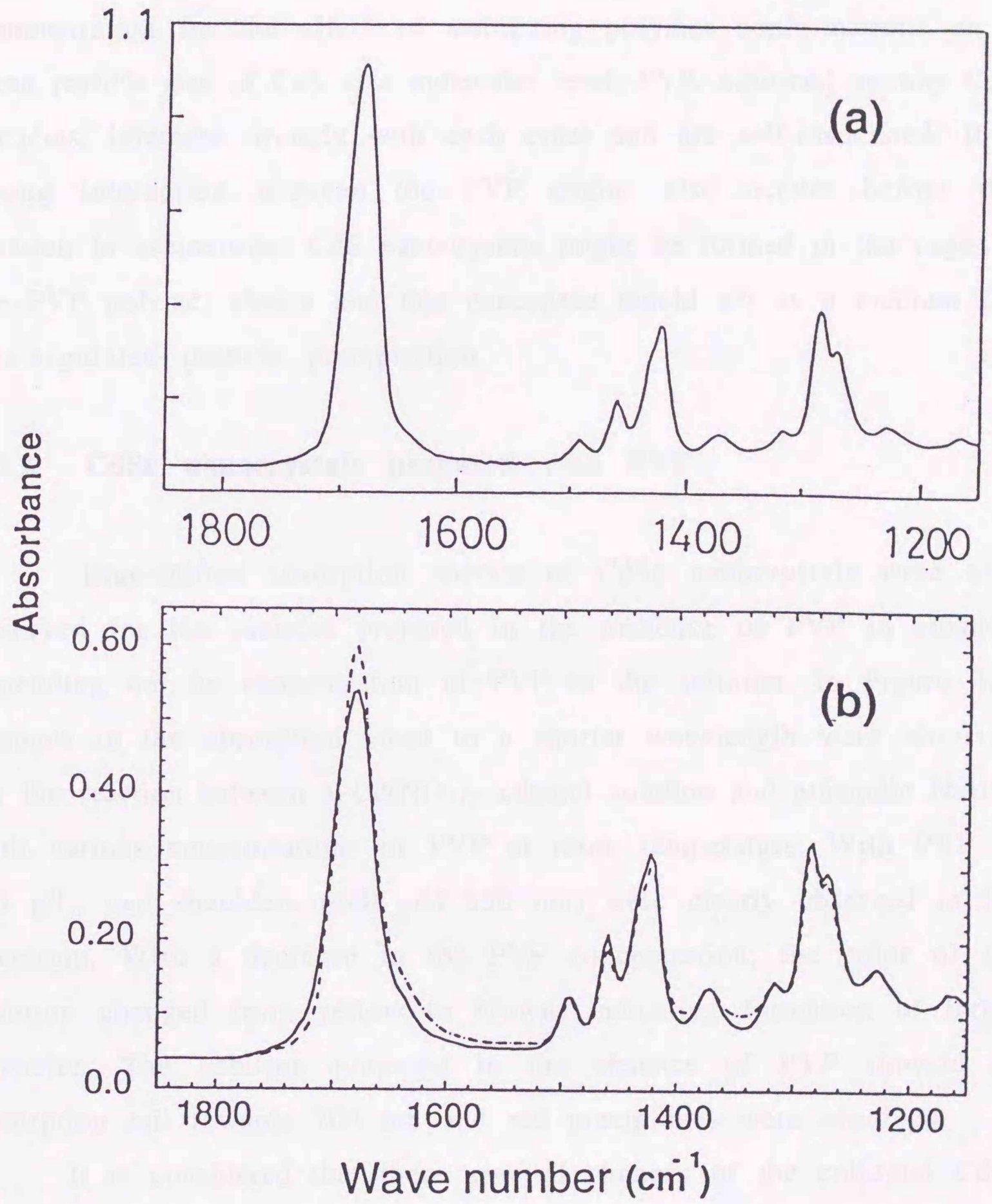

Figure 4.4. (a) FT-IR spectrum of *yellow* PVP-coated CdS powder (6.5 nm CdS coating). (b) FT-IR spectra of PVP (dot) and *white* PVP-coated CdS powder (2.0 nm CdS coating: solid).

Thus this band narrowing indicates that associated lactam species disappear due to adsorption on the surface of large CdS nanocrystals. The FT-IR spectra of the PVP-coated CdS nanocrystals are the first demonstration for the effect of stabilizing polymer conformations on a mean particle size of CdS at a molecular level. PVP, adsorbed on tiny CdS particles, interacts strongly with each other and are self-associated. If a strong interaction between the PVP chains also occurs before the reaction in acetonitrile, CdS nanocrystals might be formed in the cage of the PVP polymer chains and this nanospace would act as a medium for size-regulated particle precipitation.

4.3.2 CdSe nanocrystals prepared with PVP.

Blue-shifted absorption spectra of CdSe nanocrystals were also observed for the samples prepared in the presence of PVP in ethanol, depending on the concentration of PVP in the solution. In Figure 4.5, changes in the absorption onset to a shorter wavelength were observed for the reaction between a $Cd(NO_3)_2$ ethanol solution and ethanolic NaHSe with various concentrations of PVP at room temperature. With PVP of 8.0 g/L, two shoulders (400 and 350 nm) were clearly observed in the spectrum. With a decrease in the PVP concentration, the color of the solution changed from yellow to brown, indicating formation of larger particles. The solution prepared in the absence of PVP showed an absorption tail towards 700 nm and red precipitates were observed.

It is considered that these spectral changes of the colloidal CdSe solutions are due to the quantum size effect, which has been also observed in the case of the CdS organo-sol samples. The spectrum of

CdSe prepared with 8.0 g/L of PVP is almost the same as that of "small" CdSe nanocrystals prepared at -80 °C in methanol.[16]

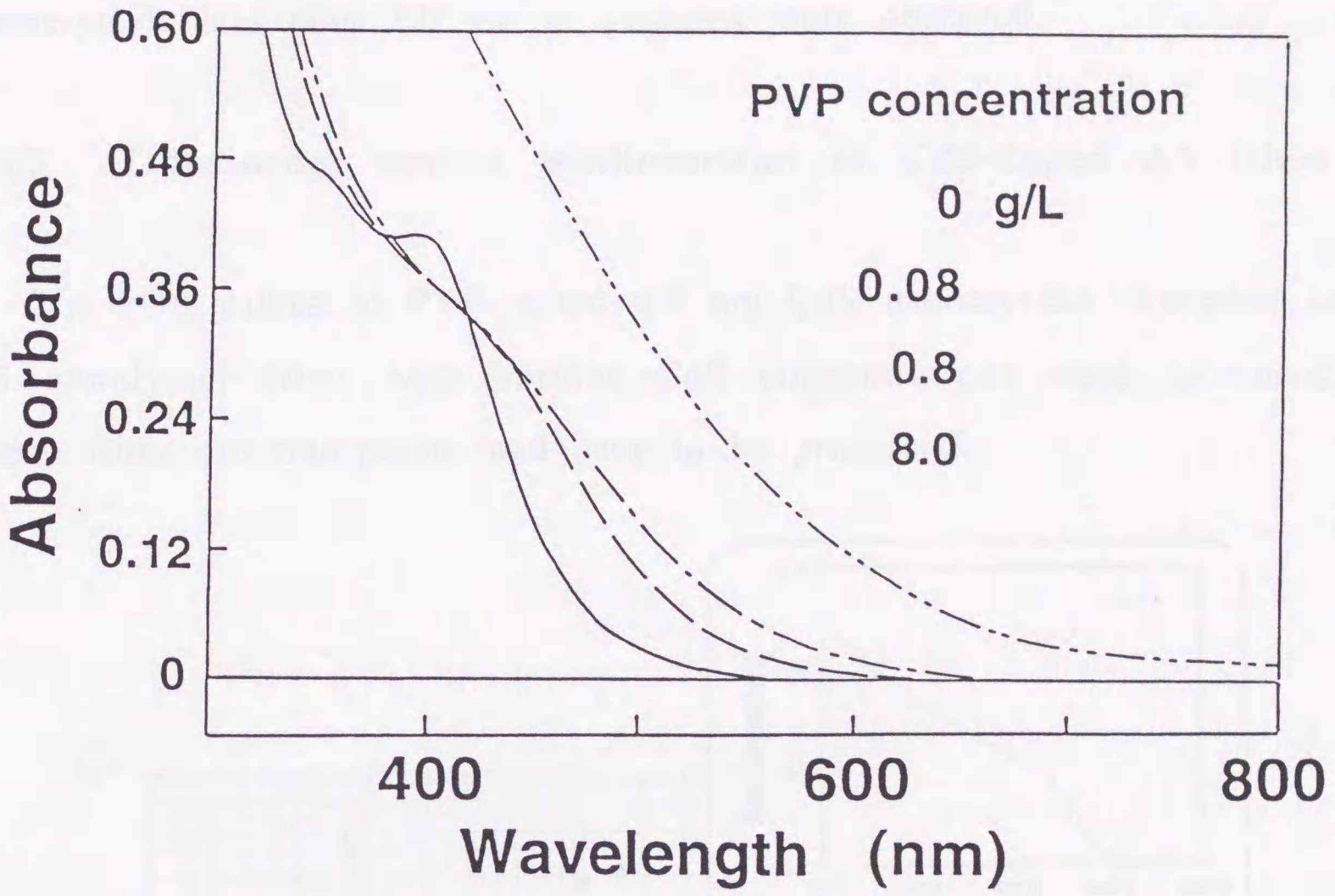

Figure 4.5. Absorption spectra of CdSe nanocrystals in ethanol with various PVP concentrations.

The spectrum prepared without PVP is also similar to that of "large" particles prepared with PVA (polyvinyl alcohol) in water at room temperature.[16] PVP showed the same effect on the stabilization of CdSe nanocrystals with CdS. A shoulder at around 350 nm was also observed for the smallest CdSe nanocrystals. This energy is about 0.45 eV higher than that of the peak at 400 nm, indicating a $1S_e$-$1S_h$ transition with the hole in the spin-orbit-split valence band.[17] TEM images of CdSe nanocrystals prepared with 8.0 g/L or 0.8 g/L of PVP in ethanol were not obtained, since small nanocrystals were adhered by the thick PVP

lumps. However, their diameters were estimated to be ~1.4 and ~1.8 nm, for the samples with 8.0 and 0.8 g/L, respectively, by empirical pseudopotential calculations.[18] In a colloid with 0.08 g of PVP, CdSe nanocrystals less than 2.0 nm in diameter were observed.

4.3.3 Third-order optical nonlinearities of CdS-doped AS films

The $|\chi^{(3)}|$ values of PVP-coated 6.5 nm CdS nanocrystals dispersed in AS copolymer films with various CdS concentrations were measured. These films are transparent and easy to be processed.

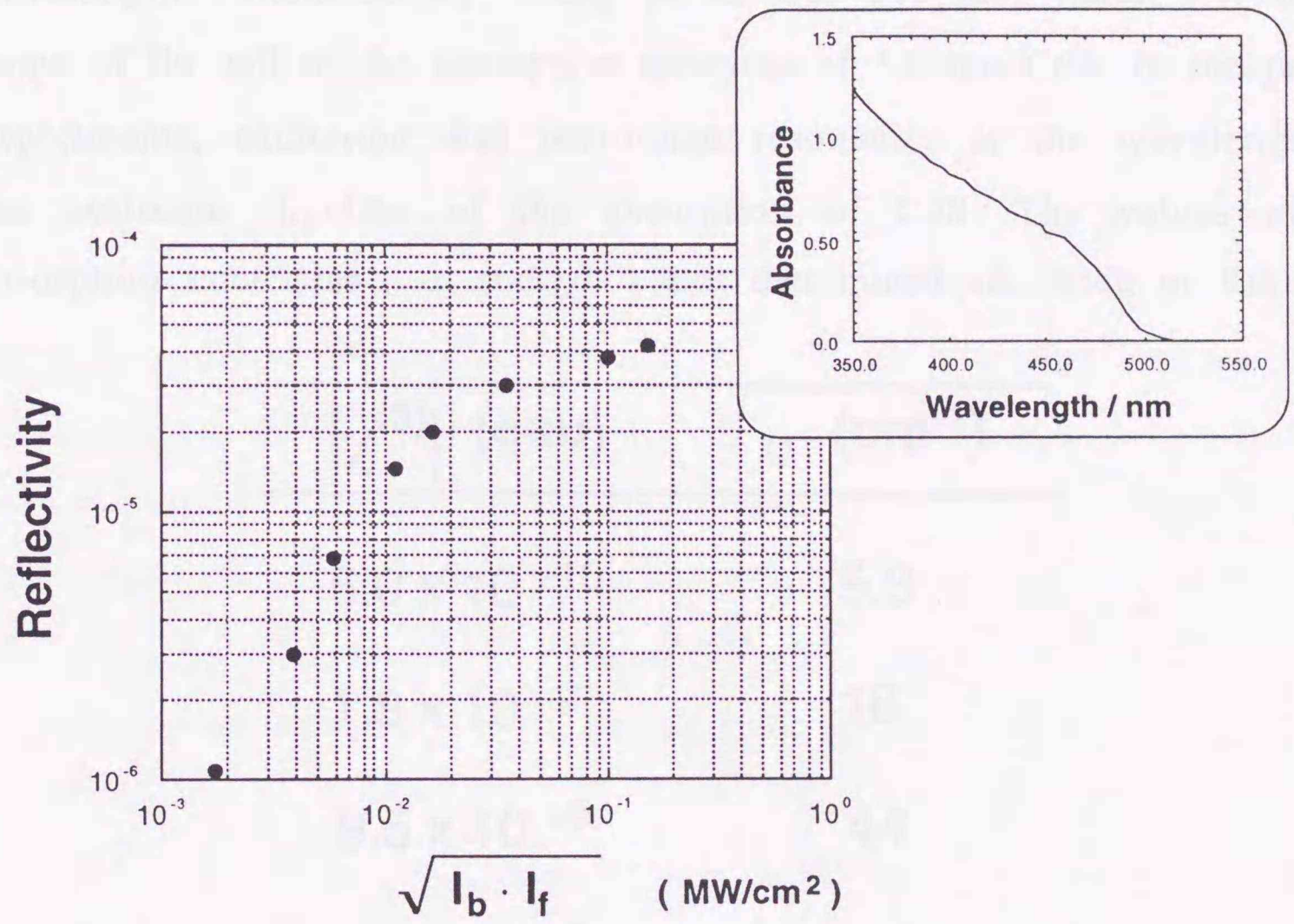

Figure 4.6. DFWM reflectivity of 6.5 nm CdS nanocrystals dispersed in an AS copolymer film. The inset shows the absorption spectrum of the film used for the measurements.

Figure 4.6 shows typical data of a relationship between the DFWM reflectivity (R) and a pump intensity $(I_b I_f)^{1/2}$ for the film (c) (sample with 0.1 g of *yellow* PVP-coated CdS, film thickness: 105 μm) together with the relevant absorption spectrum. The reflectivity was saturated above the pump intensity of 0.02 MW/cm^2. $|\chi^{(3)}|$ was obtained from the slope of the curve below the intensity of 0.02 MW/cm^2, at which a quadratic dependence of the reflectivity was observed. The saturation intensity was about one hundred times lower than that of the 5.0 nm-CdS sample obtained by Wang and Mahler.[7] The discrepancy in the saturation intensity is mainly caused by a pump wavelength. The pump wavelength conducted by Wang *et al.* was 505 nm, which was in the range of the tail of the absorption spectrum of 5.0 nm CdS. In the present experiments, excitation was performed resonantly at the wavelength of the excitonic shoulder of the absorption of CdS. The values of the absorption coefficient, α, and $|\chi^{(3)}|$ thus determined are listed in Table I.

$\lvert\chi^{(3)}\rvert$ (esu)	α (cm^{-1})
5.0×10^{-10}	5.3
1.8×10^{-9}	16
9.5×10^{-9}	44
6.0×10^{-8}	140

Table I. $|\chi^{(3)}|$ values of AS copolymer films with various concentrations of 6.5 nm CdS nanocrystals.

The values increased with increasing the concentration of PVP-coated CdS nanocrystals in the AS film. The TEM images of the cross section of the film (d), which had the highest density of CdS in the film, indicated that the volume fraction of CdS nanocrystals in the AS copolymer was about 1.0 %, and relevant $|\chi^{(3)}|$ value was ~ 6.0 x 10^{-8} esu. The large optical nonlinearities were originated substantially from the state filling of an electron-hole pair (exciton bleaching) in the CdS nanocrystals.[19]

4.3.4 Third-order optical nonlinearities of CdS- or CdSe-doped PHEMA films

CdS (6.5 nm in diameter) or CdSe (2.0 nm in diameter) nanocrystals dispersed in PHEMA were also prepared to measure $|\chi^{(3)}|$ values. The advantages of using this polymer are as follows. (i) The polymer can be dissolved in alcoholic solvents. Since PVP-coated CdS nanocrystals are more soluble in alcoholic solvents than in DMF, high loading of the particles into PHEMA is possible. (ii) PHEMA is insoluble in water. Films, resistant to a humidity, were easily obtained. $|\chi^{(3)}|$ of the CdS-doped PHEMA films (volume fraction: ~4%) with a thickness of 10 μm was 1.1 x 10^{-7} esu (α~560 cm^{-1}). To our knowledge, this is the largest value for semiconductor nanocrystals dispersed in organic matrices.

$|\chi^{(3)}|$ of the CdSe-doped PHEMA films was 3.9 x 10^{-11} esu. The absorption coefficient of the film was 20.7 cm^{-1} at 460 nm, indicating low loading of particles. The reflectivity of the signal did not saturate below a power density of 0.3 MW/cm^2, which was about ten times larger than that for CdS-doped organic films, and about two orders of magnitude smaller than that for CdSe-doped inorganic glasses.[20] The reasons were not clear, but the results are probably due to the poor

crystallinity of the particles. $|\chi^{(3)}|$ value of the CdSe colloidal solutions with a similar absorption coefficient was also determined to be about 3.0 x 10^{-11} esu.

Comparing organic and inorganic hosts for semiconductor nanocrystals, organic hosts are preferable since identical semiconductor nanocrystals can be embedded more easily in various organic host polymers. Since the organic polymer network structures are different from glass structures, microscopic environments around the nanocrystals will differ. Functional groups of the host polymer chain can be changed. This is different from the case of a glass host, since glasses consist mostly of oxides. Thus when an electron (hole) affinity of the functional group is varied, the band offset of the polymer (electronic energy levels of the ground and the excited state) would also be widely controlled. For instance, the penetration of the electron wave function outside the potential wall was affected by the polymer chain and its functional groups.[21] In the case of glass matrices, a selection of materials to control a band offset is restricted. In the present experiments, the same PVP-coated CdS nanocrystals were dispersed in different host polymers; AS copolymer and PHEMA. The functional groups of the host polymers were different. The $|\chi^{(3)}|/\alpha$ value was reduced by a factor of ~0.5 under the condition of a high nanocrystal concentration. Therefore the measured optical nonlinearity was probably related to the interaction between the surface state of CdS nanocrystals and the host polymers. According to Wang and Herron,[22] generation of a surface-trapped electron is effective to obtain large third-order optical nonlinearities, since it is capable of localizing the hole, which induces efficient exciton bleaching. Since an electron was reported to be surface-trapped within 1 ns for CdS

nanocrystals,[23] the contribution of a surface-trapped electron-hole pair to the observed nonlinearities was reasonable.

It is worth investigating the method of dispersing semiconductor nanocrystals densely into "organic" hosts for novel nonlinear optical materials.

4.4 Summary

(1) CdS and CdSe nanoparticles were prepared in organic solvents in the presence of poly(N-vinyl-2-pyrrolidone) (PVP). PVP plays an essential role in preventing the flocculation of concentrated nanoparticles (> 0.1 M), and in controlling the particle size under the influence of the solvent used. FT-IR measurements were performed to study the effect of the functional groups of PVP on particle size control at molecular levels.

(2) The PVP-coated CdS and CdSe nanoparticles obtained were dispersed in acrylonitrile-styrene (AS) copolymer or poly(2-hydroxyethyl methacrylate) (PHEMA) organic films, and third-order nonlinear optical susceptibilities $|\chi^{(3)}|$ of these films were measured. Differences for the optical nonlinearity between the organic hosts (present work) and the inorganic ones (mostly examined previously by others) were described.

4.5 References and Notes

(1) Yao, H.; Takahara, S.; Mizuma, H.; Kozeki, T.; Hayashi, T. *Jpn. J. Appl. Phys. part 1* **1996**, *35*, 4633.

(2) Park, S. H.; Morgan, R. A.; Hu, Y. Z.; Lindberg, M.; Koch, S. W.; Peyghambarian, N. *J. Opt. Soc. Am.* **1990**, *B7*, 2097.

(3) Gabel, A.; DeLong, K. W.; Seaton, C. T.; Stegeman, G. L. *Appl. Phys. Lett.* **1987**, *51*, 1682.

(4) Shinojima, H.; Yumoto, J.; Uesugi, N. *Appl. Phys. Lett.* **1992**, *60*, 298.

(5) Steigerwald, M. L.; Brus, L. E. *Acc. Chem. Res.* **1990**, *23*, 183.

(6) Jain, R. K.; Lind, R. C. *J. Opt. Soc. Am.* **1983**, *73*, 647.

(7) Wang, Y.; Mahler, W. *Opt. Commun.* **1987**, *61*, 233.

(8) Misawa, K.; Yao, H.; Hayashi, T.; Kobayashi, T. *J. Chem. Phys.* **1991**, *94*, 4131.

(9) Rossetti, R.; Hull, R.; Gibson, J. M.; Brus, L. E. *J. Chem. Phys.* **1985**, *82*, 552.

(10) Fojtik, A.; Weller, H.; Koch, U.; Henglein, A. *Ber. Bunsenges. Phys. Chem.* **1984**, *88*, 969.

(11) Ramsden, J. J.; Webber, S. E.; Grätzel, M. *J. Phys. Chem.* **1985**, *89*, 2740.

(12) Rossetti, R.; Ellison, J. L.; Gibson, J. M.; Brus, L. E. *J. Chem. Phys.* **1984**, *80*, 4464.

(13) This reaction is necessary for trapping hydrogen selenide (H_2Se), a strong poison gas, for safety. A H_2Se gas was generated with sodium diselenide (Na_2Se_2), which was dark red in ethanol if the ratio of reactants was stoichiometrically different from the reaction. Care should be taken to ensure the purity of $NaBH_4$ and perfect mixing of the reactants.

(14) Lippens, P. E.; Lannoo, M. *Phys. Rev.* **1989**, *B39*, 10935.

(15) Rothschild, W. G. *J. Am. Chem. Soc.* **1972**, *94*, 8676.

(16) Chestony, N.; Hull, R.; Brus, L. E. *J. Chem. Phys.* **1986**, *85*, 2237.

(17) Bawendi, M. G.; Wilson, W. L.; Rothberg, L.; Carroll, P. J.; Jedju, T. M.; Steigerwald, M. L.; Brus, L. E. *Phys. Rev. Lett.* **1990**, *65*, 1623.

(18) Borman, B.; Ramakrishna, M. V.; Friesner, R. A. *J. Phys. Chem.* **1995**, *99*, 7649.

(19) Schmitt-Rink, S.; Miller, D. A. B.; Chemla, D. S. *Phys. Rev.* **1987**, *B35*, 8113.

(20) Omi, S.; Hiraga, H.; Uchida, K.; Hata, C.; Asahara, Y.; Ikushima, A. J.; Tokizaki, T.; Nakamura, A. *CLEO91 Tech. Digest* (1991) Vol. 10, CTuE2.

(21) Nosaka, Y. *J. Phys. Chem.* **1991**, *95*, 5054.

(22) Wang, Y.; Herron, N. *J. Phys. Chem.* **1991**, *95*, 525.

(23) Serpone, N.; Sharma, D. K.; Jamieson, M. A.; Grätzel, M.; Ramsden, J. *Chem. Phys. Lett.* **1985**, *115*, 473.

Chapter 5. Third-order Optical Nonlinearities of CdS and Metal Nanoparticles Co-Dispersed in Polymer Matrices - Surface Modification Effect[1]

5.1 Introduction

In Chapter 4, the value of $\chi^{(3)}$ of CdS nanoparticles in organic hosts, whose origin was come from an electron-hole pair bleaching of CdS, were determined. In this chapter, enhancement of an optical nonlinearity is examined by controlling the bleaching efficiency. Metal particles are well studied in terms of excitation of surface plasmon. In relation to metal nanocrystals, surface-enhanced Raman scattering (SERS) is an attractive phenomenon. When molecules are adsorbed on noble metal surfaces of the colloids, the Raman scattering intensity was enhanced to $10^4 \sim 10^8$ times larger.[2,3] This effect was explained by local field enhancement near the metal surfaces due to surface plasmon excitation.[4] Absorption enhancement is also expected with similar mechanisms. According to a simple Maxwell-Garnett model, an effective dielectric constant of a metal-medium composite (ε_{MG}) is described as in eq. 5.1,

$$\varepsilon_{MG} = \varepsilon_h \left(\frac{3 + 2f\alpha}{3 - f\alpha} \right) \qquad (5.1)$$

where ε_h, f, and α represent a dielectric constant of the medium, a volume fraction of the metal nanocrystals, and a dielectric constant of the metal nanocrystals, respectively.[5] α is a function of ε_m, ε_d, and ε_h (ε_m and ε_d describe the dielectric constants of bulk metal and adsorbed molecules, respectively), and also of a shape of the metal particle.

Enhancement is induced through α originated by plasmon resonant excitation.

As described in the preceding chapters, linear and nonlinear optical properties of CdS nanocrystals embedded in polymer matrices have been studied. To obtain larger optical nonlinearity and examine the mechanism, the local field enhancement of silver metal nanoparticles in the vicinity of co-dispersed CdS nanocrystals can be employed. Poly(N-vinyl-2-pyrrolidone) (PVP) also stabilizes Ag nanoparticles. Thus, preparations and characterizations of CdS/Ag nanocrystals were performed by the organo-sol method described in chapter 4. In spite of exaggerate efforts, most of the silver particles changed into Ag_2S particles when Ag particles were added into a CdS organo-sol solution to prepare organic films. However, the effect of the addition of Ag nanoparticles or Ag^+ ions on linear and nonlinear optical properties were examined, and enhancement of the third order optical nonlinearity per unit absorption coefficient was observed. In this chapter, the origin of the nonlinearity will be discussed in terms of the CdS surface modification.

5.2 Experimental

5.2.1 Synthesis.

$Cd(NO_3)_2 \cdot 4H_2O$ (99.99%, High Purity Chemicals), $AgNO_3$ (GR grade, Junsei chemical), $NaBH_4$ (GR grade, Junsei Chemical), methanol (GR grade, Kokusan Chemicals), poly(N-vinyl-2-pyrrolidone (PVP; Mw = 40000, Wako Pure Chemical), and poly(2-hydroxyethyl methacrylate) (PHEMA; Scientific Polymer Products) were used as received.

CdS nanocrystals of about 6.0 nm in diameter were prepared in the following procedures, which were quite similar to those described in chapter 4. A small excess of an H_2S gas was injected into a methanol solution containing $Cd(NO_3)_2$ (5.48×10^{-4} mol) and PVP (1.0 g) under vigorous stirring. This method has an advantage in controlling the particle size of semiconductor colloids by changing a solvent used and the PVP concentration as described in the previous chapter. A PVP-coated CdS powder (~6.0 nm in diameter) was obtained by evaporating methanol at 30~35 °C under reduced pressure. This powder contains 6.67 wt% CdS.

Nanometer-sized CdS doped PHEMA films were prepared as follows (sample CdS/PHEMA). The PVP-coated CdS powder (0.01 g) was dissolved into 1.0 mL of methanol, and 0.15 mL of a PHEMA/methanol solution was added. Though the solution was turbid at this stage, evaporation of a small amount of methanol made it viscous and transparent. The viscous solution was casted on a glass sheet substrate, and dried slowly to obtain a clear film with a flat surface. The film thickness was 50 μm.

Silver nanoparticles were prepared by reduction of Ag^+ with sodium borohydride in a methanol solution. 50 mL of $NaBH_4$/methanol (2.38×10^{-2} M) was added into the methanol solution (200 mL) containing $AgNO_3$ (1.18×10^{-3} mol) and PVP (1.0 g) under vigorous stirring. A plasmon peak was appeared at around 400 nm. A PVP-coated Ag powder was obtained by evaporating methanol in a similar way of preparing the PVP-coated CdS powder. The size distribution was in the range of 5.0~15 nm.

PHEMA films co-dispersed with CdS and Ag nanocrystals were also prepared. After mixing the PVP-coated CdS powder, the PVP-coated Ag

powder, and PHEMA in methanol to obtain a viscous solution with a precaution mentioned above, the solution was casted on a glass sheet, and the solvent was evaporated. The mole fraction of Ag in the film was controlled, and samples *CdS/Ag^{p}(1), CdS/Ag^{p}(2), and CdS/Ag^{p}(3)* were obtained with ratios of Ag to CdS of 4.28, 8.57, 17.1 wt%, respectively. As references, PHEMA films containing both CdS nanocrystals and Ag^+ were prepared. $AgNO_3$ was used as a source for Ag^+ ions. The ratios of Ag^+ to CdS were 4.28, 8.57, 17.1 and 85.7 wt % for samples *CdS/Ag$^+$(1), CdS/Ag$^+$(2), CdS/Ag$^+$(3), and CdS/Ag$^+$(4)*, respectively. Preparation procedures are schematically shown in Figure 5.1.

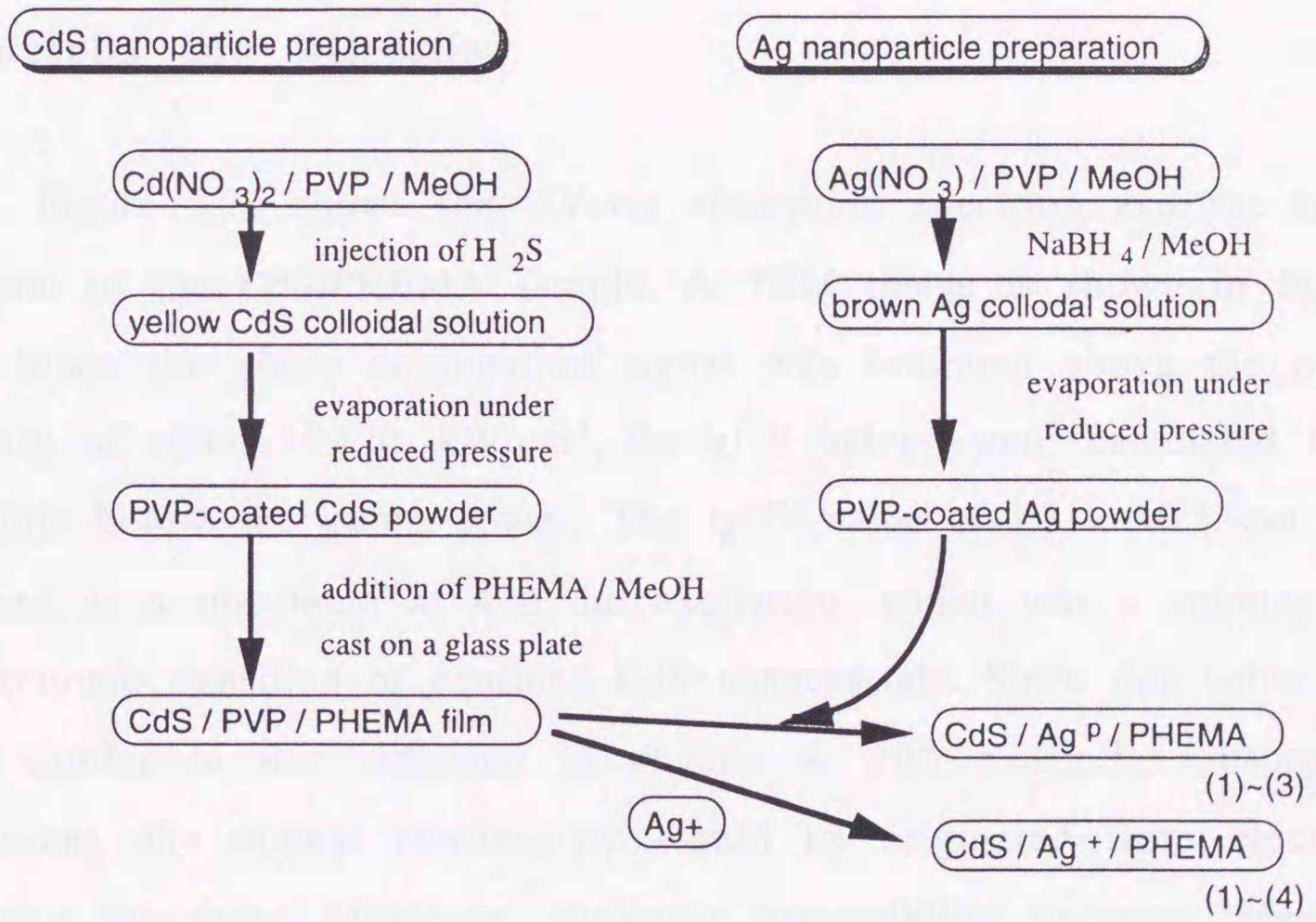

Figure 5.1. Schematic diagrams of preparation procedures of nanoparticle-doped PHEMA films.

5.2.2 Apparatus.

UV-vis absorption spectra were measured with a Shimadzu UV-2200 spectrophotometer. Fluorescence spectra were recorded on a Shimadzu RF-5000 fluorimeter. Crystal sizes were determined with a Hitachi H-300 transmission electron microscope (TEM). Measurements of a third-order nonlinear susceptibility $|\chi^{(3)}|$ were carried out with a DFWM optical setup of the phase conjugation style, which has been described in section 2.2 and Figure 2.4. The wavelengths of both pump and probe laser beams were changed from 440 to 470 nm. The $|\chi^{(3)}|$ value was calculated in the same manner as described previously.

5.3 Results and Discussion

Figure 5.2a shows the UV-vis absorption spectrum and the $|\chi^{(3)}|$ spectrum of the CdS/PHEMA sample. A TEM image is shown in Figure 5.2b. Since the phase conjugation signal was saturated above the pump intensity of about 10~20 kW/cm^2, the $|\chi^{(3)}|$ values were calculated from the plots below the pump power. The $|\chi^{(3)}|$ value of 1.3×10^{-8} esu was obtained as a maximum at 470 nm excitation, which was a shoulder of the excitonic transition of confined CdS nanocrystals. Since this value was quite similar to that obtained in chapter 4 with a similar absorption coefficient, the optical nonlinearity would be originated from electron-hole pair bleaching. Moreover, nonlinear susceptibility becomes larger as the pump wavelength approaches to the resonant transition energy of CdS.

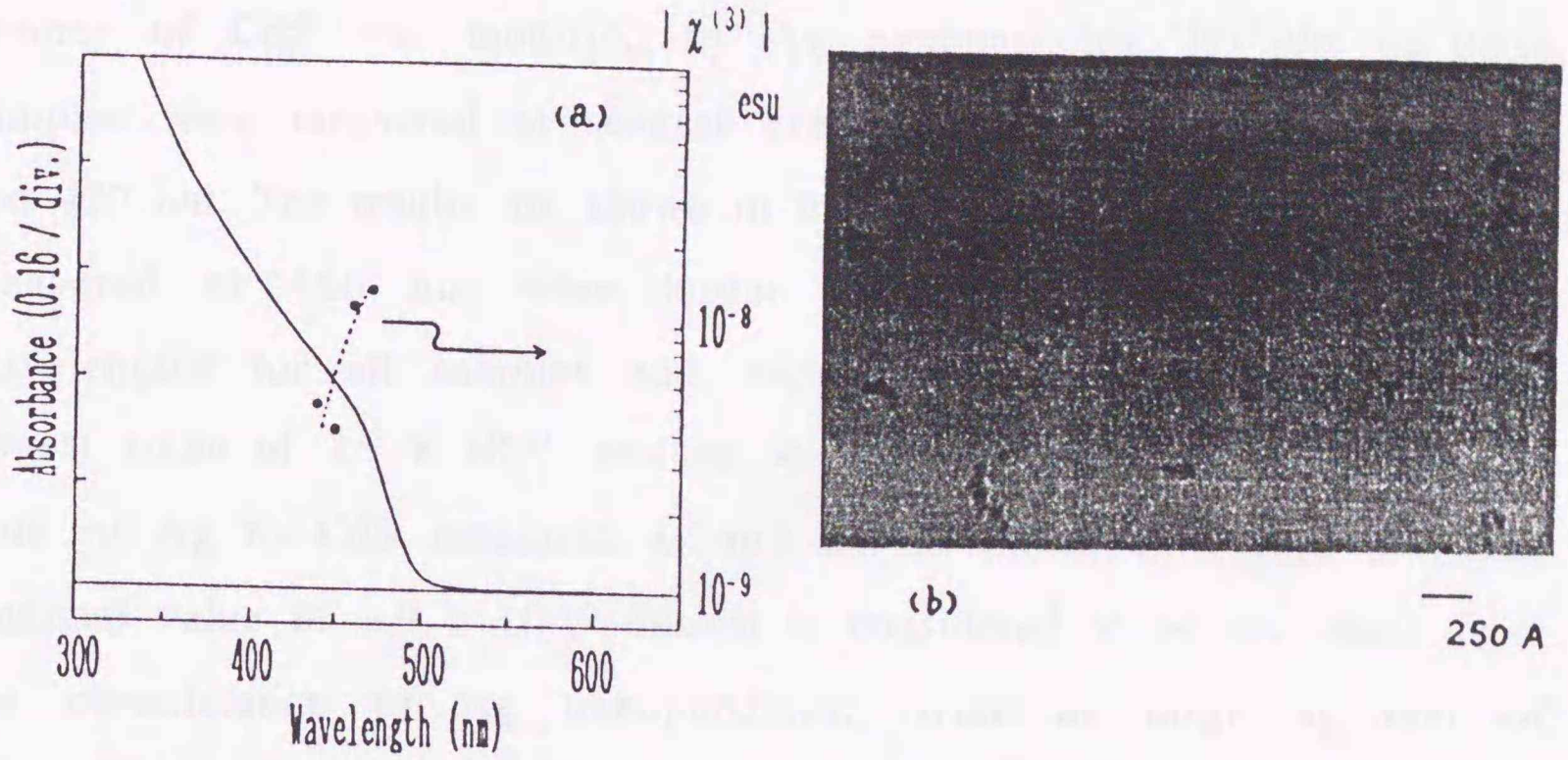

Figure 5.2. (a) Absorption spectrum and wavelength dependence of $|\chi^{(3)}|$ for the CdS/PHEMA film. (b) A TEM image of the CdS/PHEMA film.

Co-dispersion of CdS and Ag nanocrystals in PHEMA was attempted by mixing each PVP-coated powders, and the effect of the weight fraction of Ag particles in the film on $|\chi^{(3)}|/\alpha$ was studied. A surface plasmon peak of Ag nanoparticles remained for a while when CdS and Ag were mixed together in PHEMA films. After a few days, however, the peak disappeared. UV-vis absorption spectra of the *CdS/Ag^p (1)~(3)* samples with different proportions of Ag are shown in Figure 5.3a. A weak absorption tail due to the narrow band gap of Ag_2S was observed for every sample. The fact indicates that Ag nanoparticles reacted with the CdS surfaces to form Ag_2S, given as

$$CdS + 2Ag \rightarrow Ag_2S + Cd \qquad (5.2)$$

Ag nanoparticles were found to be located in the vicinity of CdS nanoparticles as revealed by a TEM image of the sample *CdS/Ag^P(3)* as shown in Figure 5.3b. Annular growth of CdS was also observed, and the surface of CdS was modified by Ag nanoparticles. $|\chi^{(3)}|/\alpha$ of these samples were measured at several excitation wavelengths between 440 and 470 nm. The results are shown in the inset of Figure 5.3a. The values measured at 460 nm were larger than those measured at other wavelengths for all samples and, especially, *CdS/Ag^P(2)* showed the largest value of 3.9×10^{-10} esu•cm. A relation between $|\chi^{(3)}|/\alpha$ and the ratio of Ag to CdS measured at 460 nm is shown in Figure 5.4. The maximal value of 3.9×10^{-10} esu•cm is considered to be the result from the co-existence of Ag nanoparticles; twice as large as that of CdS/PHEMA which does not contain Ag. Although the enhanced local field near metal nanoparticles caused by plasmon resonance might be expected when CdS nanocrystals existed on or near the surface of the metal particles,[6] the present result would not be due to this enhanced field effect because of the disappearance of a plasmon peak of the Ag nanoparticles.

To confirm the fact that the effect of Ag particle addition on the optical nonlinearity is due to surface modifications of CdS nanocrystals, $|\chi^{(3)}|$ values of CdS in the presence of Ag^+ ions were examined. Ag^+ ions are expected to react with the CdS surfaces to form easily Ag_2S, according to eq.5.1. Figure 5.5a shows absorption spectra of the *CdS/Ag⁺(1)~(4)* samples and the inset shows the dependence of $|\chi^{(3)}|/\alpha$ on the excitation wavelengths. The spectra were quite similar to those in Figure 5.2a. A TEM image of *CdS/Ag⁺(4)*, shown in Figure 5.5b, indicates that considerable particle growth occurs compared to the size obtained for the CdS/PHEMA sample.

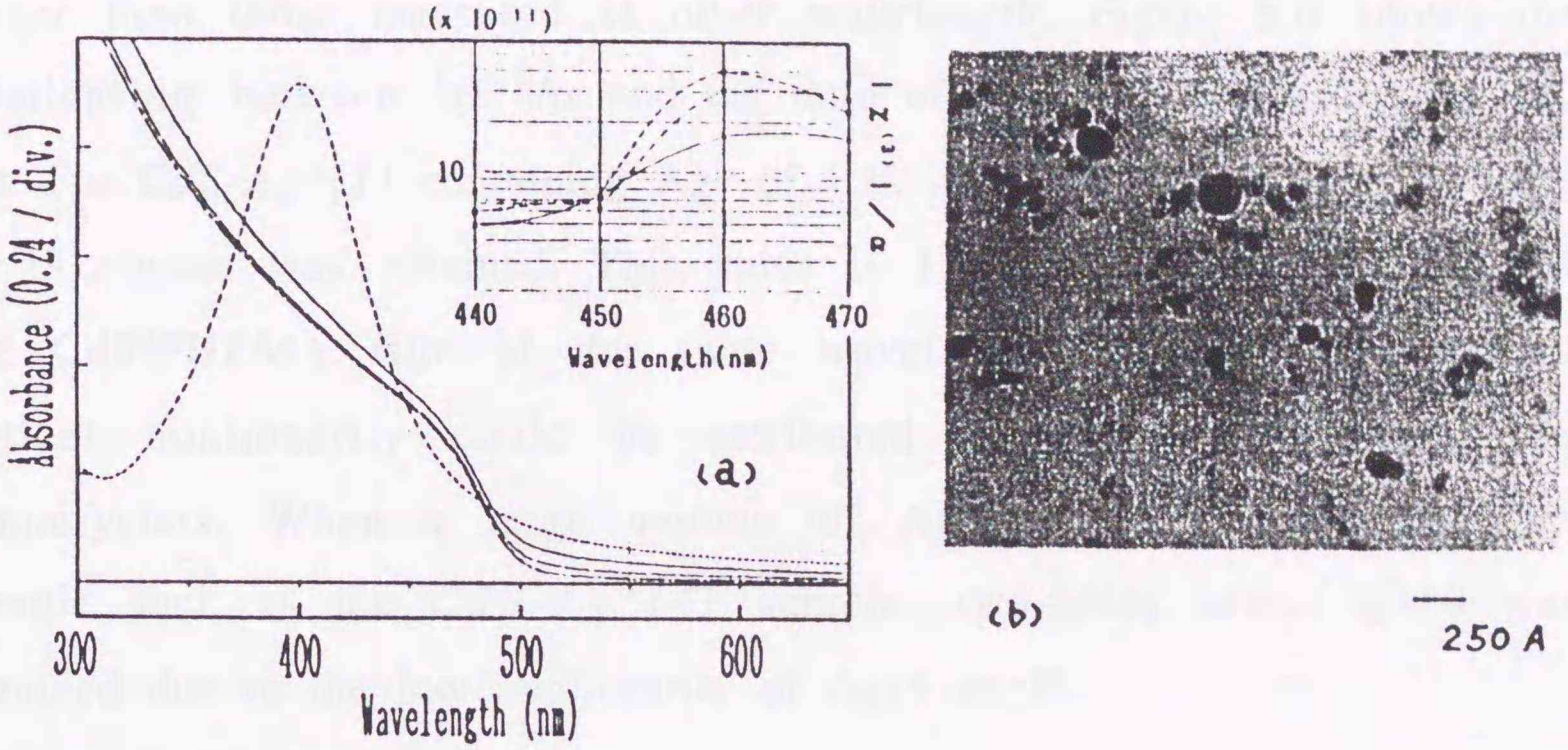

Figure 5.3. (a) Absorption spectra of *CdS/Agp (1)~(3)* samples. *CdS/Agp(1)* : dot dash, *CdS/Agp(2)*: dash, *CdS/Agp(3)*: solid, Ag colloidal solution: dot. The inset shows the dependence of $|\chi^{(3)}|/\alpha$ on pump wavelengths. (b) A TEM image of sample *CdS/Agp(3)*.

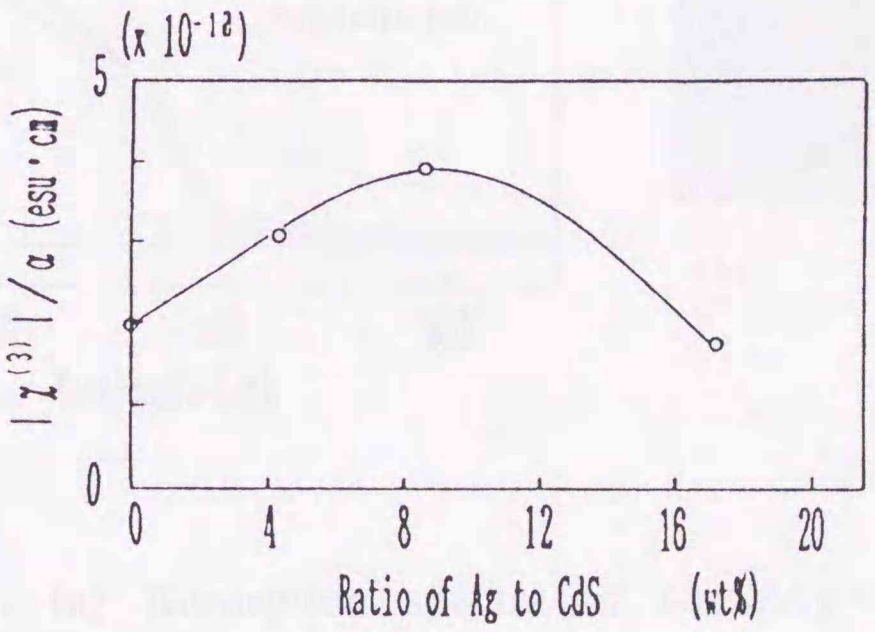

Figure 5.4. Dependence of $|\chi^{(3)}|/\alpha$ on the Ag fraction to CdS for *CdS/Agp (1)~(3)* samples. Measured at 460 nm.

This suggests that Ag nanoparticles and Ag^+ ions changed to Ag_2S at the surface of CdS nanocrystals. Values of $|\chi^{(3)}|/\alpha$ at 470 nm excitation were larger than those measured at other wavelength. Figure 5.6 shows the relationship between $|\chi^{(3)}|/\alpha$ and the ratio of Ag to CdS measured at 470 nm. For *CdS/Ag⁺(1)* containing Ag^+ of 4.28 wt%, the largest value of 4.1 x 10^{-10} esu·cm was obtained. This value is 1.5 times larger than that for the CdS/PHEMA film at the same wavelength. The enhancement of optical nonlinearity could be attributed to surface modified CdS nanocrystals. When a large amount of Ag^+ was added into the CdS sample such as the *CdS/Ag⁺(4)* sample, two-order lower $|\chi^{(3)}|$ was obtained due to the low nonlinearity of Ag_2S itself.

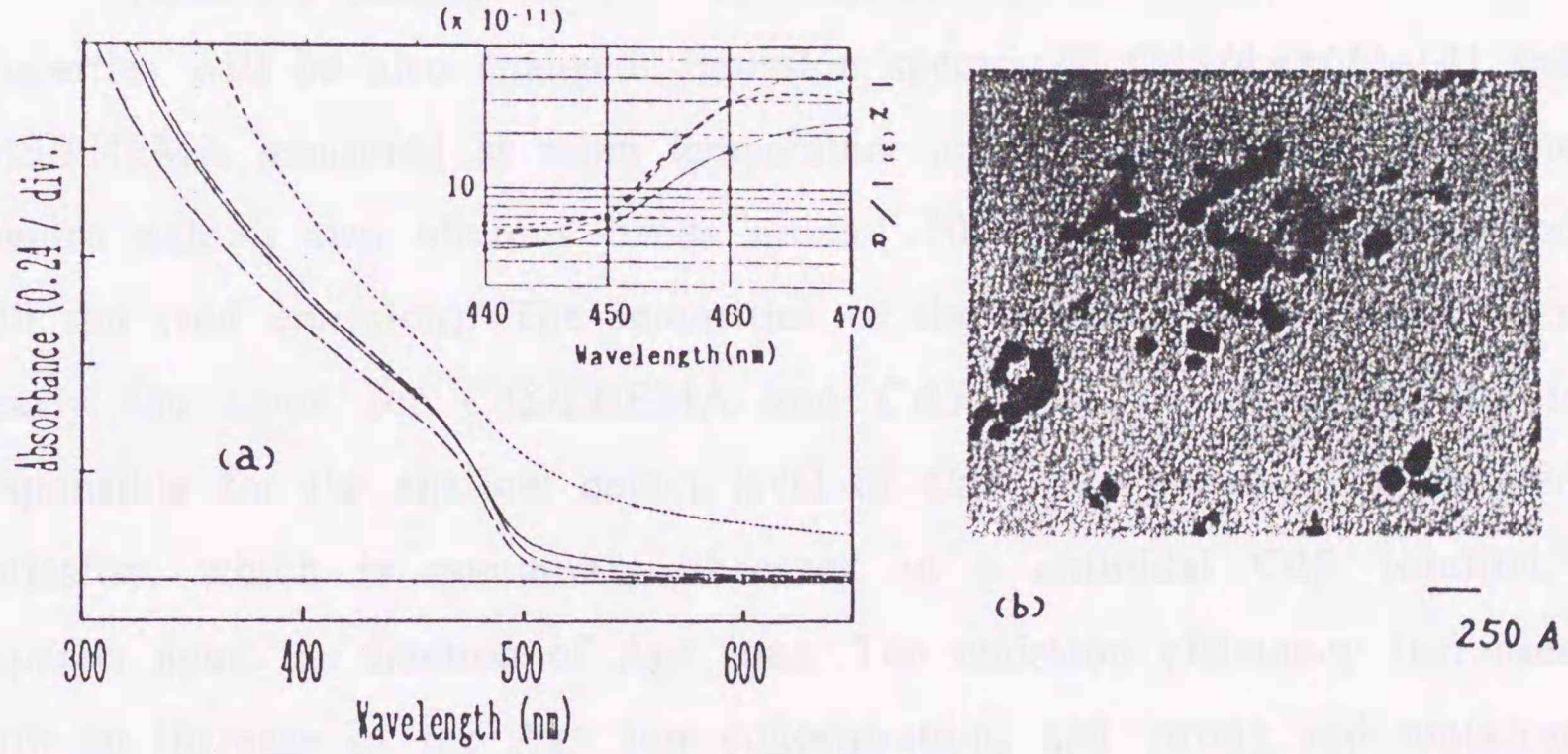

Figure 5.5. (a) Absorption spectra of *CdS/Ag⁺(1)~(4)* samples. *CdS/Ag⁺(1)* : dot dash, *CdS/Ag⁺(2)*: dash, *CdS/Ag⁺(3)*: solid, *CdS/Ag⁺(4)*: dot. The inset shows the dependence of $|\chi^{(3)}|/\alpha$ on pump wavelengths. (b) A TEM image of sample *CdS/Ag⁺(4)*.

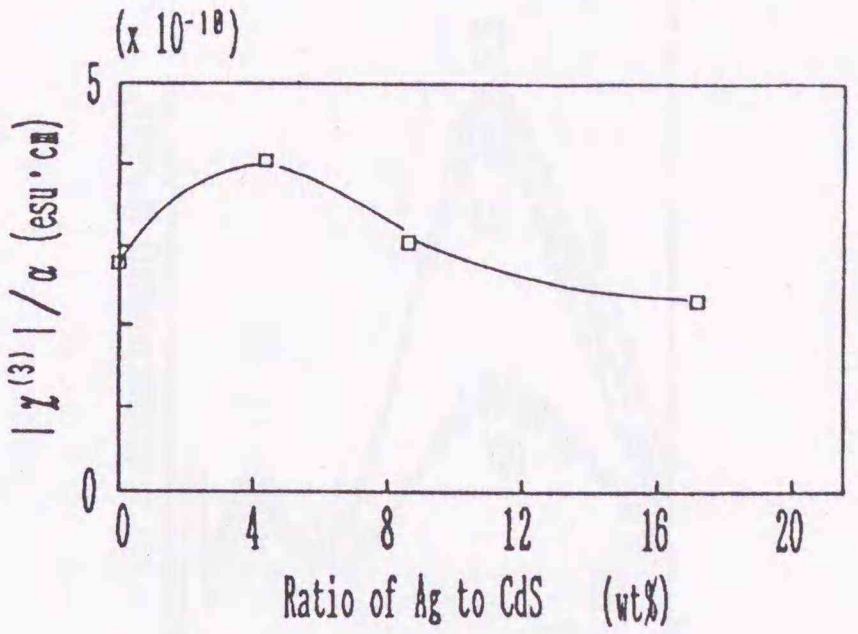

Figure 5.6. Dependence of $|\chi^{(3)}|/\alpha$ on the Ag fraction to CdS for *CdS/Ag⁺(1)~(3)* samples. Measured at 470 nm.

When the surface of CdS nanocrystals was modified, the emission properties will be also changed. Emission spectra of *CdS/Ag⁺(1)~(4)* and CdS/PHEMA measured at room temperature are shown in Figure 5.7. The spectra exhibit two obvious bands around 500 nm (green emission) and 670 nm (red emission). The intensities of the green emission band were nearly the same for CdS/PHEMA and *CdS/Ag⁺(1)~(3)*. This band is responsible for the shallow defect level of CdS. The intensity of the red emission, which is commonly observed in a colloidal CdS solution,[7] depends upon the fraction of Ag^+ ions. The emission efficiency increased with an increase of the Ag^+ ion concentration, and strong red emission was observed when the ratio of Ag to CdS was 17.2 wt%. This band is ascribed to come from the surface defects of CdS. The defects would act as a radiative center of trapped carrier recombination.[8] There appeared a difference in the Ag fraction between the maximum value of $|\chi^{(3)}|/\alpha$ and that of emission intensity.

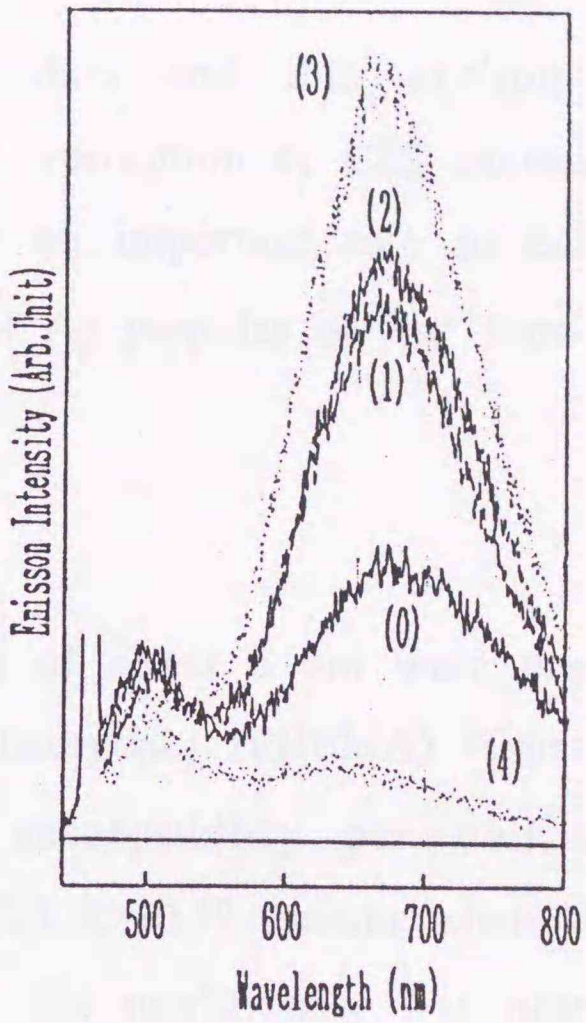

Figure 5.7. Emission spectra of CdS/PHEMA and *CdS/Ag⁺(1)~(4)* samples. Excitation wavelength was 460 nm.

The fact suggests that formation of Ag_2S with a relatively low nonlinearity in a considerable quantity lessens the $|\chi^{(3)}|/\alpha$ value when a radiationless center is modified with sufficient Ag^+ ions.

The emission properties were quite similar to those of samples *CdS/Ag⁰(1)~(3)*. The efficiency of radiationless recombination decreased as Ag particles or Ag^+ ion blocked one of the surface defects, which was responsible for radiationless processes. Thus, the increase of the emission efficiency was detected.[9]

It has been pointed out that an electron-hole pair trapped at the surface defect sites interacts with exciton and this reduces the exciton transition oscillator strength, which has been experimentally observed in optical transient absorption bleaching using a pump-probe technique for small CdS nanoparticles of 5.5 nm. The magnitude of the nonlinearity is determined by the efficiency of the bleaching process.[10] Based on the

present photoemission data and this exciton bleaching result, the saturation of the exciton absorption of CdS caused by the surface trapped electron-hole pair plays an important role in enhancement of the $|\chi^{(3)}|$ value with an addition of Ag particles or Ag^+ ions.

5.4 Summary

CdS nanoparticles of about 6 nm were prepared and embedded in poly(2-hydroxyethyl methacrylate) (PHEMA) films. The values of $|\chi^{(3)}|/\alpha$ (third-order nonlinear susceptibility per unit absorption coefficient) were determined to be 2.7×10^{-10} esu•cm when CdS was excited at 470 nm. An enhancement of the nonlinearity was observed for the first time when a small amount of Ag nanoparticles or Ag^+ ions were co-dispersed with CdS nanoparticles. The addition of Ag particles (8.57 wt%) or Ag^+ ion (4.26 wt%) enhanced the $|\chi^{(3)}|/\alpha$ value to 3.9×10^{-10} esu•cm or 4.1×10^{-10} esu•cm, respectively. The surface modification of CdS by Ag_2S is responsible for the enhancement.

5.5 References and Notes

(1) Yao, H.; Hayashi, T. *Mat. Res. Soc. Symp. Proc.* **1993**, *283*, 847.

(2) Metiu, H. *Prog. Surf. Sci.* **1984**, *17*, 153.

(3) Moskovits, M. *Rev. Mod. Phys.* **1985**, *57*, 783.

(4) Wang, D.-S.; Kerker, M.; *Phys. Rev.* **1982**, *B24*, 1777.

(5) Granqvist, C. G.; Hunderi, O. *Phys. Rev.* **1987**, *B18*, 2897.

(6) Creighton, J. A.; Blatchford, C. G.; Albrecht, M. G. *J. Chem. Soc. Faraday Trans.* **1979**, *75*, 790.

(7) Spanhel, L.; Haase, M.; Weller, H.; Henglein, A. *J. Am. Chem. Soc.* **1987**, *109*, 5649.

(8) Ramsden, J. J.; Webber, S. E.; Grätzel, M. J. *J. Phys. Chem.* **1992**, *96*, 2866.

(9) Dannhauser, T.; O'Neil, M.; Johansson, K.; McLendon, G. *J. Phys. Chem.* **1986**, *90*, 6074.

(10) Hilinski, E. F.; Lucas, P. A.; Wang, Y. *J. Chem. Phys.* **1988**, *89*, 3435.

Chapter 6. Summary

In the present thesis, several preparation methods for semiconductor nanocrystals (CdS nanocrystals)/organic polymer hybrids were developed and their optical properties were studied by spectroscopic technique in detail. Regulations of the crystal size and its distribution characteristics of CdS in polymer matrices were achieved by *in situ* synthesis of CdS under monochromatic light irradiation. The use of spherical micrometer-sized host polymers or polymer stabilizers was also successful to control the size and the distribution characteristics of CdS in the host media. These preparation methods were quite novel, and characteristic features of CdS/polymer hybrids were demonstrated in each case.

In the case of preparation of CdS under laser irradiation, a relatively narrow size-distribution of CdS was obtained when the solution containing Cd^{2+}, dilute H_2S gas and a styrene monomer was irradiated at 457.9 nm. The elaborate experiments by varying the excitation wavelength (λ) demonstrated that the crystal size and its distribution in polymers were dependent on λ. Typically, the energy difference of 21 meV (472.7 or 476.5 nm laser irradiation) was reflected on the difference in the particle diameter. This is the first demonstration for fine tuning of size-regulated synthesis of CdS under photo-illumination (Chapter 2).

In the case of *in situ* preparation of CdS from Cd^{2+} and S^{2-} in micrometer-sized chelate resin beads, characteristics of the host polymer were reflected on the properties of the CdS/polymer hybrids. The optical properties and the size distributions of CdS were controlled by the concentration of an S^{2-} solution, a host polymer particle size and an

added electrolyte (NaCl). The use of spherical microparticles possessing chelating ligands as a host medium was quite novel and, the diffusion rate of S^{2-} in the polymer particle was shown to be the most important factor governing the size and the distribution characteristics of CdS (Chapter 3).

In the case of an organo-sol method using a polymer stabilizer, solvent effects on the nanocrystal size were demonstrated. Also, this method provided dense loading of CdS nanocrystals in the polymer matrix. The CdS/polymer hybrids obtained showed high optical nonlinearity and proved to be very suitable for optical nonlinear materials (Chapter 4 and 5).

As reviewed in Chapter 1, semiconductor nanocrystals have attracted research interests in many fields such as nonlinear optical materials, photocatalysis, and so forth. However, preparation of semiconductor nanocrystal/organic polymer hybrids has been scarcely studied. From the view points of practical applications and basic science of semiconductor nanocrystals, the nanocrystal/polymer hybrids will play important roles, since the crystal size and the optical/distribution properties of nanocrystals can be controlled by several ways as demonstrated by the present study. The present study will contribute to open new basic science and materials based on semiconductor nanocrystal/polymer hybrids systems.

Acknowledgments

I would like to express my sincere gratitude to Professor Noboru Kitamura for his continuing guidance and stimulating criticism through the work of this thesis.

I am much grateful and indebted to Dr. Toyoharu Hayashi, Mitsui Toatsu Chemicals, Inc., for providing me a chance to investigate the interesting nanoscopic world and valuable discussions.

I am much grateful to Professor Kohei Uosaki, Professor Yukio Hinatu, and Associate Professor Bunsho Ohtani for the examination of this thesis.

I am grateful to Professor Takayoshi Kobayashi, and Dr. Kazuhiko Misawa, University of Tokyo, for providing me helpful discussions on nonlinear optics.

Many thanks are due to Dr. Shigeru Takahara (Faculty of Engineering, Chiba University) and Mr. Hirokazu Mizuma (Mitsui Toatsu Chemicals, Inc.) for helpful discussions. Thanks are also due to Ms. Yukako Takada, Hokkaido University, for her cooperation in this work.

I wish to thank all members of Division of Chemistry, Graduate School of Science, Hokkaido University, and of Mitsui Toatsu Chemicals, Inc. for their friendships.

Sapporo, Hokkaido

Hiroshi YAO

八尾浩史

Publication Lists

(1) Picosecond Dynamics of Intramolecular Electron Transfer in Porphyrin Dimer Model Compounds.

Mataga, N.; Yao, H.; Okada, T.; Kanda, Y.; Harriman, A. *Chem. Phys.* **1989**, *131*, 473.

(2) Charge-Transfer Rates in Symmetric and Symmetry-Disturbed Derivatives of 9,9'-Bianthryl.

Mataga, N.; Yao, H.; Okada, T.; Rettig, W. *J. Phys. Chem.* **1989**, *93*, 3383.

(3) Solvation-Induced Charge Separation in the Excited State of Composite Systems with Identical Halves and Intramolecular Excimer Formation by Recombination. Picosecond Laser Photolysis Studies on 1,2-Dianthrylethanes.

Yao, H.; Okada, T.; Mataga, N. *J. Phys. Chem.* **1989**, *93*, 7388.

(4) Picosecond Laser Photolysis Studies on Dimer Model Systems in relation to Photosynthetic Charge Separation Processes.

Mataga, N.; Yao, H.; Okada, T. *Tetrahedron* **1989**, *45*, 4683.

(5) Superradiance Quenching by Confined Acoustic Phonons in Chemically Prepared CdS Microcrystallites.

Misawa, K.; Yao, H.; Hayashi, T.; Kobayashi, T. *J. Chem. Phys.* **1991**, *94*, 4131.

(6) Size Effects on Luminescence Dynamics of CdS Microcrystallites Embedded in Polymer Films.

Misawa, K.; Yao, H.; Hayashi, T.; Kobayashi, T. *Chem. Phys. Lett.* **1991**, *183*, 113.

(7) Superradiative Emission from CdS Microcrystallites.

Misawa, K.; Yao, H.; Hayashi, T.; Kobayashi, T. *J. Cryst. Growth* **1992**, *117*, 617.

(8) Excitonic Superradiance and Its Quenching by Confined-Acoustic Phonons in CdS Microcrystallites.

T. Kobayashi, K. Misawa, H. Yao, T. Hayashi, *Nonlinear Opt.*, Proc. Toyota Conf. Nonlinear Opt. Mater. 5th 1991, ed. by S. Miyata, Elsevier, North-Holland, 153, 1992.

(9) Electromodulation Spectroscopy of CdS Microcrystal Embedded in Polymer Films.

Sekikawa, T.; Kobayashi, T.; Yao, H.; Hayashi, T. *Solid State Commun.* **1992**, *83*, 969.

(10) Quantum-confined Copper(I) Bromide Microcrystallites Embedded in Polymethyl Methacrylate Matrices.

Yao H.; Hayashi, T. *Chem. Phys. Lett.* **1992**, *197*, 21.

(11) Photoirradiation Effect on Colloidal Cadmium Sulfide Formation Processes.

Hayashi, T.; Yao, H.; Takahara, S.; Mizuma, K. *J. Phys. Chem.* **1992**, *96*, 2866.

(12) Third-order Optical Nonlinearities of Quantized CdS and Metal Ultrafine Particles Co-dispersed in Polymer Matrices. -- Surface Modification Effect.

Yao, H.; Hayashi, T. *Mat. Res. Soc. Symp. Proc.* **1993**, *283*, 847.

(13) Preparation of CdS Ultrafine Particles Dispersed in Acrylonitrile-styrene Copolymer Films and Their Third-order Optical Nonlinearities.

Hayashi, T.; Mizuma, H.; Yao, H.; Takahara, S. *Org. Mat. Non-Linear Opt. III*; Ashwell, G. J.; Bloor, D. Eds., Royal Society of Chemistry, 197, 1993.

(14) Wavelength Dependence of the Ratio of the Third Order Nonlinear Optical Susceptibility to the Absorption Coefficient in CdS Micro-crystallites Dispersed in the Polymer Matrix.

Hayashi, T.; Mizuma, H.; Yao, H.; Takahara, S. *Nonlinear Opt.* **1995**, *13*, 135.

(15) Micrometer Size Effect on Dye Association in Single Laser-Trapped Water Droplets.

Yao, H.; Inoue, Y.; Ikeda, H.; Nakatani, K.; Kim, H.-B.; Kitamura, N. *J. Phys. Chem.* **1996**, *100*, 1494.

(16) CdS Nanocrystals in Chelate Polymer Microparticles: Polymer Size Dependence of the Optical Properties.

Yao, H.; Kitamura, N. *Bull, Chem. Soc. Jpn.* **1996**, *69*, 1227.

(17) Linear and Nonlinear Optical Properties of CdS and CdSe Nano-particles Stabilized with Poly(N-vinyl-2-pyrrolidone).

Yao, H.; Takahara, S.; Mizuma, H.; Kozeki, T.; Hayashi, T. *Jpn. J. Appl. Phys. part 1* **1996**, *35*, 4633.

(18) Optical Control of Fusion of Microparticles in Solution and Simultaneous Spectrophotometric Measurements.

Yao, H.; Ikeda, H.; Inoue, Y.; Kitamura, N. *Anal. Chem.* **1996**, *68*, 4304.

(19) CdS Nanocrystals in Chelate Polymer Microparticles.

Yao, H.; Takada, Y.; Kitamura, N. *Hyomen*, **1997**, *37*, 32.

(20) A Microspectroscopic Study on Dye Association at a Single Laser-Trapped Water Droplet/Oil Interface.

Yao, H.; Ikeda, H.; Kitamura, N. *Langmuir*, **1997**, *13*, 1996.

(21) Electrolyte Effects on CdS Nanocrystal Formation in Chelate Polymer Particles: Optical and Distribution Properties.

Yao, H.; Takada, Y.; Kitamura, N. submitted.

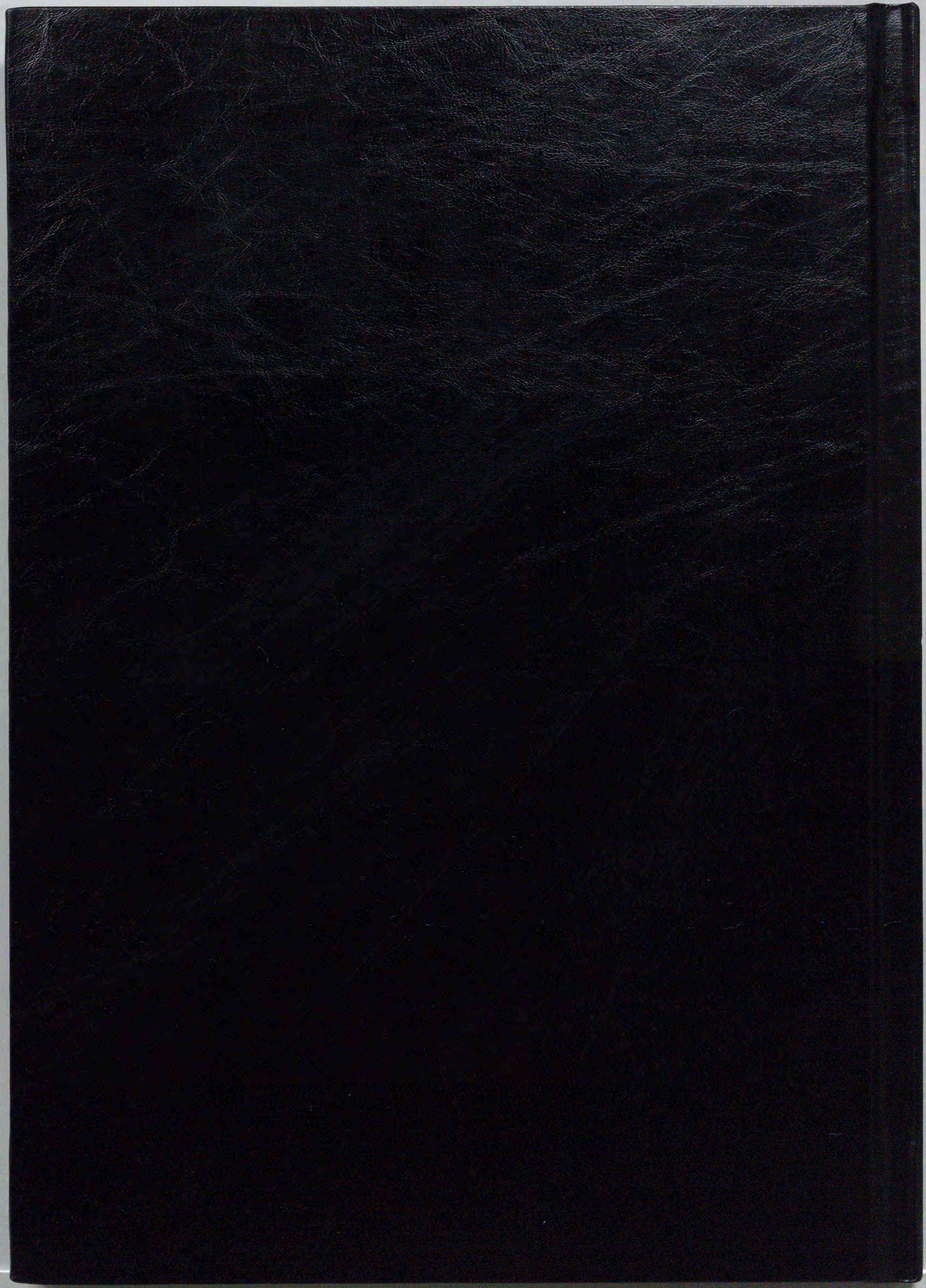

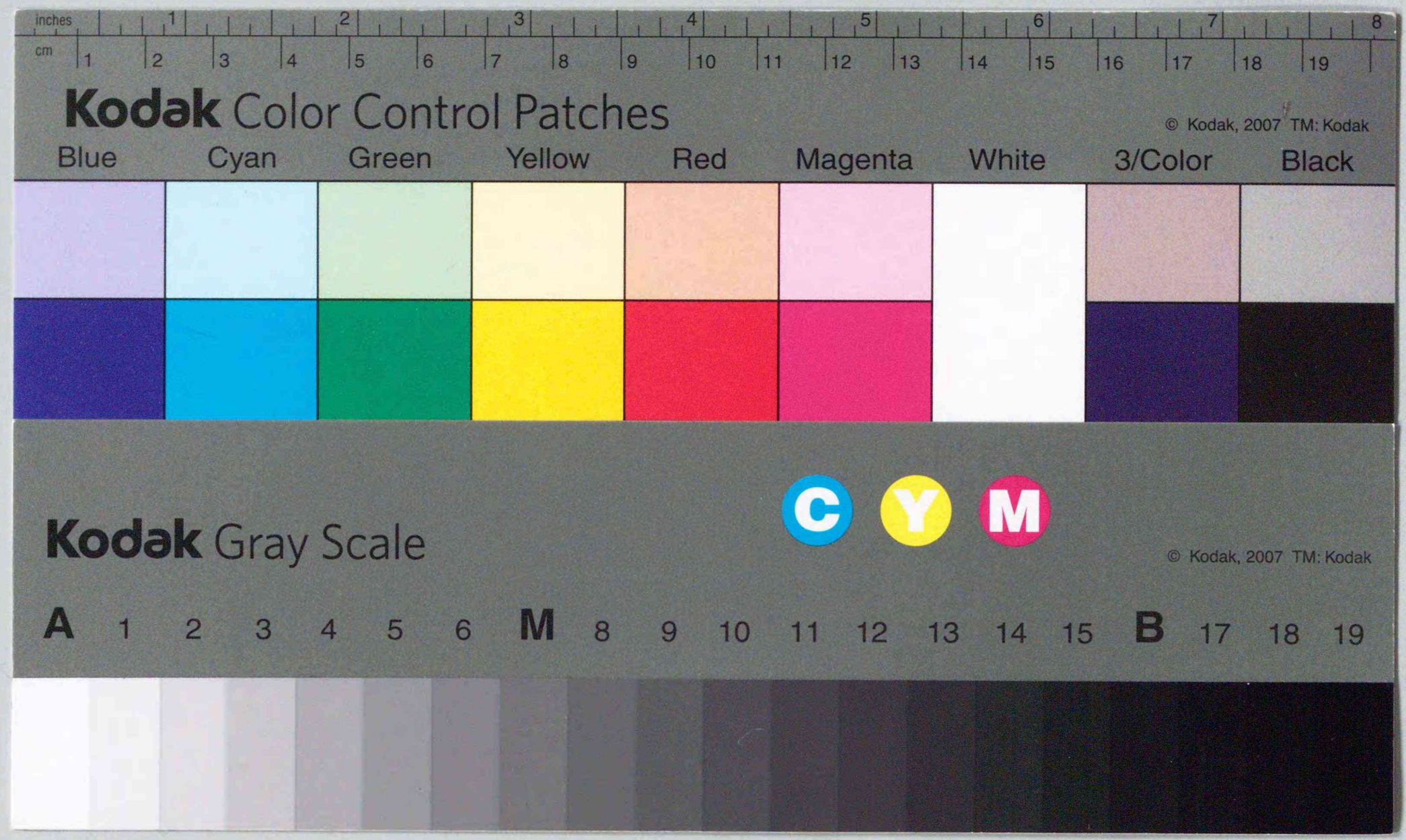
inches
cm
Kodak Color Control Patches
© Kodak, 2007 TM: Kodak
Blue
Cyan
Green
Yellow
Red
Magenta
White
3/Color
Black
Kodak Gray Scale
C
Y
M
© Kodak, 2007 TM: Kodak
A 1 2 3 4 5 6 M 8 9 10 11 12 13 14 15 B 17 18 19